1-1-2015

State Dependent Regulation of the Neural Circuit for C. Elegans Feeding

Nicholas Trojanowski
University of Pennsylvania, ntrojanowski@gmail.com

State Dependent Regulation of the Neural Circuit for C. Elegans Feeding

Abstract
Rhythmic muscular contractions are essential for many different behaviors, from locomotion to respiration. These behaviors are modulated by changes in the external environment, such as temperature shifts and presence of predators, and by internal states, such as hunger and sleep. The roundworm Caenorhabditis elegans feeds on bacteria through rhythmic contraction and relaxation of its pharynx, a neuromuscular pump innervated by a nearly independent network of just 20 neurons. Feeding rate is modulated by many environmental and physiological factors, but feeding generally persists throughout the life of the worm, ceasing only during sleep. The mechanisms by which the pharyngeal nervous system controls feeding during wake and sleep are poorly understood. I used optogenetics, genetics, and pharmacology to define the cholinergic pharyngeal circuitry that regulates feeding rate during wake, and then used similar approaches to examine how feeding is inhibited during sleep. I identified a four-neuron circuit that regulates feeding rate during wake and found that it is degenerate, meaning that multiple different classes of neurons can stimulate feeding in a similar manner. I also found that feeding quiescence is generated by distinct mechanisms during two behaviorally indistinguishable sleep states: cholinergic motor neurons are inhibited during stress-induced sleep, while the muscle is directly inhibited during developmentally timed sleep. Thus, as in mammals and despite its behavioral homogeneity, sleep in C. elegans is not a physiologically homogenous state. These results provide insight into the function of a highly conserved neural circuit that generates robust rhythmic behavior, and illustrate how this circuit can be altered in different ways to produce the same behavioral output during two distinct sleep states.

Degree Type
Dissertation

Degree Name
Doctor of Philosophy (PhD)

Graduate Group
Neuroscience

First Advisor
David M. Raizen

Second Advisor
Christopher Fang-Yen

Keywords
C. elegans, invertebrate, neural circuit, optogenetics, sleep

Subject Categories
Neuroscience and Neurobiology

STATE DEPENDENT REGULATION OF THE NEURAL CIRCUIT FOR *C. ELEGANS* FEEDING

Nicholas F Trojanowski

A DISSERTATION

in

Neuroscience

Presented to the Faculties of the University of Pennsylvania

in

Partial Fulfillment of the Requirements for the

Degree of Doctor of Philosophy

2015

Supervisor of Dissertation

_____

David Raizen, MD, Ph.D.

Asst. Prof. of Neurology

Co-Supervisor of Dissertation

_____

Christopher Fang-Yen, Ph.D.

Asst. Prof. of Bioengineering

Graduate Group Chairperson

_____

Joshua Gold, Professor of Neuroscience

Dissertation Committee:

Marc Schmidt, Ph.D., Associate Professor of Biology (Chair)

Dejian Ren, Ph.D., Professor of Biology

Michael P. Nusbaum, Ph.D., Professor of Neuroscience

Maureen Barr, Ph.D., Professor of Neuroscience, Rutgers University

STATE DEPENDENT REGULATION OF THE NEURAL CIRCUIT FOR *C. ELEGANS* FEEDING

ACKNOWLEDGMENTS

First and foremost, I would like to thank David Raizen and Chris Fang-Yen for their enthusiastic support, guidance, and mentorship, and for demonstrating the power of a true collaboration.

I would like to thank the current and former members of the Raizen and Fang-Yen labs for their input and help in various capacities, especially Matt Nelson and Olivia Padovan-Merhar, who assisted with the early stages of this work, and all of the undergraduates and technicians who poured my plates and froze my strains and made the labs run smoothly. I would also like to thank the many *C. elegans* researchers who generously shared reagents with me (most of which were used for work that was not included in this thesis).

I would like to thank my thesis committee, Marc Schmidt, Mike Nusbaum, and Dejian Ren, and the labs of Meera Sundaram, Bob Kalb, John Murray, and Todd Lamitina, for providing helpful feedback that has improved all aspects of my work, and Allan Pack for providing financial support via NIH T32-HL007953.

I would like to thank the Neuroscience Graduate Group administration, faculty, and students for providing a supportive and exciting atmosphere to become a scientist.

Finally, I would like to thank my friends and family for their support and inspiration. I would especially like to thank Brianne Connizzo for her motivation and encouragement, and for keeping me sane throughout my Ph.D.

ABSTRACT

STATE DEPENDENT REGULATION OF THE NEURAL CIRCUIT FOR *C. ELEGANS* FEEDING

Nicholas F Trojanowski

David Raizen, MD, Ph.D.

Christopher Fang-Yen, Ph.D.

Rhythmic muscular contractions are essential for many different behaviors, from locomotion to respiration. These behaviors are modulated by changes in the external environment, such as temperature shifts and presence of predators, and by internal states, such as hunger and sleep. The roundworm *Caenorhabditis elegans* feeds on bacteria through rhythmic contraction and relaxation of its pharynx, a neuromuscular pump innervated by a nearly independent network of just 20 neurons. Feeding rate is modulated by many environmental and physiological factors, but feeding generally persists throughout the life of the worm, ceasing only during sleep. The mechanisms by which the pharyngeal nervous system controls feeding during wake and sleep are poorly understood. I used optogenetics, genetics, and pharmacology to define the cholinergic pharyngeal circuitry that regulates feeding rate during wake, and then used similar approaches to examine how feeding is inhibited during sleep. I identified a four-neuron circuit that regulates feeding rate during wake and found that it is degenerate, meaning that multiple different classes of neurons can stimulate feeding in a similar manner. I also found that feeding quiescence is generated by distinct mechanisms during two behaviorally indistinguishable sleep states: cholinergic motor neurons are inhibited

during stress-induced sleep, while the muscle is directly inhibited during developmentally timed sleep. Thus, as in mammals and despite its behavioral homogeneity, sleep in *C. elegans* is not a physiologically homogenous state. These results provide insight into the function of a highly conserved neural circuit that generates robust rhythmic behavior, and illustrate how this circuit can be altered in different ways to produce the same behavioral output during two distinct sleep states.

TABLE OF CONTENTS

LIST OF TABLES

CHAPTER 1

CHAPTER 3

LIST OF FIGURES

CHAPTER 1: Introduction and Overview

Rhythmic muscle contractions are essential for a wide array of animal behaviors, from locomotion to feeding. These behaviors can be modulated both by external factors, such as temperature, and by internal states, such as sleep. The mechanisms underlying the generation of these behaviors vary widely. Some muscles, like the vertebrate heart, generate rhythmic contractions by intrinsic oscillations of membrane currents (Yaniv et al., 2015), while others, like the limb muscles that generate vertebrate locomotion, require complex neural network interactions to produce their rhythmicity (Kiehn et al., 2010).

The mechanisms that underlie rhythmic behaviors are best understood in invertebrates such as leeches, crustaceans, and molluscs, where a small number of neurons and relative ease of electrophysiological recordings allow detailed analysis of the activity of individual neurons and muscles. Over the past five decades, researchers have taken advantage of the ability to electrophysiologically identify the functional synaptic connectivity between neurons in these systems to determine the roles of intrinsic and synaptic properties of individual neurons in producing network output (Stent et al., 1979; Marder and Calabrese, 1996; Selverston, 2010). This approach has provided insight into how single neurons can function in multiple different circuits (Selverston, 2010), the ways in which activity and neuromodulators influence circuit output (Marder et al., 2014), and mechanisms by which networks maintain stable output despite variability in many underlying parameters (Golowasch, 2014).

In parallel with these electrophysiological studies, researchers have employed other model systems to study the genetic basis of rhythmic behaviors. Work initiated by Seymour Benzer on the fruit fly *Drosophila melanogaster* (Benzer, 1971; Konopka and Benzer, 1971) and by Sydney Brenner on the nematode *Caenorhabditis elegans* (Brenner, 1973; 1974) led to the development of a wide array of genetic tools for identifying the roles of individual neural and muscular genes in producing rhythmic behaviors in these organisms (Xu and Kim, 2011; Owald et al., 2015). However, just as leeches, crustaceans, and gastropods are not amenable to genetic approaches, *Drosophila* and *C. elegans* are not as suitable for electrophysiological manipulations. As a result, until recently these two broad fields of invertebrate research progressed largely independently (Marder et al., 2005). However, the development of optical methods for manipulating and monitoring neural activity has begun to bridge this gap (Kerr et al., 2000; Nagel et al., 2005). These methods enable analysis of the physiology and functional connectivity of *C. elegans* neural circuits using a conceptual approach similar to that developed in leeches, crustaceans, and gastropods while leveraging the extensive genetic toolkit available in *C. elegans*.

C. elegans is an excellent model organism for investigating the neural and genetic basis of rhythmic behaviors

C. *elegans* develops through four larval stages, each lasting 12-16 hours and followed by a molt, before becoming a 1 mm long adult three days after hatching (Corsi et al., 2015). *C. elegans* is one of the anatomically simplest model animals, and the synaptic

connections of its 302 neurons have been fully mapped (Albertson and Thomson, 1976; White et al., 1986; Hall and Russell, 1991; Jarrell et al., 2012). Despite its simplicity, *C. elegans* performs many behaviors seen in higher organisms (de Bono and Maricq, 2005), and its neurochemistry of synaptic transmission is strikingly similar to that of mammals (Bargmann, 1998). There are 91 genes predicted to encode neuropeptides and at least 100 potential neuropeptide receptor genes in *C. elegans*, a quarter of which have clear vertebrate homologs (Janssen et al., 2010; Hobert, 2013). Several of these neuropeptide signaling pathways have evolutionarily conserved functions (de Bono and Bargmann, 1998; Pierce et al., 2001; Beets et al., 2012; Garrison et al., 2012).

Although the synaptic connectivity of the *C. elegans* nervous system was first described decades ago, we are still a long way from understanding how the whole system works: the connections between neurons are simply too numerous to discern the function of any individual neuron simply by its connectivity, save for classifying some neurons as sensory or motor (Ward et al., 1975; White et al., 1986). Therefore, to understand how the nervous system works, identification of functional connectivity is necessary (Bargmann and Marder, 2013). In larger invertebrates, functional connectivity is determined by electrophysiological manipulations, but *C. elegans* neurons are too small and inaccessible for this approach to be practical (Avery et al., 1995). Instead, studies of functional connectivity in *C. elegans* have typically used laser ablation to identify the functions of neurons, where neurons are killed in young larvae and behavioral changes are assayed in adults (Sulston and White, 1980; Bargmann and Avery, 1995; Fang-Yen et al., 2012). Laser ablation has proven effective for determining the roles of neurons in some sensory behaviors, including mechanosensation (Chalfie et al., 1985),

chemosensation (Bargmann and Horvitz, 1991a; 1991b), and thermosensation (Mori and Ohshima, 1995), but this approach is insensitive to redundancy and compensatory effects, so interpreting data can be challenging.

The limitations of laser ablation can be overcome by taking advantage of the transparency of the worm and applying recently developed optical techniques, including light-sensitive ion channels and pumps and fluorescent Ca^{2+} sensors, to directly identify the roles of individual neurons in behavior (Zhang et al., 2007a). By selectively manipulating the activity of single neurons (Guo et al., 2009; Leifer et al., 2011; Stirman et al., 2011; Kocabas et al., 2012), sequential and nondestructive stimulation or inhibition of individual or multiple neurons with high temporal precision can provide a more complete picture of dynamic network function than one based on more sparse and destructive measurements.

C. elegans feeds via rhythmic contraction of a neuromuscular pump

In the wild, *C. elegans* lives in and feeds on rotting vegetation (Frézal and Félix, 2015), though in the lab it subsists on a diet of *E. coli* bacteria grown on agar plates (Brenner, 1974). *C. elegans* feeds through its pharynx, a neuromuscular pump with tri-radial symmetry (Albertson and Thomson, 1976) (Fig. 1). Pumping typically occurs 200-300 times per minute in the presence of food (Croll and Smith, 1978) and 20-60 times per minute in the absence of food (Horvitz et al., 1982), and is affected by many different factors including behavioral state (Raizen et al., 2008), touch (Chalfie et al., 1985), odorants (Li et al., 2012), mating (Gruninger et al., 2006), aging (Croll et al., 1977),

development (Cassada and Russell, 1975), cellular stress (Jones and Candido, 1999), food quality (Soukas et al., 2009), satiety (You et al., 2008), starvation (Avery and Horvitz, 1990), feeding history (Song et al., 2013), presence of food (Croll and Smith, 1978), bacterial infection (Wei et al., 2003), and hypoxia (Sharabi et al., 2014).

Anatomically and functionally, the pharynx is divided into three regions along the anterior-posterior axis (Fig. 1). The anterior part of the pharynx is known as the corpus, and contains the procorpus and the metacorpus. The posterior part of the pharynx, the terminal bulb, houses the three cuticular plates known as the grinder. The isthmus connects the corpus to the terminal bulb (Albertson and Thomson, 1976).

The muscle fibers of the pharynx are perpendicular to the lumen, so the luminal space increases when the muscles contract. The muscle cells also function as epithelial cells, as they directly abut the lumen and may secrete parts of each new cuticle formed during larval molts (Albertson and Thomson, 1976; George-Raizen et al., 2014). In between each of the three muscle cells are marginal cells (Fig. 2), which provide structural support for the pharynx (Avery and Horvitz, 1989). The muscles and marginal cells are apparently all electrically coupled (Starich et al., 1996; Li et al., 2003; Starich et al., 2003), allowing for coordinated contraction and relaxation.

Feeding occurs as two distinct but coupled pharyngeal behaviors, pumping and peristalsis (Albertson and Thomson, 1976; Shimozono et al., 2004; Song and Avery, 2012). A pump begins when the corpus and anterior isthmus muscles contract and bacterial food is sucked into the lumen (Doncaster, 1962). Nearly simultaneously, the terminal bulb muscles contract: the anterior terminal bulb muscles open the lumen in front of the

grinder, while the posterior terminal bulb muscles, whose fibers are oriented obliquely relative to the anterior-posterior axis of the pharynx, pull the grinder plates posteriorly to crush any bacteria present in the terminal bulb. After approximately 200 ms, the muscles of the corpus, anterior isthmus, and terminal bulb begin to return to their resting position (Seymour et al., 1983). The anterior tip of the corpus relaxes more rapidly than the rest of the corpus, and the corpus relaxes slightly before the anterior isthmus, so that bacteria are trapped at the anterior ends of the corpus and isthmus after relaxation (Avery and Shtonda, 2003; Lieven, 2003; Fang-Yen et al., 2009). Finally, bacteria crushed by the grinder pass through the pharyngeal-intestinal valve to the intestine (Doncaster, 1962). The second pharyngeal behavior, peristalsis, is an anterior to posterior wave along the posterior isthmus that begins while the muscles of the anterior isthmus are contracted and transports bacteria from the anterior isthmus to the anterior end of the terminal bulb. Peristalsis occurs after approximately 1 out of every 4 pumps (Avery and Horvitz, 1987).

C. elegans feeding is controlled by the pharyngeal nervous system

The pharynx is innervated by a highly interconnected subnetwork of just 20 neurons comprised of 14 types, collectively known as the pharyngeal nervous system (Albertson and Thomson, 1976) (Table 1). The pharyngeal neurons are embedded in the pharyngeal muscle, which is surrounded by a thick basement membrane (Fig. 2). The neuronal processes run along grooves through or adjacent to the muscles, and many of these neurons have sensory endings in the pharyngeal lumen (Albertson and Thomson, 1976). Pumping persists after the entire pharyngeal nervous system is killed (Avery and Horvitz,

1989), albeit at a decreased rate, demonstrating that the pharyngeal nervous system is not required for pumping. However, acetylcholine (ACh) appears to be necessary for pumping, as mutants lacking ACh do not pump (Rand, 1989).

Just 2 classes of pharyngeal neurons are essential for grossly normal and effective pharyngeal behavior, the cholinergic MC and M4 motor neurons (Avery and Horvitz, 1987; 1989). The pair of bilaterally symmetric MC neurons are essential for rapid pumping, as the pumping rate is reduced nearly 10-fold and the worms become thin and pale, like starved worms, after the MC neurons are ablated, though the pattern of muscle contraction is not dramatically altered (Avery and Horvitz, 1989; Raizen et al., 1995). Activation of the MC neurons by serotonin (5-hydroxytryptamine or 5-HT), a key regulator of pharyngeal behavior, stimulates rapid pumping (Niacaris and Avery, 2003; Song and Avery, 2012). Ablation of the M4 neuron abolishes peristalsis (Avery and Horvitz, 1987) and causes a small and variable decrease in pump rate (Raizen et al., 1995) possibly due to the luminal distension of the corpus that occurs in the absence of peristalsis. Peristalsis rate increases when the M4 neuron is activated by 5-HT (Song and Avery, 2012), and M4 can stimulate pumping under certain conditions (Chiang et al., 2006; Song and Avery, 2012; Steciuk et al., 2014).

Laser ablation of the other three classes of cholinergic pharyngeal neurons, I1, M1, and M2, causes more mild behavioral defects (Avery and Horvitz, 1989; Raizen et al., 1995; Bhatla et al., 2015). Ablation of the M1 motor neuron does not affect pump rate, but alters the behavioral response to ultraviolet light. When M1 is intact, exposure to ultraviolet light causes a decrease in pump rate and altered muscle coordination, such that

the anterior tip of the corpus no longer relaxes before the rest of the corpus so the food that has just entered the lumen is spit out. Ablation of M1 abolishes this spitting behavior (Bhatla et al., 2015). The paired I1 interneurons form the only synaptic connections between the pharyngeal and non-pharyngeal nervous systems, a pair of electrical synapses with the non-pharyngeal RIP interneurons (Ward et al., 1975; Albertson and Thomson, 1976). Ablation of the I1 neurons does not affect pumping rate in the presence of food but does cause a decrease in pumping rate in the absence of food, suggesting a role for the I1 neurons in maintaining basal pumping (David Raizen, personal communication). The I1 neurons are also required for the decrease in pumping rate in response to ultraviolet light (Bhatla et al., 2015). Ablation of the paired M2 motor neurons causes a slight but statistically significant decrease in pumping rate (Raizen et al., 1995), but nothing else is known about their function.

Among the nine classes of non-cholinergic pharyngeal neurons, four are glutamatergic: I2, M3, I5, and MI. Ablation of the paired M3 motor neurons increases pump duration, suggesting that the M3 neurons promote muscle relaxation (Avery, 1993a). The I5 interneuron likely inhibits the M3 neurons, as I5 ablation causes an M3-dependent decrease in pump duration (Avery, 1993a). The paired I2 neurons are required for pumping inhibition in response to ultraviolet light and act in parallel with the I1 neurons (Bhatla and Horvitz, 2015; Bhatla et al., 2015). Nothing is known about the function of the MI neuron. The paired serotonergic NSM neurons humorally regulate locomotion in response to the presence of food (Sawin et al., 2000; Ranganathan et al., 2001; Harris et al., 2010; 2011; Cunningham et al., 2012; Gürel et al., 2012; Flavell et al., 2013), and can modulate pumping rate under some conditions (Gruninger et al., 2006; Li et al., 2012).

Essentially nothing is known about the function of the M5, I3, I4, and I6 neurons, whose neurotransmitter(s) have not been identified. Nearly all of the pharyngeal neurons express neuropeptide genes (Schinkmann and Li, 1992; Li et al., 1999; Nathoo et al., 2001; Kim and Li, 2004) and many neuropeptides affect pumping rate (Rogers et al., 2001; Papaioannou et al., 2005; 2008; Cheong et al., 2015), but it is not known when these peptides are released or the mechanisms by which they affect feeding.

Nearly all that is known about the function of the pharyngeal nervous system has come from laser ablation experiments (Avery and Horvitz, 1987; 1989; Avery, 1993a; Raizen and Avery, 1994; Raizen et al., 1995; Chiang et al., 2006; Bhatla and Horvitz, 2015; Bhatla et al., 2015). Although this approach is powerful for identifying roles of critical neurons, it is less useful for identifying neurons with redundant functions, as this would require ablating many different combinations of neurons. Further, since ablation can only cause permanent reduction of function and behavior is typically assayed multiple days after ablation, interpretation of all results of ablation experiments are clouded by the possibility of developmental compensation (Steger et al., 2005). Optogenetic approaches are sensitive to redundancy and can be used to dynamically and bidirectionally manipulate neural activity, and have been used to study the function of neural circuits in *C. elegans* at single neuron resolution (Fang-Yen et al., 2015). However, these approaches have not yet been applied to the pharyngeal nervous system.

Many genes regulating the pharyngeal action potential have been identified

The pharyngeal muscle action potential consists primarily of five different currents (Shtonda and Avery, 2005) (Table 2). The action potential is typically initiated by the opening of the nicotinic ACh receptor (nAChR) containing the non-α EAT-2 subunit (Raizen et al., 1995; McKay et al., 2004). This receptor appears to function post-synaptically to the MC neurons, as *eat-2* mutants are pale and thin like MC-ablated animals (Avery and Horvitz, 1989; Avery, 1993b; Raizen et al., 1995) and EAT-2 is expressed in pharyngeal muscle postsynaptic to the MC neurons (McKay et al., 2004). EAT-2 interacts with EAT-18, a novel single-pass transmembrane protein of unknown function that appears to be required for proper localization of all pharyngeal nicotinic receptors (Raizen et al., 1995; McKay et al., 2004).

Electrical recordings of the pharyngeal muscle, electropharyngeograms (EPGs), reveal that during pumping at rates similar to those seen in the presence of food, small depolarizations precede each action potential (Raizen et al., 1995). These small depolarizations require both the EAT-2 subunit and the MC neurons and are absent during pumping at rates similar to those seen in the absence of food or after MC ablation, further evidence that the MC neurons promote rapid pumping by depolarizing the muscle via the EAT-2-containing receptor (Raizen et al., 1995). The activity patterns of the MC neurons have not yet been determined, so it is not clear if these depolarizations represent post-synaptic potentials generated by discrete excitation of the muscle by action potentials fired by the MC neurons, or if they represent opening of the EAT-2-containing receptor that is not triggered by rhythmic activity of the MC neurons.

The depolarization produced by opening the EAT-2-containing receptors activates the low-threshold T-type Ca^{2+} channel that contains the α_1 subunit CCA-1 (Shtonda and Avery, 2005; Steger et al., 2005), which further depolarizes the muscle until it reaches the activation threshold for the L-type Ca^{2+} channel that contains the α_1 subunit EGL-19 (Shtonda and Avery, 2005). EGL-19 inactivates slowly, creating a depolarization that lasts ~200 ms, similar to the long action potentials of the vertebrate heart (Lee et al., 1997). When the EAT-2 nAChR subunit is mutated, the resting membrane potential spontaneously depolarizes and action potentials arise spontaneously when the membrane potential reaches the CCA-1 threshold, suggesting that pharyngeal excitability can be homeostatically regulated (Steger et al., 2005).

The glutamatergic M3 neurons modulate the timing of muscle relaxation by firing a series of action potentials that activate the glutamate-gated Cl^- channel AVR-15 during muscle contraction (Avery, 1993a; Raizen and Avery, 1994; Dent et al., 1997; Li et al., 1997; Lee et al., 1999a). The M3 neurons have putative sensory endings adjacent to the pharyngeal muscle, suggesting their firing may be triggered directly by muscle contraction (Raizen and Avery, 1994). Along with inactivation of the L-type Ca^{2+} channel EGL-19, M3 activity promotes the activation of the hyperpolarization-activated K^+ channel EXP-2 (Davis et al., 1999; Fleischhauer et al., 2000; Espinosa et al., 2001; Shtonda and Avery, 2005). Although EXP-2 is molecularly similar to the Kv family of K^+ channels, its functional properties are more akin to those of the human HERG channel: it activates slowly but inactivates rapidly (Davis et al., 1999; Fleischhauer et al., 2000). A current with the same properties as the EXP-2 current was first identified in the pharyngeal muscle of the nematode *Ascaris lumbricoides*, where it was termed the

"negative spike current" (Byerly and Masuda, 1979) due to its similarity to the voltage gated Na^+ channel (Campbell and Hille, 1976), but with inverse voltage dependence. Resting membrane potential in the pharyngeal muscle is regulated by the Na^+/K^+ ATPase EAT-6 (Davis et al., 1995), in addition to other unidentified channels (Franks et al., 2002; Vinogradova et al., 2006).

ACh can also regulate pumping through the muscarinic ACh receptor GAR-3, which acts upstream of Gαq signaling (Brundage et al., 1996; Robatzek and Thomas, 2000; Steger and Avery, 2004). Loss of GAR-3 decreases pump duration, suggesting GAR-3 signaling is involved in muscle contraction (Steger and Avery, 2004). The identity of the neuron releasing the ACh that activates GAR-3 is unknown.

Feeding is inhibited during two conserved *C. elegans* sleep states

Feeding persists throughout the life of the worm, ceasing only during sleep (Raizen et al., 2008; Hill et al., 2014). In mammals, sleep states are identified by changes in brain-wide activity patterns recorded by electroencephalography (EEG). However, since *C. elegans* is not amenable to *in vivo* electrophysiology, its sleep states are identified by reversible cessation of feeding and locomotion, increased threshold for arousal, and homeostatic response to deprivation, behavioral characteristics of sleep conserved across species (Campbell and Tobler, 1984; Allada and Siegel, 2008; Cirelli and Tononi, 2008; Siegel, 2008; Zimmerman et al., 2008). By these criteria, *C. elegans* has two sleep states: developmentally-timed sleep (DTS or lethargus) occurs during larval transitions immediately preceding each of the four molts (Cassada and Russell, 1975; Singh and

Sulston, 1978; Raizen et al., 2008), whereas stress-induced sleep (SIS) can occur at any developmental stage in response to cellular stressors (Jones and Candido, 1999; Hill et al., 2014). These states are behaviorally indistinguishable.

Many pathways that regulate sleep in the fruit fly *Drosophila melanogaster*, a well-established invertebrate sleep model (Cirelli, 2009), also have a role in DTS or SIS. EGF (Van Buskirk and Sternberg, 2007; Hill et al., 2014) and FMRFamide (Nelson et al., 2014) signaling pathways, which regulate *Drosophila* sleep (Foltenyi et al., 2007; Lenz et al., 2015), have been implicated in SIS regulation. DTS is coupled to a larval timing mechanism that involves the *C. elegans* homolog of the PERIOD gene (Jeon et al., 1999; Monsalve et al., 2011), a core member of the circadian clock in *Drosophila* (Konopka and Benzer, 1971). Many other regulatory signaling pathways are conserved between DTS and *Drosophila* sleep, including PDF signaling (Parisky et al., 2008; Choi et al., 2013), PKA signaling (Hendricks et al., 2001; Belfer et al., 2013; Iwanir et al., 2013; Nagy et al., 2013; Nelson et al., 2013), neuropeptide Y signaling (Choi et al., 2013; He et al., 2013; Shang et al., 2013), Gαo signaling (Raizen et al., 2008; Guo et al., 2011; Schwarz and Bringmann, 2013), Notch signaling (Seugnet et al., 2011; Singh et al., 2011), insulin signaling (Driver et al., 2013; Cong et al., 2015), PKG signaling (Raizen et al., 2008; Donlea et al., 2012), glutamate signaling (Choi et al., 2015; Tomita et al., 2015), and more (Singh et al., 2014).

There is also evidence that DTS and SIS may serve functions similar to the putative functions of mammalian sleep. DTS has been implicated in synaptic plasticity (Dabbish and Raizen, 2011) and synthetic metabolism (Frand et al., 2005; Driver et al., 2013) and

SIS is important for recovery following exposure to cellular stressors (Hill et al., 2014), while mammalian sleep is associated with changes in synaptic plasticity (Tononi and Cirelli, 2014), anabolic metabolism (Mackiewicz et al., 2007), and stress response (Toth and Krueger, 1988; Rampin et al., 1991). State-dependent neural processing, a well-established feature of mammalian sleep (Livingstone and Hubel, 1981), has also been demonstrated during *C. elegans* sleep (Choi et al., 2013; Cho and Sternberg, 2014; Choi et al., 2015). Although there are likely important differences between sleep regulation in worms and mammals, such as the lack of ~24-hour regulation of *C. elegans* sleep, the many conserved aspects of *C. elegans* sleep suggest that insights gained from *C. elegans* may be applicable to sleep in higher organisms.

DTS and SIS require different interneurons

Three classes of peptidergic neurons have been implicated in DTS and SIS regulation: the GABAergic RIS interneuron and the paired glutamatergic RIA interneurons are required for quiescence during DTS (Nelson et al., 2013; Turek et al., 2013), while the ALA neuron is required for quiescence during SIS (Van Buskirk and Sternberg, 2007; Hill et al., 2014) (Table 3). The RIS interneuron is active during DTS and required for locomotion quiescence during this state. Activation of RIS inhibits locomotion, an effect that requires neuropeptide processing but not GABA synthesis, suggesting that RIS releases an unidentified somnogenic neuropeptide (Turek et al., 2013). The RIA interneurons also release a neuropeptide, NLP-22, which inhibits both feeding and locomotion during DTS (Nelson et al., 2013; Serrano-Saiz et al., 2013). During SIS, the

ALA interneuron, releases the seven neuropeptides encoded by the gene *flp-13* (Table 4) in response to EGF signaling (Van Buskirk and Sternberg, 2007; Hill et al., 2014; Nelson et al., 2014). The FLP-13 neuropeptides are not required for quiescence during DTS (Nelson et al., 2014), suggesting that the mechanisms that underlie the cessation of feeding and locomotion in these two behaviorally indistinguishable states may be distinct. However, sensory neuron Ca^{2+} levels are decreased during DTS as well as after overexpression of the EGF ligand LIN-3 (mimicking SIS) (Cho and Sternberg, 2014), indicating that the physiology immediately proximal to the increased arousal threshold is similar between these two states. Therefore, it is unclear if the NLP-22 and FLP-13 neuropeptides act via the same or different neural and molecular pathways to inhibit feeding and locomotion during DTS and SIS.

Objective

The goal of this thesis was to use optogenetics, pharmacology, and genetics to understand the neural and genetic mechanisms that underlie *C. elegans* feeding behavior during wake and sleep. In Chapter 2, I will describe experiments I performed to understand how cholinergic neurons regulate feeding. In Chapter 3, I investigate how the neural circuit that regulates feeding is altered when feeding is inhibited during two sleep states. I will discuss my conclusions and future directions in Chapter 4. The Appendix contains a detailed protocol for optogenetically manipulating individual neurons.

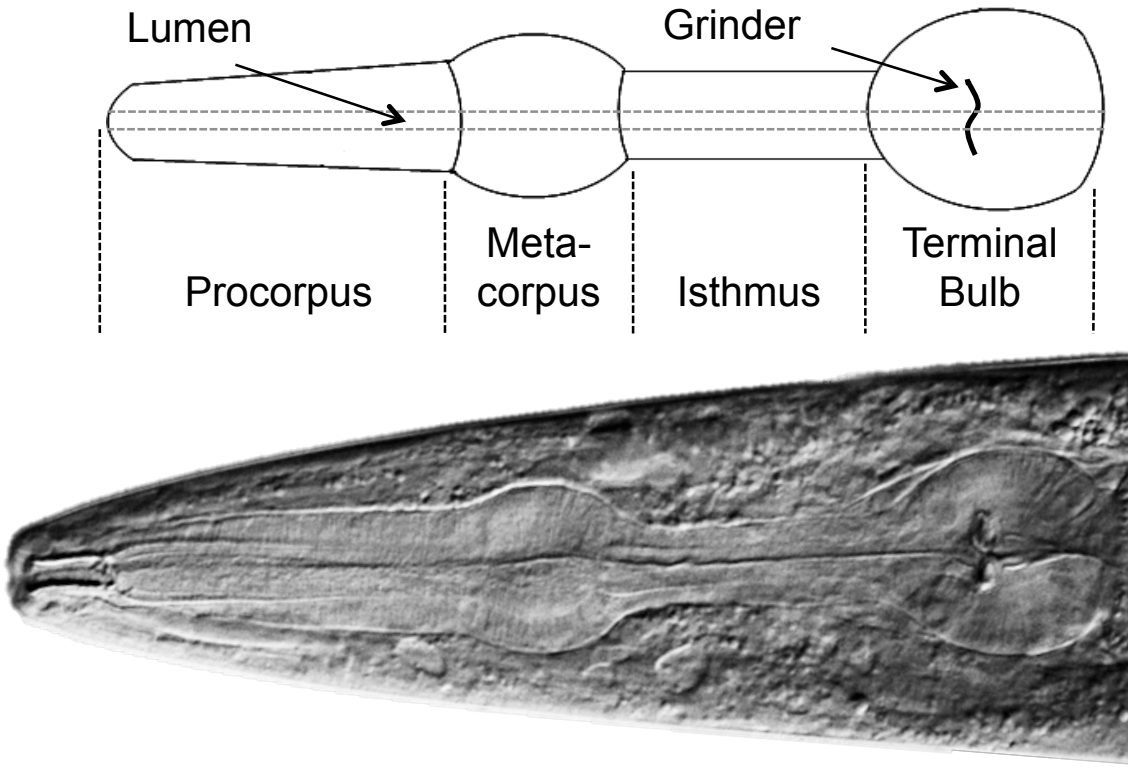

Figure 1.1: Lateral view of the pharynx. The procorpus and metacorpus draw bacterial food into the lumen, where it is transported to the terminal bulb by the isthmus. The cuticular grinder plates crush the bacteria before it is transported to the intestine. Micrograph reproduced from wormatlas.com.

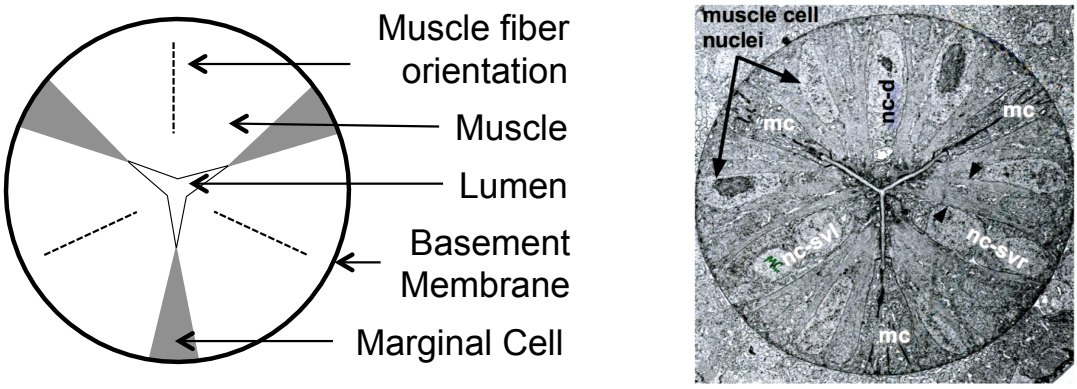

Figure 1.2: Cross section of the pharynx. The muscles of the tri-radially symmetric pharynx are oriented with their fibers perpendicular to the lumen. Marginal cells provide structural support, and the entire organ is surrounded by a thick basement membrane. Neuronal processes run adjacent or through the muscle cells. Electron micrograph reproduced from wormatlas.com.

Table 1.1: *C. elegans* pharyngeal neurons

Cell	#	NT	NP	Function
NSM	2	5-HT	Y	Humorally regulates locomotion rate in response to food
M1	1	ACh		Promotes spitting in response to UV light
M2	2	ACh	Y	Ablation causes slight decrease in feeding rate
M3	2	Glutamate	Y	Promotes relaxation via the AVR-15 receptor
M4	1	ACh	Y	Required for peristalsis
M5	1		Y	
MC	2	ACh	Y	Promotes rapid pumping via the EAT-2 receptor
MI	1	Glutamate	Y	
I1	2	ACh	Y	Inhibits pumping in response to UV light
I2	2	Glutamate	Y	Inhibits pumping in response to UV light
I3	1		Y	
I4	1		Y	
I5	1	Glutamate	Y	Inhibits M3
I6	1		Y	

ACh: Acetylcholine; NT: Neurotransmitter; NP: Neuropeptide genes

Table 1.2: Genes expressed in pharyngeal muscle that affect pumping

Name	Function	Role in pharyngeal pumping
EAT-2	Nicotinic ACh receptor non-α subunit	Initiates action potential, depolarizes the membrane to CCA-1 threshold
EAT-18	Novel single-pass transmembrane protein	Required for proper localization of all the pharyngeal nicotinic receptors
CCA-1	T-type Ca^{2+} channel a_1 subunit	Promotes depolarization to the EGL-19 threshold
EGL-19	L-type Ca^{2+} channel a_1 subunit	Necessary for the plateau phase of the action potential
AVR-15	Glutamate-gated Cl^- channel	Modulates muscle repolarization timing in response to M3 activity
EXP-2	Kv type K^+ channel	Negative spike channel, required for rapid muscle repolarization
EAT-6	Na^+/K^+ ATPase	Controls resting membrane potential
GAR-3	Muscarinic ACh receptor	Promotes muscle contraction

Table 1.3: Neurons implicated in the regulation of *C. elegans* sleep

Cell	#	NT	NP	Function
RIS	1	GABA	Y	Neuropeptide release required for DTS quiescence
RIA	2	Glutamate	Y	Secrete NLP-22 neuropeptide during DTS
ALA	1		Y	Secretes FLP-13 neuropeptides during SIS

NT: Neurotransmitter; NP: Neuropeptide genes

Table 1.4: *C. elegans* sleep-associated neuropeptides

Neuropeptide	Sequence
FLP-13-1	AMDSPLIRFamide
FLP-13-2	AADGAPLIRFamide
FLP-13-3	APEASPFIRFamide
FLP-13-4	ASPSAPLIRFamide
FLP-13-5	SPSAVPLIRFamide
FLP-13-6	ASSAPLIRFamide
FLP-13-7	SAAAPLIRFamide
NLP-22	SIAGRAGFRPamide

CHAPTER 2: Neural and genetic degeneracy underlies *Caenorhabditis elegans* feeding behavior

Nicholas F Trojanowski[1, 2, 3], Olivia Padovan-Merhar[2, 3], David M. Raizen[1], Christopher Fang-Yen[2, 3]

(1) Department of Neurology, Perelman School of Medicine

(2) Department of Bioengineering, School of Engineering and Applied Science

(3) Department of Neuroscience, Perelman School of Medicine

University of Pennsylvania, Philadelphia, PA 19104

This chapter is a slightly modified version of a paper published in the Journal of Neurophysiology.

Olivia Padovan-Merhar assisted with the initial MATLAB programming.

David Raizen and Christopher Fang-Yen assisted with planning experiments, interpreting data, and revising the paper.

All of the data presented in this chapter are my own.

Abstract

Degenerate networks, in which different elements can perform the same function or yield the same output, are ubiquitous in biology. Degeneracy contributes to the robustness and adaptability of networks in varied environmental and evolutionary contexts. However, how degenerate neural networks regulate behavior *in vivo* is poorly understood, especially at the genetic level. Here, I identify degenerate neural and genetic mechanisms that underlie excitation of the pharynx (feeding organ) in the nematode *C. elegans* using cell-specific optogenetic excitation and inhibition. I show that the pharyngeal neurons MC, M2, M4, and I1 form multiple direct and indirect excitatory pathways in a robust network for control of pharyngeal pumping. I1 excites pumping via MC and M2 but not M4. I identify nicotinic and muscarinic receptors through which the pharyngeal network regulates feeding rate. These results identify two different mechanisms by which degeneracy is manifest in a neural circuit *in vivo*.

Introduction

All living systems possess mechanisms for maintaining their function in varied internal and external environments. One mechanism which generates this adaptability is degeneracy, the ability of distinct elements to perform the same function or yield the same output under specific conditions (Tononi et al., 1999). Degeneracy is a ubiquitous property of biological systems at all levels of organization (Edelman and Gally, 2001), and supports robustness and adaptability by providing the capability to produce a variety of actions, both overlapping and unique, depending on context (Tononi et al., 1999). The degeneracy of a system has been proposed to correlate with its complexity (Tononi et al., 1999; Edelman and Gally, 2001). However, studies in the crustacean stomatogastric ganglion have demonstrated that even small neural circuits can be highly degenerate; similar functional network performance can be achieved with many different network parameters but using the same structural elements (Prinz et al., 2004; Saideman et al., 2007; Grashow et al., 2010; Marder and Taylor, 2011; Gutierrez et al., 2013; Rodriguez et al., 2013). However, the mechanisms by which different network activity patterns generate similar behaviors *in vivo* are poorly understood.

Here I investigate degeneracy in the pharyngeal nervous system of the nematode *C. elegans.* The worm feeds on bacteria via rhythmic contractions and relaxations of the pharynx, which trap the bacteria, crush it, and transport it to the intestine (Doncaster, 1962) (Fig 1A,B). The pharynx has two stereotyped behaviors: (1) pumping, which is a rhythmic contraction and relaxation of the corpus, anterior isthmus, and terminal bulb, and (2) isthmus peristalsis, which normally occurs after one out of every three to four

pumps, and transports food particles from the anterior isthmus to the terminal bulb and intestine.

The pharynx is innervated by a well-mapped and highly interconnected pharyngeal nervous system containing 20 identified neurons of 14 types and fewer than 60 unique chemical and electric synapses (Albertson and Thomson, 1976), though the pathways of non-synaptic transmission are poorly understood. The pharyngeal nervous system is synaptically connected to the 282-neuron somatic nervous system by a single pair of gap junctions (Albertson and Thomson, 1976).

Pharyngeal pumping requires the neurotransmitter acetylcholine (Avery and Horvitz, 1990; Alfonso et al., 1993), which is synthesized by 5 pharyngeal neuron types (Fig. 1A,C). By using laser ablation to kill individual neuron classes, Avery and colleagues identified the paired cholinergic MC cells as the only neurons required for rapid feeding (Avery and Horvitz, 1989; Raizen et al., 1995). However, ablation of other cholinergic pharyngeal motor neurons, such as M2 and M4, only slightly decreases feeding rate (Avery and Horvitz, 1989; Raizen et al., 1995), demonstrating that the network that regulates feeding rate is robust to the absence of some neurons. In fact, feeding continues even after ablation of all pharyngeal neurons, albeit in a slow and uncoordinated manner (Avery and Horvitz, 1989).

Work with other nematode species suggests that the pharyngeal nervous system is highly evolutionarily adaptable and more functionally complex than the *C. elegans* ablation results alone indicate. The structural connectivity of the pharyngeal nervous system of the nematode *Pristionchus pacificus* has recently been shown to be very similar to that of *C.*

elegans (Bumbarger et al., 2013). Although *C. elegans* and *P. pacificus* diverged approximately 300 million years ago (Pires-daSilva and Sommer, 2004; Dieterich et al., 2008) and have different feeding strategies, there is near-perfect homology of pharyngeal neurons between these species (Bumbarger et al., 2013). Strikingly, the morphologies of the neuronal processes are nearly identical, and a remarkable number of connections are conserved (Bumbarger et al., 2013). As in *C. elegans*, M4 ablation in *P. pacificus* causes a mild decrease in feeding rate (Chiang et al., 2006). M2 ablation in the nematode *Panagrolaimus sp.* PS1159 also causes a mild decrease in feeding rate (Chiang et al., 2006). Pharyngeal neuron homology has also been observed in nematode species with very diverse pharyngeal functions (Zhang and Baldwin, 2000; Ragsdale et al., 2010). This evolutionary adaptability and robustness suggests that the nematode pharyngeal nervous system is highly degenerate, but this hypothesis has not been directly tested.

Testing for degeneracy and functional complexity requires identification of distinct neural elements or networks capable of producing identical outputs. In laser ablation experiments, neurons are killed in young larvae and behavior is observed in adult worms (Avery and Horvitz, 1987; 1989; Avery, 1993a; Raizen et al., 1995). This approach causes irreversible elimination of neuron function, is potentially confounded by redundancy and compensatory changes during development, and may fail to uncover effects on adult feeding behavior due to early larval lethality (Avery and Horvitz, 1987). Optogenetic tools, which permit temporally precise manipulation of neural activity, can overcome limitations of laser ablation and directly identify roles of individual neurons in generating or regulating behavior (Zhang et al., 2007a). Functional dissection of neural circuits using optogenetics requires either cell-specific opsin expression (Schmitt et al.,

2012) or selective illumination of the neuron of interest after broad opsin expression (Guo et al., 2009; Leifer et al., 2011; Stirman et al., 2011; Kocabas et al., 2012).

To determine the roles of cholinergic pharyngeal neurons in pumping regulation and the pathways through which they act, I developed a technique for optogenetic manipulation of single neuron activity *in vivo*. Because pharyngeal behavior is completely internal to the animal, immobilizing the worms affords increased spatial resolution such that it is possible to simultaneously optogenetically manipulate individual pharyngeal neurons and record behavior. I confirm the endogenous excitatory role of MC and identify endogenous degenerate excitatory roles for M2, M4, and I1 in a robust network that regulates feeding rate. I identify the neurons that act post-synaptically to I1, and I illuminate degeneracy at the genetic level by identifying two molecular mechanisms that mediate the stimulatory role of MC.

Materials and Methods

Worm strains

ZM3265 *lin-15(n765ts) X; zxIs6[Punc-17::ChR2(H134R)::YFP; lin-15(+)] V*, **ZX499** *lin-15(n765ts) X; zxIs5[Punc-17::ChR2(H134R)::YFP; lin-15(+)] X*, and **ZX830** *lite-1(ce314) X; zxEx620[Punc-17::Mac::YFP; Pelt-2::mCherry]* were gifts from A. Gottschalk (Liewald et al., 2008; Husson et al., 2012). After verification of expression in cholinergic pharyngeal neurons, I crossed ZM3265 into **LX929** *vsIs48[Punc-17::GFP] X*, which has bright cytoplasmic GFP fluorescence in cholinergic neurons, to create **YX11** *lin-15(n765ts) X; zxIs6[Punc-17::ChR2(H134R)::YFP; lin-15(+)] V; vsIs48[Punc-17::GFP] X*. I then crossed YX11 into **DA1113** *eat-2*(*ad1113) II* (Avery, 1993b), **DA1110** *eat-18*(*ad1110) I* (Raizen et al., 1995), and **CB933** *unc-17(e245) IV* (Brenner, 1974)to create **YX46** *eat-2(ad1113) II; vsIs48[unc-17::GFP] X; zxIs6[Punc-17::ChR2(H134R)::YFP; lin-15(+)] V,* **YX47** *eat-18(ad1110) I; vsIs48[Punc-17::GFP] X; zxIs6[Punc-17::ChR2(H134R)::YFP; lin-15(+)]*, and **YX48** *unc-17(e245) IV; vsIs48[Punc-17::GFP] X; zxIs6[Punc-17::ChR2(H134R)::YFP; lin-15(+)]*, respectively. Since *gar-3* and *zxIs6* are both located on chromosome V, I had difficulty obtaining *gar-3; zxIs6* cross progeny and adopted a different approach for experiments involving *gar-3*. I crossed **VC657** *gar-3(gk305))* (Liu et al., 2007) with DA1110 and with ZX499 to form **YX66** *eat-18(ad1110) I; gar-3(gk305) V* and **YX68** *gar-3(gk305) V; zxIs5[Punc-17::ChR2(H134R)::YFP; lin-15(+)] X*, respectively. I identified the presence of the *gk305* deletion mutation by PCR followed by agarose gel electrophoresis (primer sequences were TGTTCTGAGTTTTTGCATTAAA and GGACATTTTCTGTATTTCTTTTTAC. I crossed YX66 into YX68 to create **YX69** *eat-*

18(ad1110) I; gar-3(gk305) V; zxIs5[Punc-17::ChR2(H134R)::YFP; lin-15(+)] X. To rescue the *gar-3* defect, I used an Eppendorf FemtoJet microinjection system on a Leica DMIRB inverted DIC microscope to inject the fosmid *WRM0627cH05* at 10 ng/µL, in combination with 5 ng/µL *pCFJ104(myo-3::mCherry)*. I performed all experiments involving inhibition with ZX830. I grew all worms in the dark at 20°C on NGM (Brenner, 1974) plates inoculated with 250 µL of a suspension of OP50 bacteria in LB medium. Where needed, I added 2 µL of 100 mM all-*trans* retinal (ATR) in ethanol to the bacterial suspension immediately before seeding. I stored ATR-seeded plates at 4°C for up to one week before use. All optogenetics experiments were performed on first-day adult hermaphrodites.

Laser ablations

I performed MC and M2 laser ablations as described (Bargmann and Avery, 1995; Fang-Yen et al., 2012). Briefly, I immobilized L1 larvae in 15 mM sodium azide on 5% agarose pads within 4 hours after hatching. With differential interference contrast (DIC) optics on a Leica DM5500B upright microscope equipped with a 100x Plan Apo oil-immersion objective lens with N.A.=1.4, I identified and ablated neurons with 60-80 pulses from a Photonics Micropoint laser. All ablations were confirmed via observation of DIC and/or fluorescence 2-3 days after the operation. All animals with collateral damage were discarded. Controls for laser ablation experiments were subject to the same immobilization protocols as operated animals but the laser was not fired.

Optogenetic stimulation of individual neurons

I mounted worms on 10% agarose pads containing 10 mM serotonin (5-HT) and immobilized them using 1.5 μL of a 2.5% (v/v) suspension of 50 nm diameter polystyrene beads (Kim et al., 2013). I included 5 mM atropine in the agarose pad where indicated; I reduced the 5-HT concentration to 5 mM for these atropine experiments to compensate for the increased ionic concentration. This atropine concentration is half that previously used to study the roles of muscarinic receptors in *C. elegans* feeding behavior (You et al., 2006). The *C. elegans* cuticle and intestinal lining generally limit drug uptake, and it is not unusual for polar drugs to be applied at concentrations 1000-fold higher than their predicted target affinities (Holden-Dye and Walker, 2007).

For each worm, I first illuminated the entire head with blue light for <1s in order to image the fluorescent cholinergic neurons. Next, I subjected each relevant neuron type to a stimulus protocol consisting of 10 cycles of 5 second illumination and 5 second darkness. The stimulus area was determined by outlining a region slightly larger than the neural cell body – about 2-3 μm in diameter – to allow constant stimulation as the neural cell bodies move during the pump. *unc-17* mutants did not immobilize well, likely due to their coiling behavior, so for these worms I used a larger spot of illumination, often covering the entire metacorpus. I performed experiments within 90 minutes of worm immobilization, and performed each experiment on 7-10 animals unless otherwise indicated. This sample size was selected based on pilot data. For additional description of the approach, see the results section.

Microscopy and imaging

I used a setup similar to that described previously (Leifer et al., 2011) (Fig. 1E). I performed optogenetic experiments on a Leica DMI3000B microscope with a Leica Plan Apo 63X oil immersion objective lens with N.A.= 1.4. To optogenetically stimulate individual neurons, I expanded a 473 nm laser beam (SLOC Lasers) using a telescope composed of two planoconvex lenses and projected it onto a 1024 by 768 pixel digital micromirror device (DMD) (Discovery 4100 DLP, Texas Instruments/Digital Light Innovations). I aligned the DMD such that when the DMD was in the 'on' state, the reflected beam was aligned with the optical axis of the microscope objective after entering the microscope through a right side auxiliary port. The light from the DMD was projected onto the back of the objective using an optical system composed of 3 lenses and a dichroic mirror. I mounted the dichroic mirror, which reflects 473 nm light while allowing transmission of wavelengths greater than 500 nm, on a custom filter cube in the microscope filter turret. The irradiance of the laser at the objective was approximately 37 mW/mm^2, well above the saturation irradiance of ChR2 (Grossman et al., 2011). To image behavior, I placed a red filter in the transillumination light path. I used an image splitter (Photometrics DV2) to simultaneously record fluorescence and bright-field images. I acquired images at a rate of 32.7 frames per second on a cooled CCD camera (Andor iXon 885). I analyzed the images using custom MATLAB scripts, as well as the freely available package PIVlab, a Time-Resolved Digital Particle Image Velocimetry Tool for MATLAB.

Software and analysis

I used Andor SOLIS software to acquire images. I controlled the DMD using the Discovery 4100 software; DMD scripts were created in MATLAB using custom scripts. After data acquisition, I used MATLAB to identify times when the stimulation was switched between off and on states and to determine pumping rate and other parameters. MATLAB scripts are available upon request. Student's *t*-test was used for all statistical comparisons unless otherwise noted, and each bar represents mean +/- SEM. Sample sizes are given in the figure captions.

Measurement of ChR2 expression

ChR2 expression was approximated by calculating the average fluorescence pixel values of a region surrounding the cell body of each pharyngeal neuron that expressed *zxIs6[Punc-17::ChR2(H134R)::YFP; lin-15(+)] V*).

Results

Optogenetic manipulation of specific pharyngeal neurons in intact, behaving animals

I used a digital micromirror device (DMD) and laser with 473 nm wavelength to illuminate individual neurons (Guo et al., 2009; Leifer et al., 2011) in worms expressing specific opsins in all cholinergic neurons. To excite neurons, I used a YFP-tagged blue light-sensitive Channelrhodopsin-2 (ChR2) (Nagel et al., 2003; 2005). To inhibit neurons, I used a YFP-tagged blue light-powered proton pump (Mac) from *Leptosphaeria maculans* (Waschuk et al., 2005; Chow et al., 2010; Husson et al., 2012). In some experiments, I co-expressed cytoplasmic GFP along with YFP-ChR2 in order to more easily visualize the neurons. I physically immobilized the animals against agarose pads using polystyrene nanoparticles (Kim et al., 2013). This immobilization causes a cessation of pumping, so I added 10 mM serotonin (5-HT) to the agarose pads to induce a submaximal basal pumping rate; a nonzero but submaximal pumping rate allowed me to measure inhibitory as well as excitatory effects. To locate each cholinergic pharyngeal neuron, I first acquired a full-field fluorescence image of the worm's head (Fig. 1C). I then specified a region for illumination based on the fluorescence image, and used the DMD to illuminate the specified region (Fig. 1D). To image behavior and fluorescence simultaneously on the same camera while avoiding non-specific opsin activation, I performed the experiments with a red glass filter in the transillumination light path (Fig. 1E). I imaged the worms through a DualView2 image splitter with RFP and GFP filters: the RFP channel captured DIC images and the GFP channel captured fluorescence, which

allowed me to both ensure proper targeting of each neuron and to correlate behavior with neuron stimulation.

Machine vision quantification of pharyngeal behavior during optogenetic stimulation

I used a particle image velocimetry (PIV) algorithm in MATLAB to track the velocity of a region of the anterior terminal bulb to quantify pumping rate (red box in Fig. 1B). The velocity was found to be biphasic in shape (Fig. 1F). Each positive spike in velocity represented movement of the grinder toward the posterior, and each negative spike represented its return to the resting position. For each experiment I set a velocity threshold, the crossing of which signified a single pump. This threshold was set to approximately half of the maximum velocity. I wrote MATLAB scripts to calculate the average pump rate during stimulus intervals (blue bars in Fig. 1F and 1G), which were determined post-hoc by automated detection of changes in fluorescence occurring when a GFP and/or YFP-expressing neuron is illuminated. My system for automated detection of pharyngeal pumps was in excellent agreement with results from a manual counting of pumps based on slow-motion review of videos, with 99.3% sensitivity and 99.5% specificity.

The MC motor neurons are excitatory for pharyngeal pumping

The paired MC neurons have cell bodies in the metacorpus, putative sensory endings in the pharyngeal lumen near the posterior end of the procorpus, and form synapses with

pharyngeal muscles in the posterior metacorpus and anterior isthmus (Fig 1A, C) (Albertson and Thomson, 1976). Because laser ablation of the MC neurons in young larvae causes an 83% decrease in pump rate in adult animals (Raizen et al., 1995), I hypothesized that optogenetic stimulation of the MCs would increase pump rate. Indeed, I found that optogenetic excitation of the MC neurons stimulated pumping (Fig. 2A). MC illumination did not excite pumping in the absence of the essential ChR2 cofactor all-*trans* retinal (ATR) (Fig. 2A), indicating that the increased pump rate during MC illumination was due to activation of ChR2.

Processes of other cholinergic neurons pass close to the MC cell bodies (Fig. 1A, C) (Albertson and Thomson, 1976), raising the possibility that the optogenetic illumination was stimulating pumping via non-targeted neurons. To test this possibility, I performed larval ablation of the MC neurons and tested whether stimulation of the region corresponding to the usual location of the MC cell bodies results in an increased pumping rate. I found no increase in pump rate (Fig. 2A), indicating that off-target effects of this optogenetic stimulation are negligible.

Serial section electron microscopic analysis of the pharyngeal nervous system has shown that the MC neurons make no chemical synapses onto other neurons and possess gap junction connections only with the paired M2 neurons (Albertson and Thomson, 1976). To determine whether the behavioral effect of optogenetic stimulation of MC occurs wholly via effects on M2, I performed optogenetic excitation of the MCs in animals in which the M2 neurons were laser-ablated. Stimulation of the MCs still excited pumping after the ablation of the M2 neurons (Fig. 2A), demonstrating that the MCs can directly stimulate pumping.

The M2 motor neurons are excitatory for pharyngeal pumping

Anatomical data suggest that the paired M2 neurons make chemical synapses only onto pharyngeal muscles in the isthmus and metacorpus (Fig 1A, C) (Albertson and Thomson, 1976). However, ablation of the M2 neurons in young larvae results in only a 16% decrease in pump rate in adults (Raizen et al., 1995), suggesting a minor role for the M2s in pumping regulation. To my surprise, I found that optogenetic stimulation of the M2s increased pump rate to a similar level as that observed during MC stimulation (Fig. 2B). As with the MCs, this effect was ATR-dependent (Fig. 2B) and did not occur when the same region was stimulated after M2 ablation (Fig. 2B), demonstrating that specific activation of the M2s excites pumping. Furthermore, M2 excitation stimulated pumping in the absence of the MC neurons (Fig. 2B), demonstrating that the M2s, like the MCs, can stimulate pumping directly.

The M4 motor neuron is excitatory for pharyngeal pumping and isthmus peristalsis

The M4 neuron synapses only on the pharyngeal muscles in the isthmus and terminal bulb (Fig 1A, C) (Albertson and Thomson, 1976) and is the only neuron required for isthmus peristalsis (Avery and Horvitz, 1987; 1989). Laser-ablation experiments have shown a 28% reduction in pump rate in adult animals after M4 ablation in young larvae (Raizen et al., 1995). However, interpretation of this experiment is confounded by the peristalsis defect seen after M4 ablation: defective peristalsis causes both starvation, which itself causes a reduction in pump rate (Avery and Horvitz, 1990), and distention of

the corpus by bacteria, which may affect pharyngeal behavior via abnormal activation of mechanosensory endings (Avery and Horvitz, 1987; Raizen et al., 1995). My optogenetic approach allowed me to directly test whether M4 could stimulate pumping rate in well-fed animals with normal peristalsis. I found that optogenetic excitation of the M4 neuron caused an increase in pumping to a similar level as that observed during MC or M2 stimulation (Fig. 2C). No cholinergic pharyngeal neurons send processes behind the M4 cell body, so the effect of M4 stimulation is due to specific activation of M4. Consistent with its proposed role in regulating isthmus peristalsis, optogenetic excitation of M4 caused a greater proportion of pumps to be followed by peristalsis than during MC stimulation. During five 10-second intervals of M4 stimulation in two worms, 97% of pumps (N=179 pumps) were followed by isthmus peristalsis, whereas during stimulation of MC in the same worms only 41% (N=204 pumps) were followed by peristalsis ($p<0.0002$, Mann-Whitney *U* test). M4 excitation caused an increase in pump rate in the absence of both the MCs and the M2s (Fig. 2C), demonstrating that M4 can directly stimulate pumping.

Stimulation of the M1 motor neuron does not excite pumping

The M1 neuron sends a process from the terminal bulb to the anterior end of the corpus, where it forms synapses on the anterior pharyngeal muscles (Fig 1A, C) (Albertson and Thomson, 1976). M1 ablation causes only an 8% reduction in pump rate (Raizen et al., 1995). In contrast to the other cholinergic pharyngeal neurons, I did not find M1 optogenetic stimulation to affect pump rate (Fig. 2D). This is unlikely to be explained by a lower level of expression of ChR2 in M1 since the average fluorescence intensity of

ChR2::YFP in M1 was similar to that measured in MC, M2, and M4 (MC: 93.8 ± 7.1; M2: 101.2 ± 11.0; M4: 91.2 ± 10.7; M1: 71.6 ± 16.7, Mean ± SEM, arbitrary units, N=6, $p>0.79$ 1-way ANOVA with Dunn's Multiple Comparison Test). These results suggest that M1 stimulation does not excite pharyngeal pumping.

The I1 interneurons excite pumping through the MCs and M2s

The paired I1 neurons form the only synaptic connections between the somatic and pharyngeal nervous systems, and are the only cholinergic pharyngeal neurons that do not synapse onto pharyngeal muscle (Albertson and Thomson, 1976). Ablation of the I1 neurons has no effect on the pump rate in the presence of food (Raizen et al., 1995). Electron microscopy data indicated that the I1s are presynaptic to six classes of neurons, including the MCs and the M2s but not M4 (Albertson and Thomson, 1976). Optogenetic stimulation of the I1 neurons increases pumping rate in an ATR-dependent manner to a level similar to that seen with MC or M2 stimulation (Fig. 3B). No cholinergic pharyngeal neurons send processes behind the I1 cell body, so the effect of I1 stimulation is due to specific activation of I1. I1 stimulation excited pumping following the ablation of either the MCs or the M2s, but not following ablation of both neuron types (Fig. 3B), demonstrating that the I1s can stimulate pumping through the MCs, through the M2s, or through both the MCs and the M2s.

The MC, M2, and M4 motor neurons stimulate pumping endogenously

My optogenetic experiments with ChR2 showed that the MC, M2, M4, and I1 neurons are capable of stimulating pumping. However, it does not necessarily follow that these neurons endogenously regulate pumping rate. To determine if these neurons stimulate pumping endogenously, I expressed the proton pump Mac in the cholinergic neurons (Husson et al., 2012) and individually inhibited these neurons using methods otherwise identical to those used with ChR2. I found that optogenetic inhibition of the MCs, the M2s, or M4 reduced pump rate, indicating that an endogenous function of these neurons is to stimulate pumping (Fig. 4A). By contrast, optogenetic inhibition of M1 had no effect on pump rate, suggesting that M1 is not required for pump rate regulation. Simultaneous inhibition of the MCs and the M2s caused a greater inhibition of pumping than inhibition of either alone, consistent with an endogenous role for the M2s in pumping rate regulation (Fig. 4A).

The I1 interneurons regulate pumping endogenously via the MCs and the M2s

As with MC, M2, and M4, I found that I1 inhibition caused a decrease in pumping (Fig. 4B). To test whether the I1s endogenously act through the MCs and the M2s to regulate pump rate, as my ChR2 experiments suggested, I simultaneously inhibited the I1s and either the MCs, the M2s, or both the MCs and the M2s. Inhibition of the I1s simultaneously with inhibition of the MCs caused a stronger reduction in pump rate than inhibition of the MCs alone, suggesting that the I1s can function independently of the MCs. Similarly, inhibition of the I1s simultaneously with inhibition of the M2s caused a stronger pump rate reduction than inhibition of the M2s alone, suggesting that the I1s can

function independently of the M2s. However, inhibition of the I1s simultaneously with inhibition of both the MCs and the M2s did not cause slower pumping than that seen with inhibition of the MCs and the M2s alone (Fig. 4B), indicating that effect of I1 inhibition on pumping rate requires the MCs and the M2s. Together with my ChR2 stimulation data, these results indicate that the I1s endogenously excite pumping via both the MCs and the M2s.

The MC neurons can stimulate pumping through a non-nicotinic mechanism

Mutations in the gene *eat*-2, which encodes a nicotinic acetylcholine receptor subunit expressed in pharyngeal muscle postsynaptic to the MCs (McKay et al., 2004), causes a reduced pump rate that mimics the phenotype observed after MC ablation (Avery, 1993b; Raizen et al., 1995). This observation suggested that the mechanism by which the MC neurons stimulate feeding is via activation of a nicotinic acetylcholine receptor containing EAT-2. Therefore, I expected that stimulation of the MCs in *eat-2* mutants would not increase pump rate. To my surprise, I found that stimulation of the MC neurons in *eat-2* mutants causes an increase in pumping, albeit less than in wild-type worms (Fig. 5 vs. Fig. 2A). Stimulation of the same region following MC ablation in wild type worms did not cause an increase in pumping (Fig. 2A), demonstrating that this effect is not due to off-target excitation of nearby processes. These results demonstrate that the MCs can stimulate pumping through an EAT-2-independent mechanism.

To test the possibility that the MCs can stimulate pumping via an alternative nicotinic ACh receptor in the absence of EAT-2, I studied animals lacking EAT-18, a single

transmembrane protein required for the pharyngeal response to bath-applied nicotine (Raizen et al., 1995; McKay et al., 2004). In *eat-18* mutants, the staining of the pharynx with alpha-bungarotoxin, which binds to nicotinic acetylcholine receptors, is also eliminated (McKay et al., 2004). As in the absence of EAT-2, optogenetic stimulation of the MCs resulted in a pumping increase in the absence of EAT-18 (Fig. 5), suggesting that the MCs can excite pumping via a non-nicotinic mechanism.

The MC neurons directly stimulate pumping via a non-nicotinic cholinergic mechanism

To further explore the nature of the EAT-2- and EAT-18-independent MC-induced pumping, I examined mutants for the gene *unc-17*, which encodes a transporter required for loading acetylcholine into vesicles prior to release (Alfonso et al., 1993). Since *unc-17* null mutations are lethal, I used the hypomorphic allele *e245*, which had a variable basal pumping rate during immobilization. Stimulation of the pharyngeal metacorpus, which includes the MC cell bodies and processes, did not increase pumping rate in *unc-17* mutants (Fig. 5), demonstrating that MC stimulation of pumping requires cholinergic neurotransmission.

The MCs may stimulate pumping via a cholinergic non-nicotinic mechanism by acting directly on pharyngeal muscle, or they may act via their electrical connections to the M2s. To distinguish between these possibilities, I tested the effect of MC stimulation in *eat-18* mutants in which I ablated the M2 neurons. MC stimulation still increased

pumping in *eat-18* mutants in the absence of the M2s, (Fig. 5), demonstrating that the MCs can activate pumping directly via a cholinergic non-nicotinic mechanism.

The MC neurons stimulate pumping in part via the muscarinic receptor GAR-3

Ionotropic cholinergic receptors insensitive to nicotine have been identified in *C. elegans* (Richmond and Jorgensen, 1999; Francis et al., 2005; Touroutine et al., 2005), suggesting the possibility that MC stimulates pumping in an *eat-18* genetic background through such a channel. Alternatively, the MCs may be acting through a muscarinic receptor. To distinguish between these possibilities, I used the muscarinic antagonist atropine (You et al., 2006). In the presence of atropine, MC stimulation failed to excite pumping in *eat-18* mutants (Fig. 5), demonstrating that in the absence of *eat-18*, the MCs stimulate pumping via an atropine-sensitive receptor and hence likely a muscarinic acetylcholine receptor.

The *C. elegans* genome contains three genes that encode for muscarinic receptors: *gar-1* (Lee et al., 1999b), *gar-2* (Lee et al., 2000), and *gar-3* (Hwang et al., 1999). Of these, only *gar-3* has been reported to be expressed in pharyngeal muscle (Steger and Avery, 2004). Loss of GAR-3 has been shown to cause decreased action potential duration in pharyngeal muscle, and excessive GAR-3 signaling can cause muscle contraction to outlast muscle depolarization (Steger and Avery, 2004), consistent with an excitatory role for GAR-3 in response to MC stimulation. I therefore tested if the MCs excite pumping via GAR-3 in an *eat-18* mutant background. MC stimulation did not excite pumping in *eat-18; gar-3* double mutants (Fig. 5), demonstrating that the MCs activate pumping in part through the muscarinic acetylcholine receptor GAR-3. A transgene containing the

gar-3 gene restored the ability of MC stimulation to excite pumping in *eat-18; gar-3* double mutants (Fig 5), confirming that the *gar-3* mutation caused the defect in the ability of the MCs to excite pumping in the absence of EAT-18.

Discussion

By optogenetically manipulating individual *C. elegans* neurons while recording feeding behavior, I have shown that the cholinergic MC, M2, and M4 motor neurons stimulate pharyngeal pumping in a degenerate manner (Fig. 6), and that the cholinergic I1 interneurons stimulate pumping via the MCs and the M2s. By analysis of mutants I identified nicotinic and muscarinic pathways through which the MCs regulate pumping rate. Taken together, these results demonstrate that this robust and evolutionarily adaptable network is degenerate at both the neural and genetic levels, and that the same behavior can be stimulated by multiple neurons and through different types of receptors.

An optogenetic approach reveals novel functions for multiple neurons

While optogenetic tools have played an important role in clarifying the functional dynamics of identified neural networks, to my knowledge they have not been previously used to identify new functional roles of circuit elements in *C. elegans* (Husson et al., 2013). In contrast to laser ablation, single neuron optogenetic manipulation allowed me to test the roles of individual neurons in regulating behavior while avoiding the possibilities of developmental compensation and ablation-induced developmental abnormalities, phenomena which would be expected to occur in degenerate networks (Marder and Taylor, 2011). For example, M4 ablation results in early larval lethality (Avery and Horvitz, 1987), which prevents accurate assessment of its effects on feeding rates in adult animals. In *eat-2* mutants, the resting membrane potential of the terminal bulb is depolarized and unstable relative to wild type worms (Steger et al., 2005). It is possible

that similar compensation occurs after ablation of pharyngeal neurons, either in the muscle or other neurons.

The candidate neuron and gene approach I demonstrate here is especially well-suited for identifying components of degenerate networks, in which ablation of individual classes of neurons may not cause obvious phenotypes. For example, although laser ablation of the M2s yields only a small reduction in pumping rate (Raizen et al., 1995), I found that M2 excitation directly stimulates rapid pumping. It is possible that other excitatory cholinergic neurons, such as the MCs and M4, replace this function of the M2s after their ablation. Likewise, while *gar-3* mutants have only subtle feeding defects (Steger and Avery, 2004), I found that the MCs can act via GAR-3 to stimulate pumping in the absence of EAT-18. Indeed, one characteristic of degenerate neural networks is that specific faults in the system, such as focused neurological lesions, often do not cause changes in outputs (Gazzaniga, 1995).

My approach is also well suited for identifying the molecular mechanisms through which individual neurons can stimulate pumping. I have identified two distinct cholinergic receptors post-synaptic to the MCs, and I expect that receptors downstream of other neurons could be identified by a similar approach of testing whether optogenetic stimulation of individual neurons can still stimulate pumping in mutants for candidate genes. For example, testing the effects of mutations in different nicotinic acetylcholine receptor subunits expressed in pharyngeal muscle on the excitatory effects of stimulating the M2s or M4 should lead to the identification of the receptors postsynaptic to these neurons.

Another advantage of my approach is its ability to individually assess the function of multiple classes of neurons in the same animal. Studies in the crustacean stomatogastric ganglion have observed significant animal-to-animal variability in the tuning of neuron conductance parameters despite similar network output (Prinz et al., 2004; Marder, 2011). Therefore, sequentially and nondestructively manipulating the activity of individual or multiple neurons in a single animal can provide a more complete picture of network function than one based on more sparse measurements in multiple animals.

Degeneracy at two levels allows robust responses to unpredictable environmental and physiological signals

My work has revealed that a circuit that tightly regulates response to various intrinsic and extrinsic cues has degeneracy at both the neural and genetic levels. Feeding rate in *C. elegans* is influenced by a multitude of factors, including mechanosensation (Chalfie et al., 1985), chemosensation (Li et al., 2012), heat stress (Jones and Candido, 1999), aging (Huang et al., 2004), mating (Gruninger et al., 2006), starvation (Avery and Horvitz, 1990), food quality (Soukas et al., 2009), feeding history (Song et al., 2013), satiety (You et al., 2008), molting (Cassada and Russell, 1975), sleep (Raizen et al., 2008), and infection (Los et al., 2013). Degeneracy at multiple levels may play a role in the ability of the pharyngeal nervous system to integrate these inputs to determine feeding rate (Greer et al., 2008; Cunningham et al., 2012; Li et al., 2012). The neural degeneracy of the system allows multiple neurons to perform similar functions in response to different modulators, while the genetic degeneracy allows neurotransmitters and neuropeptides to differentially activate subsets of neurons or muscles, or to activate different cell signaling

cascades within the same neuron or muscle. Having improved the definition of the circuit that regulates feeding rate, we are now in a better position to understand the circuit mechanisms by which intrinsic and extrinsic cues affect behavior.

Depolarization and 5-HT stimulation of the same pharyngeal neuron can cause similar or distinct behaviors

Serotonin (5-HT) is a potent modulator of many *C. elegans* behaviors, including feeding (Chase and Koelle, 2007). I found that basal pumping is almost completely abolished in immobilized worms in the absence of 5-HT, but MC, M2, M4, or I1 stimulation caused a small but variable increase in pump rate (data not shown). This is likely because when the worm is immobilized, the stimulus-response curve of the neurons is not linear, so that even a large stimulus causes only a small neural response.

The 5-HT G-protein coupled receptor SER-7 is expressed in many pharyngeal neurons including the MCs, the M2s, and M4 (Fig. 6) (Hobson et al., 2006). 5-HT stimulates pumping primarily by activating SER-7 in the MCs (Song and Avery, 2012). I suspect that the basal pumping rate I observe in the presence of 5-HT is also due to activation of SER-7 in the MCs, since MC ablation dramatically decreases the pump rate on 5-HT in my experiments (Fig. 2A). Interestingly, while activation of SER-7 in M4 causes increased peristalsis but not pumping (Song and Avery, 2012), I found that optogenetic stimulation of M4 causes an increase in both pumping and peristalsis rates. It is likely that depolarization and SER-7 activation stimulate intracellular pathways that are at least

partially distinct, which in turn evokes neurotransmitter release that may differ in location, amount, or molecular identity.

Functional conservation and evolutionary adaptability of the pharyngeal nervous system

It has been postulated that the processes of evolution and natural selection necessarily are accompanied by degeneracy (Edelman and Gally, 2001), but this is a challenging idea to test experimentally. The prevalence of evolutionarily divergent nematode species and the relative ease with which their pharyngeal nervous systems can be anatomically mapped makes them interesting models for studying the role of degeneracy in evolution. However, despite the apparent simplicity of the anatomic connectivity of the pharynx, inferring the function of the pharyngeal nervous system from the wiring diagram alone is difficult. The sign of physiological connections is often unknown and the number of synapses between two cells does not always correlate with the importance of this connection (Chalfie et al., 1985; Bargmann and Marder, 2013), and non-synaptic communication can also play important roles in regulating behavior. For example, though the M2s form 60 synapses on pharyngeal muscle and the MCs form just four (Albertson and Thomson, 1976; Avery and Thomas, 1997; McKay et al., 2004; Avery and You, 2012), I find that effects of stimulation of these two neuron types on pumping rate in immobilized animals are equivalent (Fig. 2A, B). Thus, without knowledge of the functional connectivity, it is difficult to interpret the differences between the wiring of *C. elegans* and other species, such as *Pristionchus pacificus,* in an evolutionary context (Bumbarger et al., 2013).

Laser ablation data from other nematode species may be informative. Ablation of M4 causes a reduction in isthmus peristalsis in every species in which it has been tested, including *P. pacificus*, demonstrating a conserved function (Chiang et al., 2006). The M2s synapse on the anterior pharyngeal muscle in *C. elegans* and *P. pacificus*, and ablation of the M2s in *Panagrolaimus sp.* PS1159 causes a decrease in anterior isthmus peristalsis, a behavior observed in neither *C. elegans* nor *P. pacificus* (Chiang et al., 2006). Ablation of either the MCs or M4 in *P. pacificus* and either the M2s or M4 in *Panagrolaimus sp.* PS1159 causes a decrease in pumping rate (Chiang et al., 2006), demonstrating that the networks regulating feeding are also degenerate in these species. While further experiments are necessary to draw firm conclusions, these data are consistent with evolutionary adaptability, functional conservation, and degeneracy of pharyngeal nervous system function in different species.

A circuit-level framework for feeding modulation

By identifying the pathways of cholinergic input that regulate pharyngeal pumping rate (Fig. 6), this work defines a framework within which I can investigate how feeding is integrated with other physiological processes and behaviors in response to changing environmental and internal states. The method described here can be used to further develop this circuit-level framework by identifying roles for the remaining nine classes of pharyngeal neurons, as well as the molecular mechanisms through which they interact. This method can also be combined with genetically encoded Ca^{2+} indicators to visualize intracellular Ca^{2+} dynamics during optogenetic manipulation (Husson et al., 2013). The

functional connectivity of the pharyngeal circuit forms a foundation for exploring how mutations affect the activity of a degenerate network and how the network adapts to robustly regulate behavior.

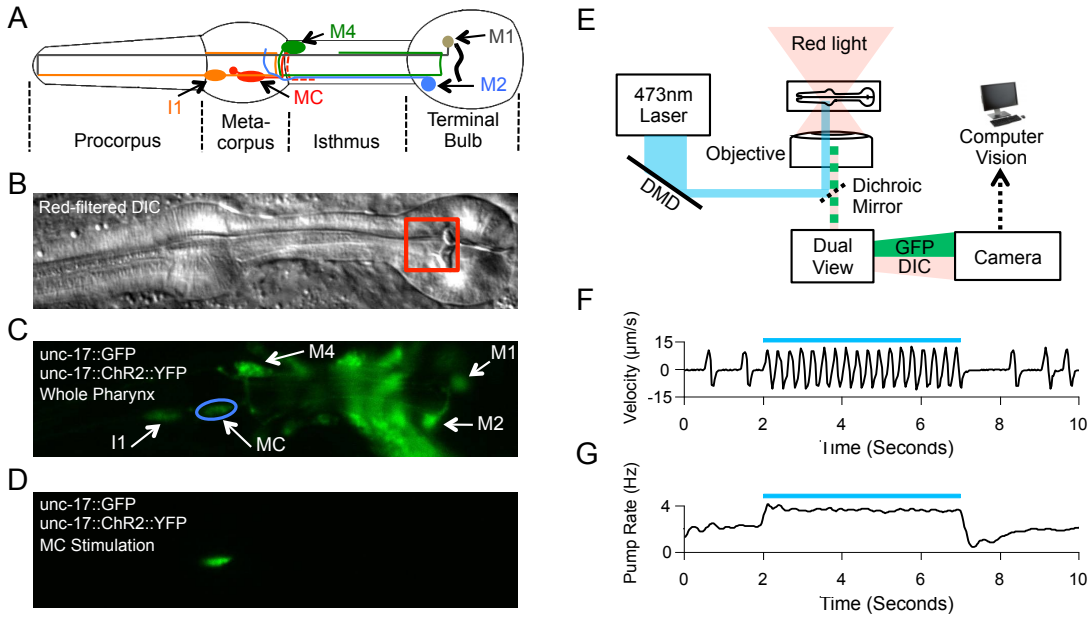

Figure 2.1: Optogenetic stimulation of the pharyngeal cholinergic nervous system and machine vision quantification of pumping. **A**: Cholinergic pharyngeal neurons. Only one of each of the paired I1, MC, and M2 neurons is shown. In A-D, anterior is to the left and ventral is toward the bottom. **B**: DIC image of the pharynx. Red box denotes region used for velocity calculations. **C**: wide field GFP fluorescence image of the same field of view as in B. The blue circle represents a stimulus region for an MC soma. **D**: GFP fluorescence image of the same field of view as in B and C, during selective illumination of an MC soma. **E**: Experimental schematic. A laser beam with wavelength 473 nm is shaped by a DMD and enters a microscope to selectively stimulate neurons of interest expressing either GFP and ChR2 or Mac. Pharyngeal behavior is imaged using a red filter and DIC optics. **F**: Velocity from machine vision algorithm during ChR2-mediated stimulation of the MCs. Each peak in the velocity represents a pump. **G**: Mean pump rate from nine intervals of MC excitation in each of 10 worms. In F and G, the blue bar denotes timing of laser illumination.

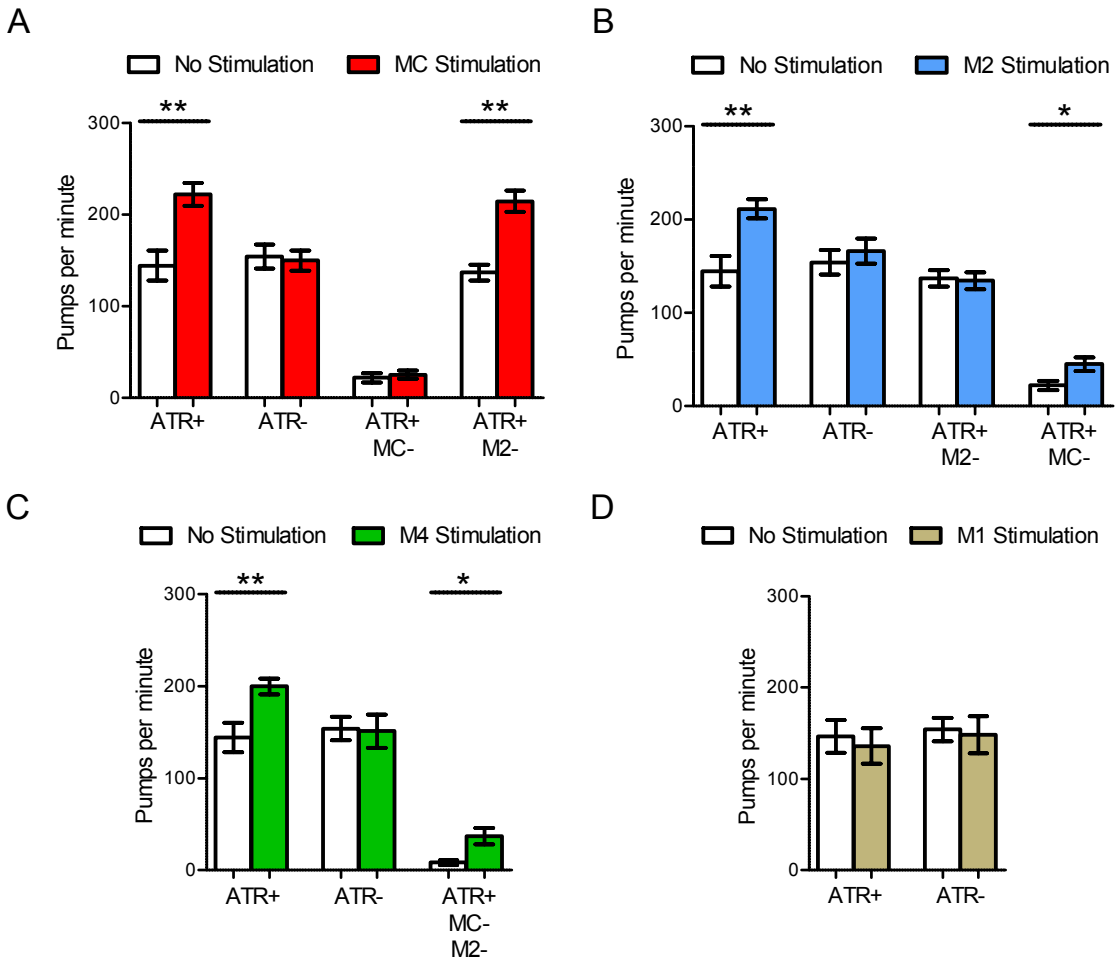

Figure 2.2: **Cholinergic motor neurons MC, M2, and M4, but not M1, are excitatory for pumping. A**: MC stimulation excites pumping in an all-*trans* retinal (ATR) dependent manner. This effect is abolished when the MCs are ablated but not when the M2s are ablated. N=10, 7, 10, 9 animals for each pair of bars, respectively. **B**: M2 stimulation excites pumping in an ATR-dependent manner. This effect is abolished when the M2s are ablated but not when the MCs are ablated. N=10, 7, 10, 9 animals for each pair of bars, respectively. **C**: M4 stimulation excites pumping in an ATR-dependent manner. This effect persists when the MCs and the M2s are ablated. N=10, 7, 7 animals for each pair of bars, respectively. **D**: M1 stimulation does not excite pumping. N=9, 7

animals for each pair of bars, respectively. 10 mM 5-HT was used for each experiment. Each bar represents mean +/- SEM. Statistical significance was calculated using the two-tailed Student's *t*-test. * and ** denote $p<0.05$ and $p<0.01$ respectively.

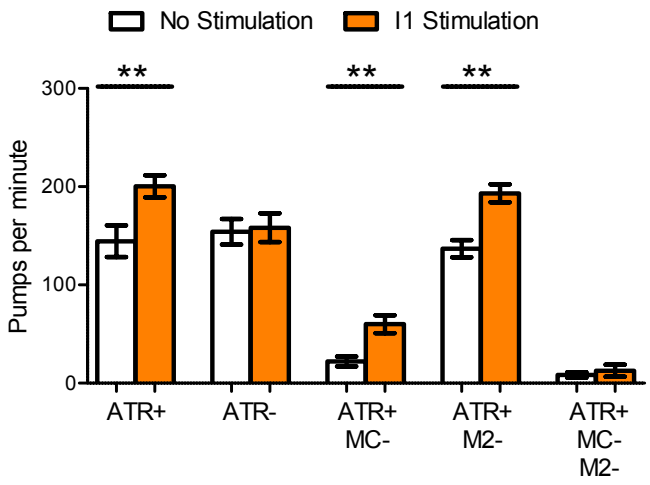

Figure 2.3: **The I1 interneurons stimulate pumping via the MCs and the M2s.** I1 stimulates pumping in an all-*trans* retinal (ATR) dependent manner and in the absence of either the MCs or the M2s but not both. N=10, 7, 10, 9, 7 animals for each pair of bars, respectively. 10 mM 5-HT was used for each experiment. Each bar represents mean +/- SEM. Statistical significance was calculated using the two-tailed paired Student's *t*-test. * and ** denote $p<0.05$ and $p<0.01$ respectively.

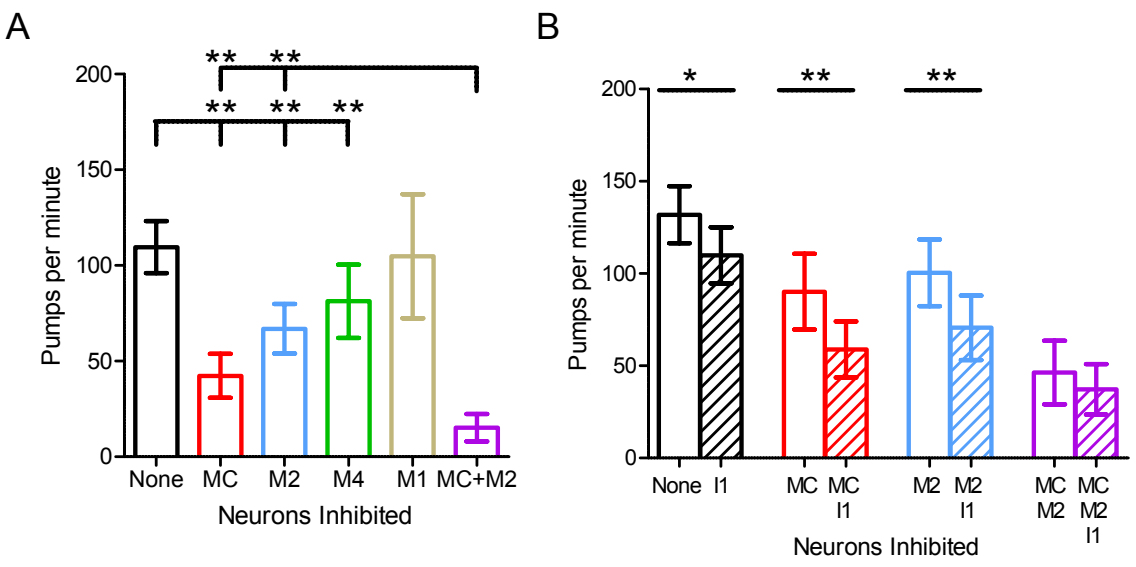

Figure 2.4: Optogenetic inhibition of pharyngeal cholinergic neurons inhibits 5-HT-stimulated pumping. A: Optogenetic inhibition of the MCs, the M2s, and M4, but not M1, inhibits 5-HT-stimulated pumping. Simultaneous inhibition of the MCs and the M2s causes an inhibition of pumping greater than that observed during inhibition of either the MCs or the M2s alone, consistent with an endogenous role for the M2s in pumping regulation. "None" indicates that no neurons were inhibited. N=15 for control, 14 for the MCs, 13 for the M2s, 9 for M4, and 4 for M1. **B**: Inhibition of the I1s inhibits 5-HT-stimulated pumping. Simultaneous I1 inhibition increased the effects of individual MC inhibition or M2 inhibition, but not of combined MC and M2 inhibition, indicating that I1 stimulates pumping endogenously via the MCs and the M2s. N=9 for each bar. 10 mM 5-HT was used for each experiment. Each bar represents mean +/- SEM. Statistical significance was calculated using the two-tailed Student's *t*-test. * and ** denote $p<0.05$ and $p<0.01$ respectively.

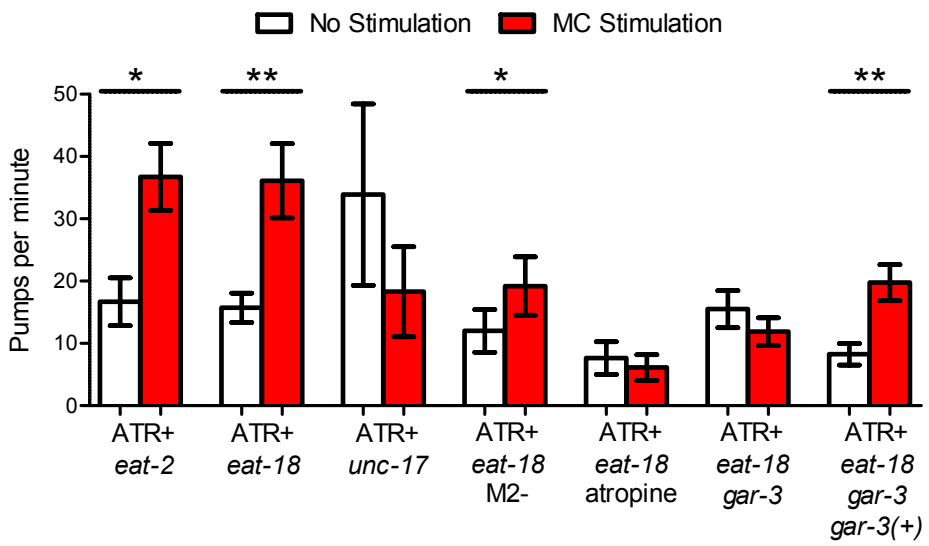

Figure 2.5: **The MCs can directly excite pumping via both nicotinic and muscarinic receptors.** Optogenetic MC stimulation increases pumping in both *eat-2* and *eat-18* nicotinic receptor mutants but not in *unc-17* (vesicular acetylcholine transporter) mutants, demonstrating that MC can act via a non-nicotinic cholinergic pathway in addition to the known EAT-2/EAT-18 nicotinic pathway. Serial section electron microscopy suggests that the MCs and M2s form gap junctions; MC stimulation directly increases pumping in the absence of the M2s in *eat-18* mutants. MC stimulation does not increase pumping in *eat-18* mutants in the presence of the muscarinic antagonist atropine. GAR-3 is a muscarinic receptor expressed in pharyngeal muscle, MC stimulation does not increase pumping in *eat-18; gar-3* double mutants. Injection of a transgene containing the *gar-3* genomic region restores the ability of MC stimulation to excite pumping in *eat-18*; *gar-3* mutants. N=10, 10, 8, 9, 9, 10, 10 animals for each pair of bars respectively. 10mM 5-HT was used for each experiment except those with atropine, where I used 5 mM 5-HT and 5 mM atropine. Each bar represents mean +/- SEM. Statistical significance was calculated using the two-tailed Student's *t*-test. * and ** denote $p<0.05$ and $p<0.01$ respectively.

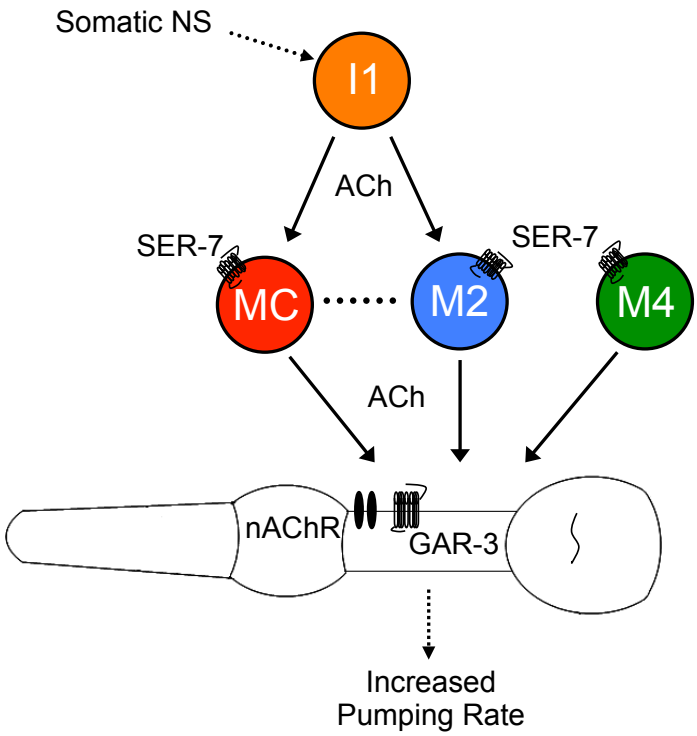

Figure 2.6: **Model of the cholinergic network regulating feeding rate.** The MCs, the M2s, and M4 can directly stimulate pumping, and the I1s can stimulate pumping via the MCs and the M2s. The MCs and the M2s are connected by gap junctions. The serotonin receptor SER-7 is expressed in the MCs, the M2s, and M4. The MCs stimulate pumping via a nicotinic receptor containing EAT-2 and EAT-18 and also via the GAR-3 muscarinic receptor.

CHAPTER 3: Distinct mechanisms underlie quiescence during two *Caenorhabditis elegans* sleep states

Nicholas F Trojanowski[1, 2, 3], Matthew D. Nelson[4], Steven W. Flavell[5], Christopher Fang-Yen[2, 3], David M. Raizen[1]

(1) Department of Neurology, Perelman School of Medicine

(2) Department of Bioengineering, School of Engineering and Applied Science

(3) Department of Neuroscience, Perelman School of Medicine

University of Pennsylvania, Philadelphia, PA 19104

(4) Department of Biology, Saint Joseph's University, Philadelphia, PA 19131

(5) Howard Hughes Medical Institute, Lulu and Anthony Wang Laboratory of Neural Circuits and Behavior, The Rockefeller University, New York, NY 10065

This chapter is a slightly modified version of a paper in press at the Journal of Neuroscience, with the addition of my contribution to George-Raizen JB, Shockley KR, Trojanowski NF, Lamb AL, and Raizen DM. Dynamically-expressed prion-like proteins form a cuticle in the pharynx of *Caenorhabditis elegans*. Biology Open, 2014.

Matthew Nelson and Steven Flavell provided unpublished reagents.

Christopher Fang-Yen and David Raizen assisted with planning experiments, interpreting data, and revising the paper.

All of the data presented in this chapter are my own.

Abstract

Electrophysiological recordings have enabled identification of physiologically distinct yet behaviorally similar states of mammalian sleep. In contrast, sleep in other vertebrates and invertebrates has generally been identified behaviorally, and therefore regarded as a physiologically uniform state characterized by quiescence of feeding and locomotion, reduced responsiveness, and rapid reversibility. The nematode *Caenorhabditis elegans* sleeps under two conditions: developmentally timed sleep (DTS) occurs during larval transitions, while stress-induced sleep (SIS) occurs in response to exposure to cellular stressors. Behaviorally, DTS and SIS appear identical. Here I use optogenetic manipulations of neural and muscular activity, pharmacology, and genetic perturbations to uncover circuit and molecular mechanisms of DTS and SIS. I find that locomotion quiescence induced by DTS- and SIS-associated neuropeptides occurs via their action on the nervous system, though their neural target(s) and/or molecular mechanisms likely differ. Feeding quiescence during DTS results from a loss of pharyngeal muscle excitability, whereas feeding quiescence during SIS results from a loss of excitability in the nervous system. Finally, I demonstrate that the pharyngeal cuticle in the terminal bulb is remodeled during DTS. Together these results indicate that, as in mammals, sleep is subserved by different mechanisms during distinct sleep states in *C. elegans*.

Introduction

Over the past 15 years, the study of small non-mammalian genetic models such as zebrafish, fruit flies, and roundworms has yielded many insights into the mechanisms of sleep regulation (Crocker and Sehgal, 2010). Electrophysiological characterization of sleep states, which is routinely used to identify sleep and its sub-stages in mammals, is difficult in these smaller organisms, and consequently sleep in non-mammals has typically been defined as a behavioral state characterized by quiescence of feeding and locomotion with an elevated arousal threshold and rapid reversibility (Allada and Siegel, 2008; Zimmerman et al., 2008). However, electroencephalography (EEG) has revealed that despite its apparent behavioral homogeneity, mammalian sleep is not a physiologically homogenous state (Loomis et al., 1937). For example, despite appearing behaviorally essentially identical, REM and non-REM sleep are regulated by different circuit and neurochemical mechanisms (Siegel, 2005).

The presence of distinct states of mammalian sleep raises the important question of whether behaviorally indistinguishable sleep states can be physiologically distinct in animals for which EEG is not feasible. In the nematode *C. elegans*, two behaviorally indistinguishable sleep states have been observed. Developmentally timed sleep (DTS), or lethargus, occurs during larval transitions preceding each molt (Raizen et al., 2008), and is coupled to a larval timing mechanism involving LIN-42, a homolog of the circadian timing protein PERIOD (Jeon et al., 1999; Monsalve et al., 2011). Stress-induced sleep (SIS) follows exposure to conditions that induce cellular stress, and requires the epidermal growth factor (EGF) LIN-3 (Hill et al., 2014). Both states are characterized by a cessation of locomotion and feeding as well as reduced responsiveness

to weak sensory stimuli, and animals in DTS or SIS resume movement but not feeding in response to a strong mechanical stimulation (Cassada and Russell, 1975; Jones and Candido, 1999; Raizen et al., 2008; Hill et al., 2014). Sensory neuron Ca^{2+} levels are decreased both during DTS as well as after somatic overexpression of EGF (mimicking SIS), demonstrating that the physiology immediately proximal to increased arousal threshold is similar between these states (Cho and Sternberg, 2014). The molecular genetic regulation of DTS (Choi et al., 2013; Nelson and Raizen, 2013; Schwarz and Bringmann, 2013; Singh et al., 2014) has several similarities to the regulation of circadian-timed sleep in *Drosophila* (Renn et al., 1999; Hendricks et al., 2001; Joiner et al., 2006; Parisky et al., 2008; Guo et al., 2011; He et al., 2013), while the molecular genetic regulation of SIS (Nelson et al., 2014) has similarities to the regulation of stress-induced sleep in *Drosophila* (Zimmerman et al., 2008; Lenz et al., 2015), demonstrating conserved mechanisms of quiescence regulation between *C. elegans* and other animals.

Recent evidence suggests that there might be differences in the underlying molecular and circuit mechanisms that regulate behavioral quiescence during DTS and SIS. For example, disruption of the function of the ALA interneuron results in severely defective quiescence after cellular stress (Hill et al., 2014) but only minor changes in quiescence during larval development (Van Buskirk and Sternberg, 2007), while key neurotransmitters used by the ALA interneuron to induce quiescence, the seven FMRFamide-like neuropeptides encoded by the *flp-13* gene, are required for normal quiescence during SIS but not DTS (Nelson et al., 2014).

In this study, I aimed to elucidate differences and similarities in the circuit and molecular mechanisms underlying behavioral quiescence during DTS and SIS. My results suggest that despite the outwardly identical appearance of DTS and SIS, feeding and locomotion inhibition arise from fundamentally distinct circuit and molecular mechanisms during these states.

Materials and Methods

Worm strains and cultivation

I performed all experiments with hermaphrodites. Unless otherwise specified, animals were cultivated on the surface of NGM agar in a 20ºC incubator. To conditionally overexpress *nlp-22* and *flp-13*, I used the strains **NQ251** *qnIs142 [Phsp-16.2::nlp-22; Phsp-16.2::GFP; Pmyo-2::mCherry; unc-119(+)]* (Nelson et al., 2013) and **NQ570** *qnIs303[Phsp-16.2::flp-13; Phsp-16.2::GFP; Prab-3::mCherry]* (Nelson et al., 2014), respectively. The mutant strains I used in my candidate screen are **KG421** *gsa-1(ce81gf) I* (Schade et al., 2005), **KG518** *acy-1(ce2gf) III* (Schade et al., 2005), **KG744** *pde-4(ce268) II* (Charlie et al., 2006), **KG532** *kin-2(ce179) X* (Schade et al., 2005), **JT734** *goa-1(sa734) I* (Robatzek and Thomas, 2000), **PS998** *goa-1(sy192dn) I* (Mendel et al., 1995), **CG21** *egl-30(tg26gf) I* (Doi and Iwasaki, 2002), **JT609** *eat-16(sa609) I* (Hajdu-Cronin et al., 1999), **KP1097** *dgk-1(nu62) X* (Nurrish et al., 1999), **NL594** *gpa-12(pk322) X* (Jansen et al., 1999), **MJ500** *tpa-1(k501) IV* (Tabuse and Miwa, 1983), **DA467** *eat-6(ad467) V* (Avery, 1993b), **MT6129** *egl-19(n2368gf) IV* (Lee et al., 1997), **VC223** *tom-1(ok285) I* (Dybbs et al., 2005), **NM1968** *slo-1(js379) V* (Wang et al., 2001), **DR1089** *unc-77(e625gf) IV* (Brenner, 1974), **MC339** *unc-64(md130) III* (Saifee et al., 1998), **CB5** *unc-7(e5) X* (Brenner, 1974), **MT9455** *tbh-1(n3247) X* (Alkema et al., 2005), **MT1074** *egl-4(n479) IV* (Trent et al., 1983). Other strains I used include **N2** (Brenner, 1974), **VC1669** *aptf-1(gk794) II* (Turek et al., 2013), **NQ596** *nlp-22(gk509904) X* (Nelson et al., 2013), **NQ602** *flp-13(tm2427) IV* (Nelson et al., 2014), **NQ670** *qnEx95[Phsp16.2::nlp-22; Pmyo-2::mCherry; unc-119(+)]* (Nelson et al., 2013), **NQ230** *ceh-17(np1) I; qnEx95[Phsp16.2::nlp-22; Pmyo-2::mCherry; unc-119(+)]* (Nelson et al., 2013), **NQ777**

ceh-17(np1) I; qnIs303[Phsp-16.2::flp-13; Phsp-16.2::GFP; Prab-3::mCherry] (Nelson et al., 2014), **ZM3265** *lin-15(n765ts) X; zxIs6[Punc-17::ChR2(H134R)::YFP; lin-15(+)] V* (Liewald et al., 2008), **YX11** *vsIs48[Punc-17::GFP] X; zxIs6[Punc-17::ChR2(H134R)::YFP; lin-15(+)] V* (Trojanowski et al., 2014), **YX62** *qnIs142[Phsp-16.2::nlp-22; Phsp-16.2::GFP; Pmyo-2::mCherry; unc-119(+)]; vsIs48[Punc-17::GFP] X; zxIs6[Punc-17::ChR2(H134R)::YFP; lin-15(+)] V*, **YX63** *qnIs303[Phsp-16.2::flp-13; Phsp-16.2::GFP; Prab-3::mCherry]/+; vsIs48[Punc-17::GFP] X; zxIs6[Punc-17::ChR2(H134R)::YFP; lin-15(+)] V*, **SJU8** *kin-2(ce179); qnEx448[Punc-17::kin-2(+); Pmyo-3::mCherry]*, **NQ902** *kin-2(ce179) X; qnIs303[Phsp-16.2::flp-13; Phsp-16.2::GFP; Prab-3:mCherry]; qnEx448[Punc-17::kin-2(+); Pmyo-3::mCherry]*, **NQ903** *kin-2(ce179) X; qnIs142[Phsp-16.2::nlp-22; Phsp-16.2::GFP; Pmyo-2::mCherry; unc-119(+)]; qnEx448[Punc-17::kin-2(+); Pmyo-3::mCherry]*, **NQ820** *qnEx390[Pmyo-2::GCaMP6s::SL2::dsRed; rol-6(d)]***, CX16557** *kyIs5640[Pmyo-2::Chrimson; Pelt-2::his-4.4-mCherry],* and **NQ904** *qnEx390[Pmyo-2::GCaMP6s::SL2::dsRed; rol-6(d)]; kyIs5640[Pmyo-2::Chrimson; Pelt-2::his-4.4-mCherry]*.

Strain construction

To rescue the *kin-2* defect specifically in cholinergic neurons, we used an Eppendorf FemtoJet micro-injection system on a Leica DMIRB inverted differential interference contrast (DIC) microscope to inject *Punc-17::kin-2::unc-54utr* in CFJ151 at 25 ng/µL in combination with 5 ng/µL of pCFJ104*(Pmyo-3::mCherry)*. We created the *Punc-17::kin-2::unc-54utr* construct using standard Gateway cloning procedures. Briefly, we

recombined *Punc-17* in pDONR P4P1r and *kin-2* cDNA in pDONR221 into the CFJ151 destination vector. To create *qn390*, we used overlap extension PCR (Nelson and Fitch, 2011) to generate *Pmyo-2::GCaMP6s::SL2::dsRed*. We then injected *Pmyo-2::GCaMP6s::SL2::dsRed* at 20 ng/µL and *pRF4* at 100 ng/µL into N2. We created *Pmyo-2::Chrimson* by subcloning the *myo-2* promoter into the pSM-Chrimson vector (Gordus et al., 2015) using FseI and AscI. To generate *kyIs5640,* we injected *Pmyo-2::Chrimson* at 0.4 ng/µL in combination with 5 ng/µL P*elt-2::his-4.4-mCherry*. The resulting extrachromosomal array spontaneously integrated during the course of strain maintenance (Mello et al., 1991).

To construct the strains used to test gene mutation effects on the behavioral quiescence conferred by neuropeptide overexpression, we followed the red fluorescent reporter on the transgene array (*Pmyo-2::mCherry* or *Prab-3::mCherry*) and the visible phenotypes of the gene mutation. In cases where the phenotype of the gene mutation was difficult to identify, we made use of balanced chromosomes marked with GFP fluorescence (Edgley et al., 2006).

Acute heat shock

Unless otherwise indicated, I triggered stress-induced sleep by acute heat shock, performed as described in "protocol 1" by Nelson et al. (Nelson et al., 2014). I heat-shocked day one adults at 35ºC in a water bath for 30 minutes on standard NGM agar plates seeded with DA837. I then counted pumping rate as previously described (Raizen et al., 2012) for individual worms between 35 and 45 minutes after the end of heat shock.

Conditional neuropeptide overexpression

Unless otherwise indicated, to induce neuropeptide overexpression I placed day one adults on NGM agar plates seeded with DA837 in a 33ºC water bath for 30 minutes and allowed them to recover at room temperature for 2-3 hours, at which time the effects of acute heat shock had worn off (Nelson et al., 2013; 2014). To screen for mutants with abnormal *flp-13*- or *nlp-22*-induced quiescence, I tested all of the candidate strains overexpressing one neuropeptide gene on the same day, and the experimenter was blinded to the genotype of the strains. I counted the number of pumps per 20 seconds and the number of body bends per 20 seconds (where one full back and forth movement of the anterior body was counted as one body bend) for each of 12-15 worms. I tripled each value to convert to pumps per minute or body bends per minute. For experiments testing the effect of *ceh-17* mutation on *nlp-22* and *flp-13* overexpression induced quiescence, I used NQ670 and NQ570 as the respective control strains.

Effects of 5-HT

To test the effect of 5-HT on feeding after neuropeptide overexpression, during SIS, or during DTS, I immobilized worms on agarose pads containing 10 mM 5-HT as previously described (Trojanowski et al., 2014).

Single neuron optogenetics

I performed optogenetic stimulation of single neurons after neuropeptide overexpression as previously described (Trojanowski et al., 2014), except the worms were first submitted to the conditional neuropeptide overexpression protocol, as described above. I examined worms between 2 and 3 hours after heat shock.

Wide-field optogenetics

To stimulate pharyngeal neurons during SIS or DTS, I grew ZM3265 worms on OP50 containing all-*trans* retinal (ATR) as previously described (Trojanowski et al., 2014). For SIS, I performed acute heat shock as described above, except plates seeded with ATR-containing OP50 were used. I then illuminated these worms with blue light (using GFP optics, irradiance = 0.66 mW/mm^2) from a mercury halide lamp on a Leica MZ16F stereomicroscope, and quantified pump rate in 20-second intervals (Raizen et al., 2012). I tripled these values to calculate pumps per minute.

Pharyngeal muscle optogenetics

I performed optogenetic stimulation of pharyngeal muscle during wake and DTS similarly to stimulation of single neurons, with some modifications because Chrimson was not tagged with a fluorescent protein. First, I stimulated the entire head region of the worm instead of only the pharynx by setting the digital micromirror device (DMD) to illuminate the entire field of view. Next, I used a pulse generator (Stanford Research

Systems DG535) to generate 5V pulses of a specified duration and frequency and connected this output to the modulation input of the laser to control stimulus timing. To identify the stimulus interval on the camera, I attached a red collimated LED to the same pulse generator output via a relay and directed this light towards the objective, allowing me to detect a small increase in bright-field intensity when the laser was on. All other aspects of the experiment were unchanged.

Ca^{2+} imaging

I performed experiments using GCaMP6s the same way as pharyngeal muscle optogenetics experiments with slight modifications. With the laser continuously illuminating the field of view, I recorded the *Pmyo-2::GCaMP6s* signal for about 30 s (1000 frames at 30 frames per second). I then identified the maximum and minimum fluorescence values in a region of the metacorpus during this time, and calculated the difference between these values to determine the maximum fluorescence change during this interval. The laser power I used here was the same as for optogenetics experiments.

Time-lapse imaging

To image the pharynx during L4 DTS, we immobilized the animals against agarose pads using polystyrene nanoparticles (Kim et al., 2013). Images were captured at 3.75 frames per second using an Imaging Source DMK 31BU03 camera on a Leica DM 2500 P upright microscope at 63X and analyzed using IC Capture 2.2 software (Imaging Source).

Statistics

For the candidate mutant screens, I used Dunnett's multiple comparison tests to determine which mutants were significantly different from the control. For the single neuron optogenetics, I performed a one-way ANOVA to determine if there was an effect of neuron stimulation on pumping rate. For stress-induced sleep experiments, I used a Mann-Whitney test without post-hoc correction to determine which mutants were significantly different from the control. See figure legends for details.

Results

Feeding quiescence during SIS does not require pathways that regulate DTS

Two classes of neurons are known to be required for normal quiescence during DTS: the paired RIA neurons, which release the neuropeptide NLP-22, and the RIS neuron, which requires the AP2 transcription factor APTF-1 (Nelson et al., 2013; Turek et al., 2013). The ALA neuron, which secretes the neuropeptides encoded by *flp-13*, is the only neuron known to be required for SIS (Van Buskirk and Sternberg, 2007; Hill et al., 2014; Nelson et al., 2014) (Fig. 1A). Although SIS and DTS are behaviorally indistinguishable, it is unclear to what extent there is overlap between the mechanisms of behavioral quiescence during these states.

While *flp-13* mutants have defective feeding and locomotion quiescence after cellular stress induction, their quiescence during larval transitions is normal (Nelson et al., 2014). To further compare the mechanisms of quiescence during DTS and SIS, I examined SIS feeding quiescence in mutants with defective DTS. While I detected differences in SIS feeding quiescence between wild-type worms and *flp-13* mutants, neither *nlp-22* mutants nor *aptf-1* mutants displayed a defect in SIS feeding quiescence, demonstrating that these DTS-promoting factors are not required for quiescence during SIS (Fig. 1B). Thus, some factors required for quiescence during SIS are not necessary for quiescence during DTS, and vice versa.

Overexpression of *flp-13* or *nlp-22* neuropeptide genes inhibits feeding and locomotion

I next sought to identify conserved pathways that regulate quiescence downstream of the ALA and RIA interneurons during SIS and DTS, respectively. Quiescence during SIS requires the release of the FMRFamide-like FLP-13 neuropeptides from the ALA interneuron (Nelson et al., 2014), and quiescence during DTS requires the release of the NLP-22 neuropeptide, which is structurally similar to the mammalian neuropeptide Neuromedin S, from the RIA interneuron. *nlp-22* mRNA cycles in phase with mRNA of *lin-42* (Jeon et al., 1999), the *C. elegans* homolog of the PERIOD gene, and an *nlp-22* loss-of-function mutation decreases quiescence during DTS (Nelson et al., 2013). Likewise, *flp-13* mRNA is increased after organismal stress, and a *flp-13* loss-of-function mutation decreases quiescence during SIS (Nelson et al., 2014).

I conditionally overexpressed these neuropeptides under control of the heat shock promoter (*Phsp-16.2::flp-13* and *Phsp-16.2::nlp-22*) to robustly induce quiescent behavioral states mimicking SIS and DTS (Nelson et al., 2013; 2014). This approach, similar to one recently used to study somnogenic neuropeptides in zebrafish (Woods et al., 2014), was selected for four reasons. First, in contrast to chronic loss-of-function experiments using genetic mutants, these conditional overexpression experiments are not subject to redundancy, compensation, or other developmental or physiological defects that may be part of the loss-of-function phenotype. Second, expressing the neuropeptides at supraphysiological levels is likely to activate all or nearly all of the receptors of these neuropeptides, so their effects will be limited only by the expression patterns of their receptors. Third, prolonged overexpression of the somnogenic peptides provides the

experimental advantage of inducing a behavioral state lasting longer than the endogenous behavior, facilitating the identification of defects in these behaviors and characterization of downstream signaling pathways. Finally, the temporal control afforded by this conditional approach allowed me to compare quiescence induced by the two peptides in the same early adult stage, minimizing effects of developmental time on behavior. It is important to note that while *flp-13* and *nlp-22* have been implicated in SIS and DTS respectively, it is unlikely that overexpression of these neuropeptide genes faithfully recapitulates all aspects of these sleep states.

Since SIS is triggered by acute activation of the ALA neuron by heat shock, it is possible that the somnogenic effects of overexpressing these neuropeptide genes using the heat shock-inducible promoter are affected by ALA activation, and the quiescence I observe does not reflect purely the somnogenic actions of the neuropeptides. While I attempt to avoid effects of SIS in my neuropeptide overexpression experiments by observing the animals at least two hours after heat exposure and by inducing gene expression with a less stressful 33ºC stimulus (Nelson et al., 2014), it remains possible that residual effects of SIS influence the behavior of these animals. To test for this possibility, I overexpressed *nlp-22* and *flp-13* in the *ceh-17* mutant background, which lacks a functional ALA neuron (Pujol et al., 2000). I found that worms with a *ceh-17* mutation were indistinguishable from controls two hours after transgene induction with respect to both locomotion (*nlp-22* overexpression: control: 1.0 ± 0.2 body bends per minute (bbpm), *ceh-17*: 1.6 ± 0.3 bbpm, p=0.51; *flp-13* overexpression: control: 0.6 ± 0.2 bbpm, *ceh-17*: 1.0 ± 0.2 bbpm, p=0.54; mean ± SEM, n=15) and feeding (*nlp-22* overexpression: control: 30.6 ± 4 pumps per minute (ppm), *ceh-17*: 15.2 ± 1.9 ppm,

p=0.26; *flp-13* overexpression: control: 20.4 ± 4.1 ppm, *ceh-17*: 16.2 ± 2.1 ppm, p=0.72; mean ± SEM, n=15), demonstrating that ALA activation is not required for the quiescence observed after *flp-13* or *nlp-22* overexpression.

Activation of the Gαq or Gαs pathways inhibits both *flp-13*- and *nlp-22*-induced locomotion quiescence

To identify conserved genes that regulate locomotion quiescence induced by overexpression of *flp-13* or *nlp-22*, I crossed strains overexpressing these neuropeptides into strains containing mutations in candidate genes with vertebrate homologs. Candidate genes were those that cause increased neurotransmitter release, increased membrane excitability, hyperactive locomotion, defective behavioral quiescence, or resistance to anesthetics. I focused in particular on strains with increased neurotransmitter release due to increased Gαq and Gαs signaling (Fig. 2, adapted from (Perez-Mansilla and Nurrish, 2009)), since these mutants show hyperactive locomotion and some have defects in DTS locomotion quiescence (Belfer et al., 2013; Iwanir et al., 2013; Schwarz and Bringmann, 2013; Singh et al., 2014), and therefore they might be resistant to the effects of somnogenic neuropeptides.

The Gαq signaling pathway acts antagonistically to Gαo signaling in *C. elegans* and promotes neurotransmitter release by increasing diacylglycerol (DAG) levels (Miller et al., 1999), while the Gαs pathway acts downstream of DAG to increase neurotransmitter release (Reynolds et al., 2005). Hyperactivation of the Gαq signaling pathway can be achieved either directly, using a gain-of-function mutation in the Gαq gene *egl-30* (Doi

and Iwasaki, 2002), or indirectly, using loss-of-function mutations in the Gαo gene *goa-1* (Miller et al., 1996), the regulator of G-protein signaling (RGS) gene *eat-16* (Hajdu-Cronin et al., 1999), or the diacylglycerol kinase theta (DGK-θ) gene *dgk-1* (Miller et al., 1999). Hyperactivation of the Gαs signaling pathway can also be achieved either directly, using gain-of-function mutations in the Gαs gene *gsa-1* (Schade et al., 2005) or the adenylate cyclase type IX gene *acy-1* (Schade et al., 2005), or indirectly, using loss-of-function mutations in the phosphodiesterase-4 gene *pde-4* (Charlie et al., 2006) or the cAMP-dependent protein kinase (PKA) regulatory subunit gene *kin-2* (Schade et al., 2005).

I also examined strains with mutations that increased neurotransmitter release by other means, including loss-of-function mutations in the tomosyn gene *tom-1* (Dybbs et al., 2005) and the BK channel gene *slo-1* (Wang et al., 2001), as well as mutations that generally increased membrane excitability, including a gain-of-function mutation in the L-type Ca^{2+} channel gene *egl-19* (Lee et al., 1997) and a loss-of-function mutation in the Na^{+}/K^{+} transporter α-subunit gene *eat-6* (Davis et al., 1995). I also tested strains with mutations that confer resistance to anesthesia, including a gain-of-function mutation in the NALCN channel subunit gene *unc-77* (Humphrey et al., 2007; Morgan et al., 2007; Yeh et al., 2008), a loss-of-function mutation in the innexin gene *unc-7* (Starich et al., 1996), and a neomorphic mutation affecting the syntaxin gene *unc-64* (van Swinderen et al., 1999). Finally, I tested strains with mutations that caused defects in various types of behavioral quiescence, including loss-of-function mutations in the cGMP-dependent protein kinase (PKG) gene *egl-4* (Raizen et al., 2008), the Gα12 gene *gpa-12* (van der Linden et al., 2003), the protein kinase C epsilon (PKC-ε) gene *tpa-1* (van der Linden et

al., 2003), and the tyramine β-hydroxylase gene *tbh-1* (Alkema et al., 2005). Table 1 lists all mutants tested and their effects on relevant signaling pathways and cell physiology.

Mutations that increase Gαq or Gαs signaling suppressed the locomotion quiescence induced by overexpression of either *flp-13* or *nlp-22* (Fig. 3A, B, Table 2). However, while overexpression of *nlp-22* in mutants with activated Gαs signaling caused qualitatively normal locomotion, overexpression of *flp-13* in the same mutants caused aberrant locomotion characterized by uncoordinated twitches and accordion-like contractions. Gαq pathway genes are expressed in neurons but not in body wall muscles (Nurrish et al., 1999; Bastiani et al., 2003), and cholinergic neuron stimulation during DTS causes contraction of body wall muscle (Dabbish and Raizen, 2011), suggesting that FLP-13 and NLP-22 neuropeptides both act on neurons to inhibit locomotion.

To test if these neuropeptides are acting via cholinergic neurons to regulate locomotion, we rescued the function of *kin-2*, the PKA regulatory subunit, in cholinergic neurons using the *unc-17* promoter and assessed the effect of neuropeptide overexpression on locomotion. I found that after restoring *kin-2* function in cholinergic neurons, locomotion was strongly inhibited after overexpression of either neuropeptide gene (Fig. 3C), demonstrating that decreased PKA signaling in cholinergic neurons is important for inhibiting locomotion downstream of these neuropeptides. However, since I observed different locomotion phenotypes after overexpressing *flp-13* or *nlp-22* in backgrounds with activated Gαs signaling, these neuropeptides likely act on different molecular targets and/or different subsets of cholinergic neurons.

Feeding quiescence induced by *flp-13* overexpression but not *nlp-22* overexpression is suppressed by activation of the Gαq or Gαs pathways

C. elegans feeds by rhythmic contraction of its pharynx, a neuromuscular pump possessing 20 neurons of 14 types (Albertson and Thomson, 1976). Pharyngeal contractions are easiest to measure by observing movement of the grinder, cuticular plates in the posterior region of the pharynx, the terminal bulb (Raizen et al., 2012). To identify conserved signaling pathways that regulate feeding quiescence downstream of *flp-13* and *nlp-22*, I overexpressed these neuropeptide genes in the mutant backgrounds described above and in Table 1. As with locomotion quiescence, feeding quiescence induced by *flp-13* overexpression was strongly suppressed by mutations that increase neurotransmitter release by activating either the Gαq or Gαs signaling pathways (Fig. 4A, Table 2), which are present in all or nearly all neurons (Ségalat et al., 1995; Korswagen et al., 1997; Bastiani et al., 2003). In these mutants, feeding rates were substantially higher than the control feeding rate, even though in the absence of neuropeptide overexpression many of these strains feed at rates similar to that of the control (Song and Avery, 2012). In addition, some mutations that increase neurotransmitter release by other mechanisms or confer resistance to anesthesia also suppressed the feeding quiescence caused by *flp-13* overexpression (Fig. 4A). In contrast, none of the mutants tested suppressed the feeding quiescence induced by *nlp-22* overexpression (Fig. 4B). These results indicate that FLP-13 and NLP-22 neuropeptides promote feeding quiescence via distinct molecular mechanisms.

FLP-13 inhibits feeding by acting on neurons; NLP-22 inhibits feeding downstream of neurons

Since *flp-13*-induced feeding quiescence is suppressed by mutations that increase neurotransmitter release but *nlp-22*-induced feeding quiescence is not, I hypothesized that the FLP-13 neuropeptides promote feeding quiescence by acting on the nervous system and that the NLP-22 neuropeptide promotes feeding quiescence by acting directly on the pharyngeal muscle. To test this hypothesis, we rescued the function of *kin-2*, the PKA regulatory subunit, in cholinergic neurons and assessed the effect of neuropeptide overexpression on feeding rate. I found that restoring *kin-2* function in cholinergic neurons restored pumping levels after *flp-13* overexpression to that of the control, while restoring *kin-2* function in cholinergic neurons after *nlp-22* overexpression did not affect feeding rate (Fig. 5A).

Three classes of pharyngeal cholinergic motor neurons, the paired MC and M2 neurons and the single M4 neuron, stimulate pharyngeal pumping (Avery and Horvitz, 1989; Raizen et al., 1995; Trojanowski et al., 2014). Based on the above results, I predicted that *flp-13*-induced feeding quiescence, but not *nlp-22*-induced feeding quiescence, could be overcome by perturbations that excite pharyngeal cholinergic motor neurons. To test this hypothesis, I used both pharmacological and optogenetic approaches.

First, I tested the effects of the neuromodulator serotonin (5-hydroytryptamine or 5-HT) on feeding quiescence induced by *flp-13* or *nlp-22* overexpression. 5-HT stimulates pharyngeal pumping primarily via the SER-7 5-HT receptor and downstream Gαs signaling in pharyngeal cholinergic motor neurons (Hobson et al., 2006; Song and Avery,

2012). Therefore, the effects of neuropeptides that promote feeding quiescence by acting on or upstream of pharyngeal motor neurons should be suppressed by 5-HT, while the effects of neuropeptides that act downstream of the motor neurons should be unaffected by 5-HT. I found that *nlp-22*-induced feeding quiescence was not suppressed by the excitatory effects of 5-HT, consistent with the NLP-22 acting downstream of the pharyngeal motor neurons (Fig. 5B). In contrast, *flp-13*-induced feeding quiescence was fully suppressed by 5-HT, consistent with the FLP-13 neuropeptides acting on or upstream of the pharyngeal motor neurons (Fig. 5B).

An alternative explanation for these differential effects that would be consistent with both neuropeptides suppressing feeding by the same mechanisms is that *nlp-22* is overexpressed at higher levels than *flp-13*, and that 5-HT can overcome mild overexpression but not strong overexpression. I tested this possibility two ways, both making use of the fact that the transgenes expressing the neuropeptides were under the control of a heat-inducible promoter, and I could thus vary the degree of transgene overexpression. First, I induced different degrees of expression of each neuropeptide transgene by varying the duration of the animals' exposure to 33°C. In the presence of food, an environmental stimulant to feeding rate, but in the absence of exogenous 5-HT, overexpression of either neuropeptide gene caused a similar reduction in feeding rate 2-3 hours after heat exposure that was a function of the duration of prior heat exposure (and thus a function of neuropeptide expression) (Fig. 5C). In contrast, in the presence of exogenous 5-HT but not food, overexpression of *flp-13* and *nlp-22* produced different effects on feeding rate. Similar to its effect in the presence of food, *nlp-22* overexpression caused a dose-dependent reduction in feeding rate in the presence of 5-HT. In contrast,

even strong overexpression of *flp-13* failed to inhibit feeding in the presence of 5-HT (Fig. 5D).

As a second way of testing whether the different effects of 5-HT after overexpressing *nlp-22* or *flp-13* were due to differential overexpression of transgenes, I exposed the animals to 29°C, instead of 33°C, for 30 minutes to induce a lower level of transgene expression. This lower induction temperature had the additional advantage of being less likely to trigger quiescence on the basis of acute heat exposure (Avery and Horvitz, 1989; Raizen et al., 1995; Nelson et al., 2014; Trojanowski et al., 2014). Animals carrying transgenes with the heat shock promoter driving either *flp-13* or *nlp-22* overexpression showed feeding quiescence two hours after this 30-minute 29°C heat exposure (*Phsp-16.2::flp-13*: 182.1 ± 8.7 ppm before heat, 20.1 ± 8.6 ppm after heat, $p<0.001$; *Phsp-16.2::nlp-22*: 145.2 ± 5.2 ppm before heat, 9.3 ± 3.6 ppm after heat, $p<0.001$; mean ± SEM, n=10), demonstrating that both transgenes were expressed at sufficiently high levels to induce quiescence even at this milder activation temperature. At an earlier time point (35 minutes) following the same 30-minute 29°C heat exposure, worms overexpressing *flp-13* but not worms overexpressing *nlp-22* showed feeding quiescence (*Phsp-16.2::flp-13*: 181.2 ± 8.7 ppm before heat, 11.4 ± 5.2 ppm 35 minutes after heat, $p<0.001$; *Phsp-16.2::nlp-22*: 145.2 ± 5.2 ppm before heat, 136.2 ± 16.3 ppm 35 minutes after heat, $p=0.61$; mean ± SEM, n=10). These observations suggest that the differential effects of 5-HT on feeding quiescence are not explained by reduced activation of the *flp-13* transgene relative to the *nlp-22* transgene.

Next, I used an optogenetic approach to test where the NLP-22 and FLP-13 neuropeptides act in relation to depolarization of cholinergic pharyngeal motor neurons (Fig. 5E). While 5-HT activates pumping via these neurons, optogenetic stimulation via the light-sensitive cation channel Channelrhodopsin-2 (ChR2) of individual cholinergic motor neurons in the presence of 5-HT induces an even greater increase in feeding rate during wake (Trojanowski et al., 2014). I stimulated single pharyngeal motor neurons and monitored resulting changes in feeding rate. I found that stimulation of any of the excitatory cholinergic neurons MC, M2, or M4 caused an increase in feeding rate after *flp-13* overexpression, but not after *nlp-22* overexpression (Fig. 5F). These results further support the hypothesis that the FLP-13 neuropeptides act on or upstream of the pharyngeal cholinergic neurons, while the NLP-22 neuropeptide acts downstream of cholinergic neuron excitation, likely on the pharyngeal muscle.

Feeding quiescence during SIS is abolished by activation of the Gαq but not the Gαs pathway

Having gained insight into the mechanisms through which the NLP-22 and FLP-13 neuropeptides control feeding, I next asked whether feeding is regulated by similar mechanisms in their associated sleep states. Because I found that mutations that increase Gαs or Gαq signaling suppressed *flp-13*-induced feeding quiescence, I hypothesized that these mutations would also suppress feeding quiescence during SIS. I found that mutations that increased Gαs signaling did not affect feeding quiescence during SIS, while mutations that increased Gαq signaling did suppress feeding quiescence during SIS

(Fig. 6). Thus, activation of Gαs signaling suppresses feeding quiescence induced by *flp-13* overexpression but does not suppress the feeding quiescence observed during SIS, while activation of Gαq signaling suppresses feeding quiescence after either *flp-13* overexpression or during SIS. These results suggest that other neurotransmitters released by ALA affect feeding quiescence during SIS, perhaps by acting downstream of Gαs signaling.

I also found that a loss-of-function mutation in *egl-4* (PKG) suppressed feeding quiescence during SIS (Fig. 6), suggesting that EGL-4 acts downstream of or in parallel to ALA activation. Since the *egl-4* mutation did not suppress feeding quiescence in response to *flp-13* overexpression (Fig. 4A and Table 2), *egl-4* may be acting downstream of or in parallel to a neurotransmitter distinct from FLP-13 that is released from ALA. Alternatively, FLP-13 released by *flp-13* overexpression under the heat shock promoter may act on receptors that are not engaged by FLP-13 released from ALA. These possibilities are not mutually exclusive.

The pharyngeal nervous system can excite feeding during SIS but not DTS

Based on my results from animals overexpressing either *flp-13* or *nlp-22*, I hypothesized that feeding is inhibited at the level of the pharyngeal motor neurons during SIS, while during DTS feeding is inhibited downstream of motor neuron excitation. To test this hypothesis, I again used both pharmacological and optogenetic approaches. First, I placed worms in either SIS or DTS on agarose pads containing 5-HT to determine if excitation of pharyngeal neurons with 5-HT could stimulate feeding during these states. I found that

worms in SIS but not DTS pumped in the presence of 5-HT, suggesting feeding quiescence during SIS occurs at the level of or upstream of pharyngeal cholinergic motor neurons, while feeding is inhibited at a level downstream of pharyngeal cholinergic motor neuron during DTS (Fig. 7A).

Absence of feeding induction by 5-HT during DTS could be explained by decreased 5-HT responsiveness during this state. Alternatively, it could be explained by reduced excitability of the motor neurons, or by reduced excitability of pharyngeal muscle downstream of motor neuron excitation. To further delineate the circuit mechanism of feeding cessation during SIS and DTS, I optogenetically depolarized pharyngeal cholinergic motor neurons during these states. To minimize the effects of animal immobilization on behavior and to provide as strong an excitatory input to pumping as possible, I used wide-field blue light illumination to stimulate ChR2 in all cholinergic neurons in worms on bacterially seeded agar plates. As with *nlp-22* overexpression, stimulation of cholinergic neurons did not result in feeding during DTS (Fig. 7B). However, as with *flp-13* overexpression, cholinergic neuron stimulation caused feeding during SIS. These results are consistent with NLP-22 inhibiting pharyngeal muscle during DTS, and FLP-13 inhibiting pharyngeal cholinergic motor neurons during SIS.

Pharyngeal muscle excitability is altered during DTS

My result that depolarization of pharyngeal neurons during DTS did not stimulate feeding suggests that feeding is inhibited at the level of the muscle during this state. However, another possible explanation is that neurotransmitter release is blocked during DTS. To

directly test if feeding was inhibited at the level of the muscle during DTS, I attempted to optogenetically stimulate pharyngeal muscle. I had difficulty expressing ChR2 in pharyngeal muscle, so instead we used the light-sensitive cation channel Chrimson (Klapoetke et al., 2014), which expressed well. The peak excitation wavelength of Chrimson is approximately 590 nm, but it retains adequate sensitivity (about 25% of peak) to 473 nm blue light (Klapoetke et al., 2014), so I used the same laser and power to stimulate Chrimson as I did ChR2. I found that optogenetic stimulation of pharyngeal muscle increased feeding rate during wake, but this effect was abolished during DTS (Fig. 7C). Thus, even when pharyngeal muscle was optogenetically depolarized it did not contract, suggesting that either the coupling between excitation and contraction is altered during DTS or that Ca^{2+} levels in the muscle are not rising sufficiently to generate contractions.

To test whether this uncoupling between muscle depolarization and contraction is upstream or downstream of increased Ca^{2+} levels, I imaged Ca^{2+} levels in the metacorpus region of the pharyngeal muscle (Avery and You, 2012) using the genetically encoded Ca^{2+} sensor GCaMP6s (Chen et al., 2013). During wake, I detected fluctuations in GCaMP6s fluorescence in the metacorpus (Fig. 7D, 7E); such Ca^{2+} transients are associated with pharyngeal pumps (Kerr et al., 2000; Akerboom et al., 2013). These fluctuations in GCaMP6s fluorescence were absent during DTS, demonstrating that Ca^{2+} levels in the muscle do not oscillate during DTS (Fig. 7D, 7F). Ca^{2+} transients during DTS were undetectable even when pharyngeal muscle was optogenetically depolarized (Fig. 7D), demonstrating that pharyngeal excitability is fundamentally altered during DTS such that Ca^{2+} levels cannot rise and trigger muscle contraction.

Pharyngeal cuticle is replaced during DTS

To examine whether any morphological changes associated with molting during DTS could explain why pharyngeal muscle excitability is impaired during DTS, I performed time-lapse analysis of an animal in the fourth larval stage (L4) DTS molt. I found that in early DTS, the cuticular plates in the posterior part of the pharynx, the grinder, gradually moved anteriorly (Fig. 8). As DTS progressed, this grinder became smaller in size and a new, larger grinder formed posterior to the L4 grinder, in a position similar to the one that the grinder previously occupied. Since defective molting is lethal (Frand et al., 2005), these results suggest that the decreased pharyngeal excitability observed during DTS may allow the proper deposition of new cuticle.

Discussion

My results show that, despite the behavioral similarities of DTS and SIS, the quiescence-inducing mechanisms downstream of neuropeptide release are distinct in these states. Overexpression of the DTS-associated neuropeptide gene *nlp-22* inhibits feeding via action on pharyngeal muscle and acts on the nervous system to inhibit locomotion. In contrast, the SIS-associated FLP-13 neuropeptides inhibit feeding via the pharyngeal nervous system and inhibit locomotion by acting on the nervous system through a different mechanism from that of NLP-22 (Fig. 9). Further, I found that stimulation of pharyngeal motor neurons excites feeding during SIS but not during DTS, and even direct stimulation of pharyngeal muscle does not excite feeding during DTS. It is important to note that I have focused on two particular behavioral programs observed during sleep in all animals: quiescence of feeding and locomotion. Other aspects of sleep behavior, such as an elevated sensory arousal threshold, were not studied here and may be regulated by mechanisms different from those regulating feeding and locomotion quiescence.

Nevertheless, to my knowledge this is the first *in vivo* demonstration that a non-mammalian animal can express mechanistically distinct types of quiescence during sleep states. These results raise the possibility that in other animals (e.g. fruit flies, zebrafish), quiescence during sleep under different conditions may be regulated by different mechanisms despite behavioral similarities. Indeed, there are already suggestions that this is the case. For example, mechanisms of regulation of locomotion quiescence in young *Drosophila* adults are partially distinct from mechanisms in older *Drosophila* adults (Kayser et al., 2014).

Could the effects of neuropeptide overexpression be due to altered temporal dynamics of SIS?

In my neuropeptide overexpression experiments, I used heat to induce somatic transcription of the NLP-22 or FLP-13 neuropeptides. However, as demonstrated here and previously, heat exposure can also directly trigger behavioral quiescence via induction of cellular stress (Cassada and Russell, 1975; Jones and Candido, 1999; Raizen et al., 2008; Nelson et al., 2013; Hill et al., 2014). Therefore, it is possible that the quiescence-inducing effects of neuropeptide overexpression are confounded by the quiescence observed during SIS. To minimize this possibility, I used a lower temperature, 33°C versus 35°C, and a later analysis time point, 2-3 hours after heat exposure versus 35-45 minutes after heat exposure, to examine quiescence in response to neuropeptide overexpression. Acute feeding quiescence is less severe after 33°C exposure than after 35°C exposure (Nelson et al, 2014), and the behavioral effects of a 30-minute heat shock at 33°C dissipate fully by two hours after heat exposure (Lee et al., 1997; Nelson et al., 2013; 2014). I also repeated the neuropeptide overexpression experiments in *ceh-17* mutants, which have defective SIS (Hill et al., 2014; Nelson et al., 2014), and found no changes in the quiescence observed in response to neuropeptide overexpression. Finally, I found that 35 minutes after a mild heat shock at 29°C, worms overexpressing *flp-13* were quiescent while worms overexpressing *nlp-22* were not. This suggests that the behavioral effects of *nlp-22* overexpression are not due to an interaction between neuropeptide overexpression and recovery of cellular stress. Since I did observe acute feeding quiescence using the milder 29°C exposure in animals carrying the *Phsp-16.2::flp-13*

transgene but not in wild-type animals (Nelson et al, 2014), it is possible that overexpression of *flp-13* may amplify the acute stress response, affirming the important role of *flp-13* in SIS.

Feeding quiescence during DTS results from altered pharyngeal muscle excitability

My results indicate that pharyngeal muscle is not excitable during DTS. Even with direct optogenetic stimulation of pharyngeal muscle, no Ca^{2+} increase was observed during DTS, suggesting that Ca^{2+} entry is impaired during this state. Insofar as pharyngeal Ca^{2+} increase during feeding occurs primarily via the L-type voltage-gated Ca^{2+} channel EGL-19 (Lee et al., 1997; Shtonda and Avery, 2005), my results suggest that the EGL-19 Ca^{2+} current is decreased during DTS. Transcriptional expression of the *egl-19* gene is unchanged during DTS (George-Raizen et al., 2014), so the reduction in the EGL-19 current is likely due to a post-transcriptional change. This change could occur directly, via modulation of EGL-19 protein expression or function, or indirectly, via an increase in inhibitory currents carried by potassium and/or chloride channels. My data also suggest that NLP-22 directly inhibits pharyngeal muscle during DTS, though it must act in parallel to other mechanisms because feeding quiescence is weakened but not abolished in *nlp-22* mutants (Nelson et al., 2013). NLP-22, like other neuropeptides, may act through a G-protein coupled receptor to inhibit feeding. Alternatively, like certain small peptides such as *Drosophila* SLEEPLESS (Koh et al., 2008), it may act like a toxin and interact with ion channels directly (Wu et al., 2010; Dean et al., 2011; Wu et al., 2014). The receptor for NLP-22 is unknown.

Why is quiescence during DTS and SIS engaged differently?

While feeding and locomotion quiescence are both characteristics of DTS, recent data from many labs supports my conclusion that feeding and locomotion are inhibited at different levels. Several mutants have been described with impaired locomotion quiescence throughout DTS (Raizen et al., 2008; Singh et al., 2011; Belfer et al., 2013; Choi et al., 2013; Nelson et al., 2013; Schwarz and Bringmann, 2013; Turek et al., 2013; Singh et al., 2014), and DTS locomotion quiescence can be reduced by mechanical stimulation (Raizen et al., 2008; Driver et al., 2013; Nagy et al., 2014). However, mutations that suppress locomotion quiescence do not appear to affect feeding quiescence, as no mutant has been described to feed throughout DTS. It is possible that feeding quiescence during DTS is essential for viability.

The differing mechanisms for behavioral quiescence during DTS and SIS may reflect the relative importance of the different types of quiescence for survival. DTS is accompanied by a molt (Singh and Sulston, 1978) and occurs at the end of each of the four larval stages, when the worm has not yet reached reproductive maturity. The completion of each molt is essential for survival and reproduction (Frand et al., 2005), so there is strong selection for worms that can molt successfully. The correct replacement of the pharyngeal cuticle appears to be a vital part of DTS, as defective pharyngeal molting can be lethal (Singh and Sulston, 1978). By inhibiting feeding at the level of muscle excitability, the worm increases the likelihood that the pharyngeal cuticle will form properly, since no stray neural impulses or neuromodulation could trigger muscle

contraction that might disrupt cuticular assembly. Interestingly, mutations that severely decrease quiescence during SIS can also have a small effect on quiescence during DTS (Van Buskirk and Sternberg, 2007), suggesting that molting may be stressful and weakly stimulate SIS.

In contrast to the precise timing of DTS, the environmental stresses that trigger SIS can happen at any point in the life of a worm and no SIS-associated structural or morphological changes have been identified. Failure to engage proper SIS is rarely lethal in the first 24 hours after stress (Hill et al., 2014), so pharyngeal contraction during this state may not be as detrimental to survival. In fact, by inducing quiescence at the level of the nervous system, the worm retains the ability to use other neuromodulators, such as 5-HT, to stimulate feeding during SIS. This implies that although quiescence increases the likelihood of survival in response to cellular stressors (Hill et al., 2014), there may be conditions under which feeding during this state is beneficial.

DTS and SIS may be functionally conserved, and are regulated by evolutionarily conserved signaling pathways

There is no evidence to suggest that DTS and SIS represent evolutionary forms of sub-types of mammalian sleep. However, DTS and SIS may serve functions similar to different aspects of mammalian sleep: DTS, which occurs in phase with cycling of the *C. elegans* homolog of the PERIOD gene (Monsalve et al., 2011), has been implicated in synaptic plasticity (Dabbish and Raizen, 2011) and synthetic metabolism (Frand et al., 2005; Driver et al., 2013), while SIS is important for survival following physiological

stressors (Hill et al., 2014). Likewise, mammalian sleep has been implicated in synaptic plasticity (Tononi and Cirelli, 2014), anabolic metabolism (Mackiewicz et al., 2007), and stress responses (Toth and Krueger, 1988; Rampin et al., 1991).

The signaling pathways investigated here, as well as other previously identified regulators of DTS (Raizen et al., 2008; Singh et al., 2011; Belfer et al., 2013; Choi et al., 2013; Driver et al., 2013; Iwanir et al., 2013; Nagy et al., 2013; Nelson et al., 2013; Schwarz and Bringmann, 2013; Turek et al., 2013; Nagy et al., 2014; Singh et al., 2014) and SIS (Hill et al., 2014; Nelson et al., 2014), are found in many cell and neuron types and are highly conserved. These pathways have been implicated in sleep regulation in a variety of species (Allada and Siegel, 2008; Zimmerman et al., 2008; Crocker and Sehgal, 2010; Nelson and Raizen, 2013; Singh et al., 2014), but their ubiquitous expression patterns have made identification of specific cellular and circuit functions for these pathways challenging (but see (Crocker et al., 2010)). By identifying how these genes affect circuits that regulate different sleep states, we will gain insight into the mechanisms and functions of sleep across all species.

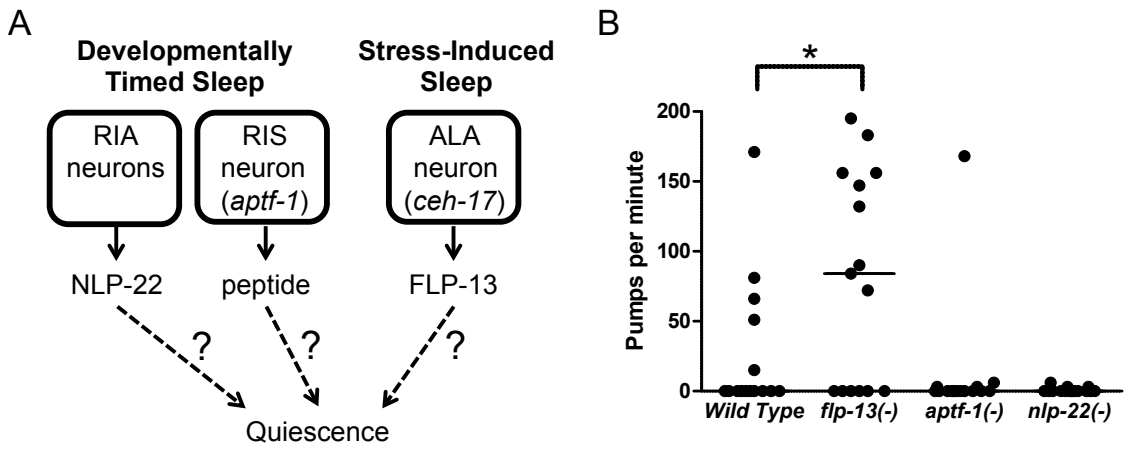

Figure 3.1: Quiescence during DTS and SIS is mediated by different neuropeptides. **A:** Schematic representing the known pathways that control quiescence during DTS and SIS. In DTS, the RIA neurons release NLP-22, while the RIS neuron releases an unidentified peptide. The *aptf-1* gene is required for the function of the RIS neuron and the *ceh-17* gene is required for the function of the ALA neuron. During SIS, the ALA neuron releases the FLP-13 neuropeptides. It is unknown how these neuropeptides lead to behavioral quiescence. **B:** Feeding quiescence during SIS does not require pathways that regulate DTS. Mutants defective in RIA and RIS signaling (*nlp-22* and *aptf-1* mutants, respectively) have normal feeding quiescence during SIS. Each point represents an observation from one worm, and the horizontal bar represents the median of each group. N=15 for each group. Statistical significance was calculated using the Mann-Whitney test. *P<0.05.

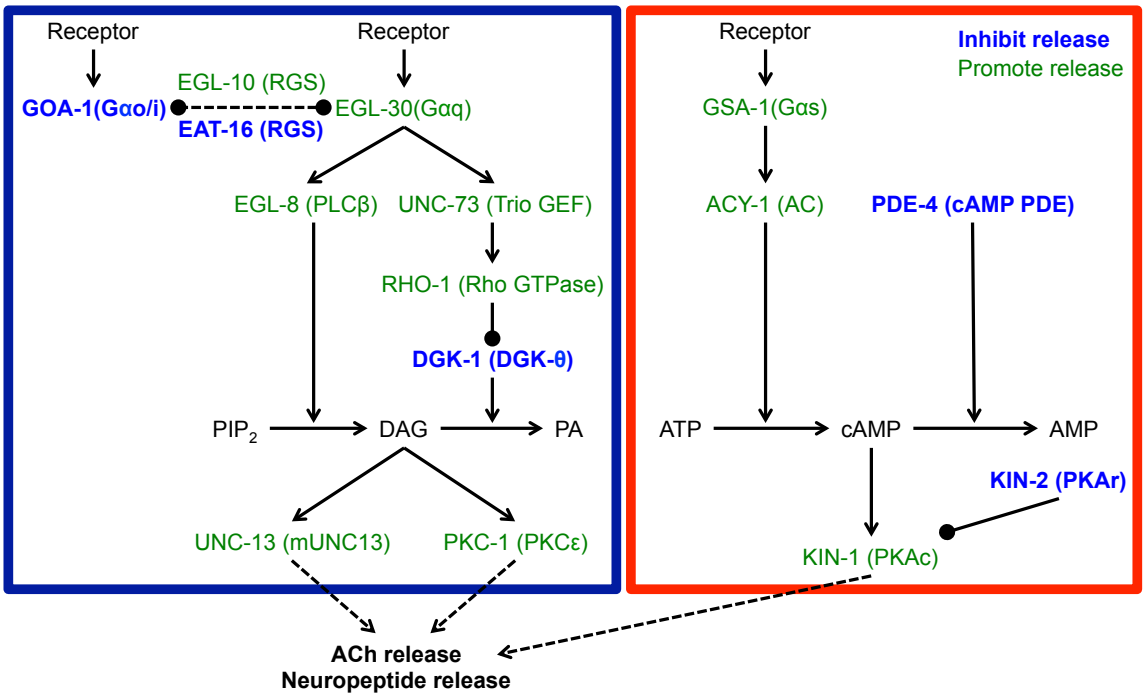

Figure 3.2: Schematic representation of the Gαq and Gαs pathways that regulate neurotransmitter secretion in *C. elegans*. Gαq signaling causes increased diacylglycerol (DAG) levels, while the Gαs pathway causes increased cAMP levels. *C. elegans* proteins names are shown in uppercase letters and mammalian homolog names are shown in parentheses. The blue box surrounds the Gαq pathway, while the red box surrounds the Gαs pathway. Proteins labeled in blue inhibit neurotransmitter release, while those in green promote release. Lines ending in arrows are positive regulation; lines ending in balls are negative regulation. Figure modeled after Perez-Mansilla and Nurrish, 2009.

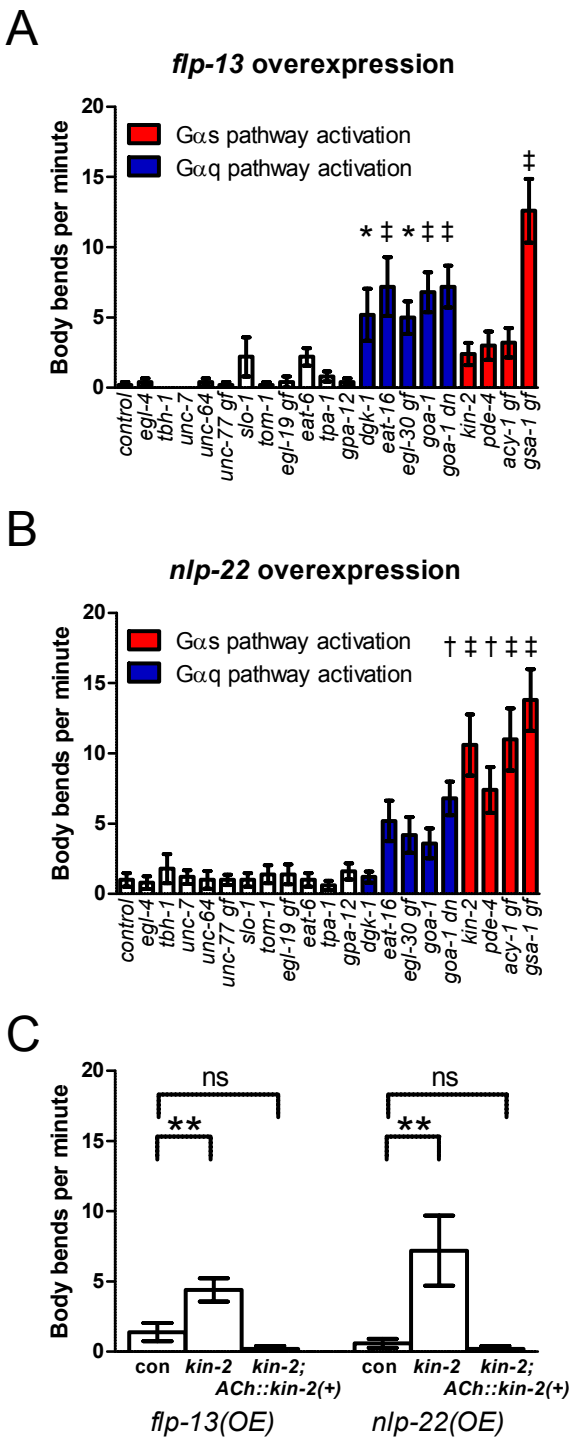

Figure 3.3: Activation of Gαq or Gαs pathways impairs locomotion quiescence caused by *flp-13* or *nlp-22* overexpression. A: Mutations that increase Gαq or Gαs

signaling impair locomotion quiescence after *flp-13* overexpression. **B:** Mutations that increase Gαq or Gαs signaling impair locomotion quiescence after *nlp-22* overexpression. For A and B, each bar represents the mean ± SEM of body bends for 12-15 worms during a 20-second window. Each bar represents the data obtained for a different mutant strain containing the designated overexpression transgene. For detailed genotypes and data, see Table 2. 'gf' denotes gain-of-function mutation, 'dn' denotes dominant negative mutation. The others are loss of function mutations. Statistical significance was calculated using one-way ANOVA followed by Dunnett's multiple comparison tests. *P<0.05, †P<0.01, ‡P<0.001. **C:** Rescuing *kin-2* function in cholinergic neurons using the *unc-17* promoter rescues the effects of the *kin-2* mutation on locomotion quiescence after *flp-13* or *nlp-22* overexpression. 'Con' designates the *flp-13* overexpression and *nlp-22* overexpression control strains, NQ570 or NQ251, respectively. N=13-15. Each bar represents mean ± SEM. Statistical significance was calculated using one-way ANOVA followed by Dunnett's multiple comparison tests. *P<0.05, **P<0.01, ***P<0.001.

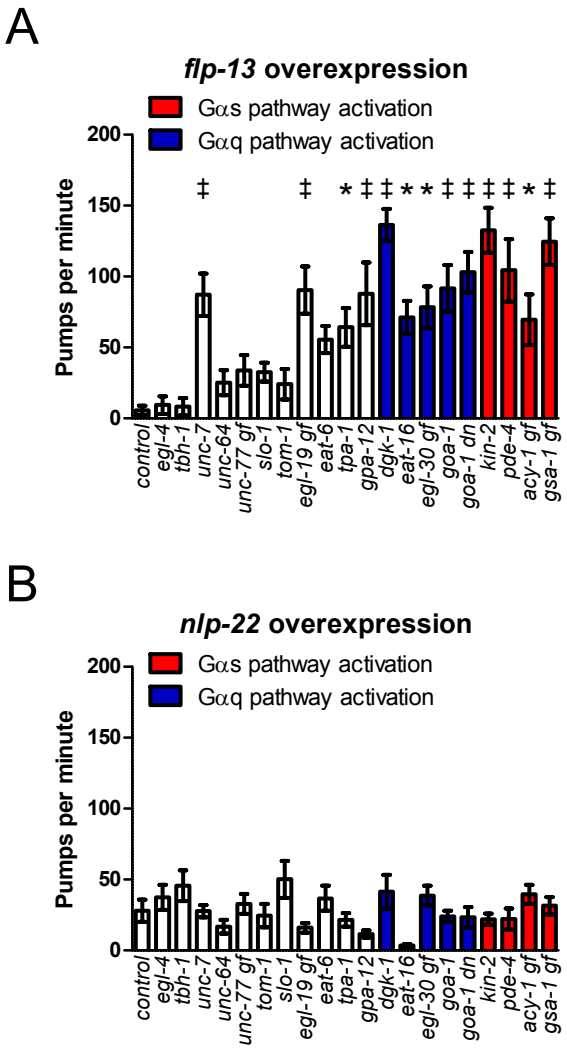

Figure 3.4: Activation of Gαq or Gαs pathways impairs feeding quiescence caused by *flp-13* overexpression but not that caused by *nlp-22* overexpression. A: Mutations that increase Gαq or Gαs signaling impair feeding quiescence after *flp-13* overexpression relative to the control *flp-13* overexpression strain. **B:** Mutations that increase Gαq or Gαs signaling do not affect feeding rate after *nlp-22* overexpression relative to the control *nlp-22* overexpression strain. 'gf' denotes gain-of-function mutation, 'dn' denotes dominant negative mutation. The others are loss of function mutations. Each bar

represents the mean ± SEM of pharyngeal pumps for 12-15 worms during a 20-second window for a different mutant strain containing the designated overexpression transgene. Statistical significance was calculated using a one-way ANOVA followed by Dunnett's multiple comparison tests. *P<0.05, †P<0.01, ‡P<0.001.

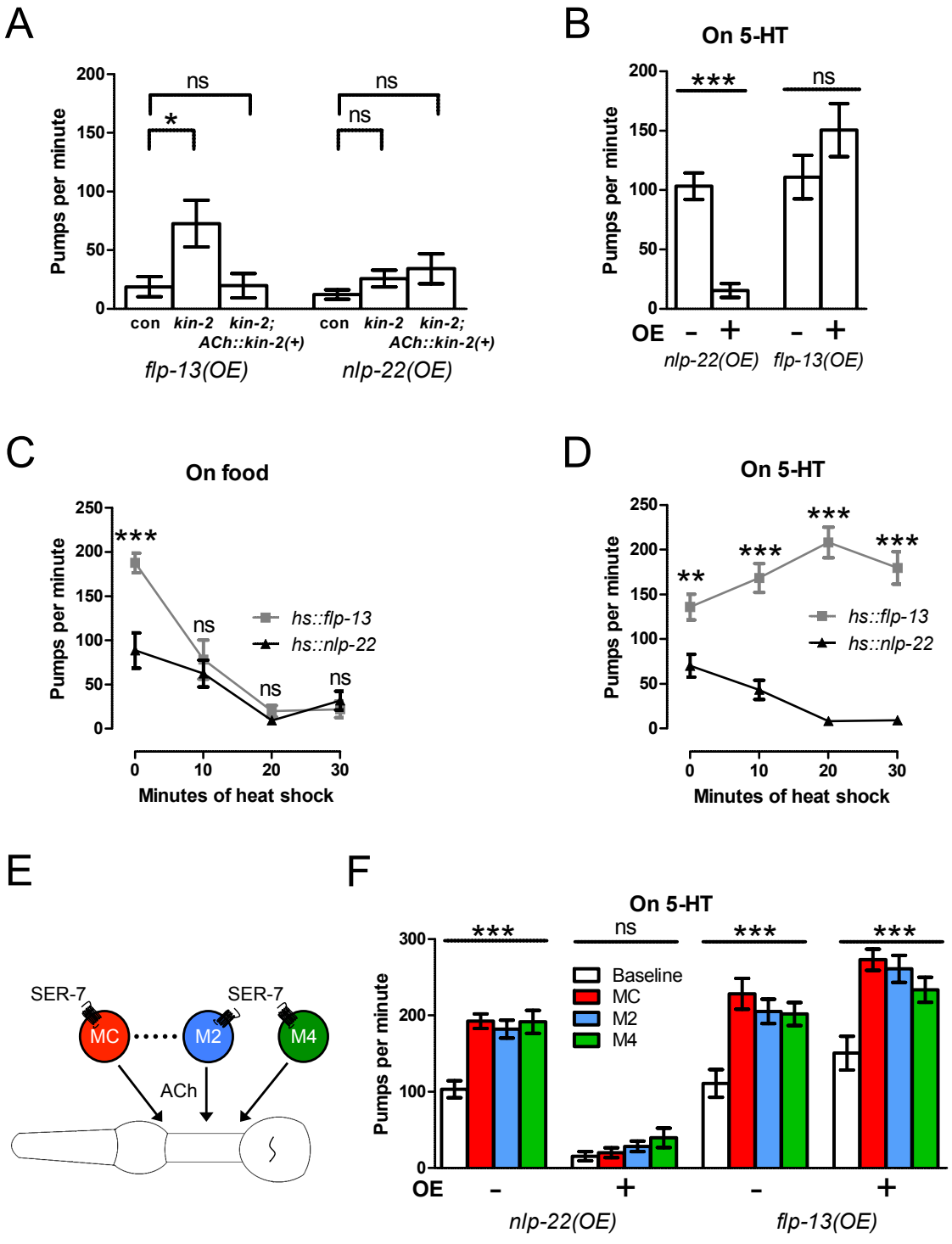

Figure 3.5: FLP-13 inhibits pharyngeal pumping by acting on neurons, but NLP-22 inhibits feeding downstream of motor neuron excitation. A: Rescuing *kin-2* function

in cholinergic neurons using the *unc-17* promoter rescues the effect of the *kin-2* mutation on feeding quiescence induced by *flp-13* overexpression but does not affect feeding quiescence induced by *nlp-22* overexpression. 'Con' designates the *flp-13* overexpression and *nlp-22* overexpression control strains, NQ570 or NQ251, respectively. N=13-15. Each bar represents mean ± SEM. Statistical significance was calculated using one-way ANOVA followed by Dunnett's multiple comparison tests. **B**: In immobilized worms, 5-HT blocks the inhibitory effect of *flp-13* overexpression on feeding but not that of *nlp-22* overexpression on feeding. N=10. Each bar represents mean ± SEM. Statistical significance was calculated using Student's *t*-test. **C**: *flp-13* overexpression and *nlp-22* overexpression cause similar effects on feeding in worms in the presence of food when overexpressed to similar degrees. N=9-15. Each point represents mean ± SEM. Statistical significance was calculated using a two-way ANOVA. **D:** The difference in the effects of 5-HT on feeding rate in immobilized worms after *flp-13* overexpression and *nlp-22* overexpression is not affected by the degree of neuropeptide overexpression. N=9-15. Each point represents mean ± SEM. Statistical significance was calculated using a two-way ANOVA. **E:** Schematic of the excitatory cholinergic pharyngeal neurons and SER-7 5-HT receptor. **F:** Optogenetic excitation of the pharyngeal cholinergic motor neurons MC, M2, and M4 stimulates pumping in immobilized worms after *flp-13* overexpression but not after *nlp-22* overexpression. N=10. Each bar represents mean ± SEM. Statistical significance was calculated using a one-way ANOVA. *P<0.05, **P<0.01, ***P<0.001.

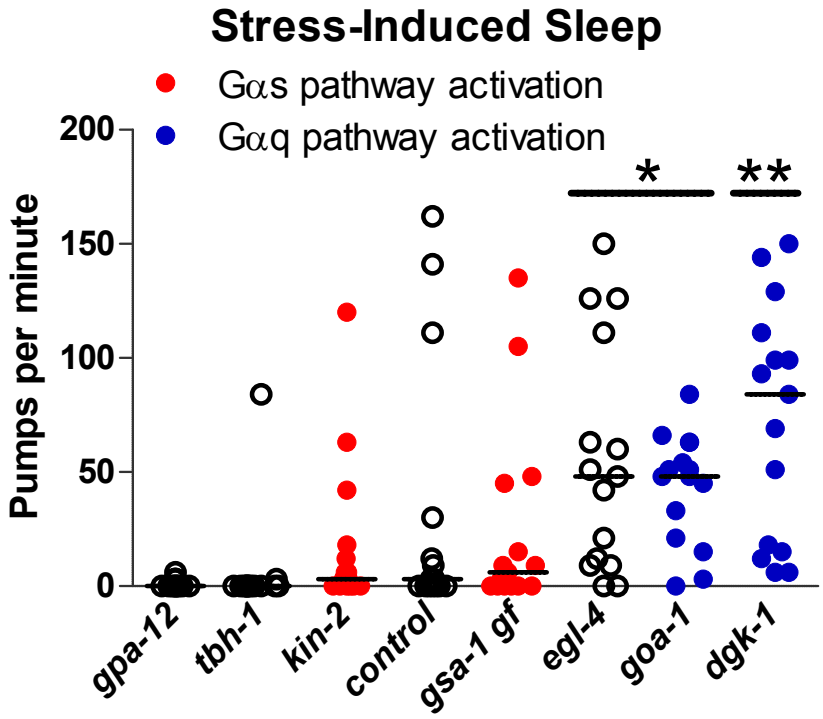

Figure 3.6: Activation of Gαq but not Gαs pathway impairs feeding quiescence during SIS. Mutants with increased DAG levels due to activation of the Gαq pathway have increased feeding during SIS, but mutants with an activated Gαs pathway do not. In addition, an *egl-4* mutation impairs feeding quiescence during SIS. Each point represents an observation from one worm, and the horizontal bar represents the median of each group. N=15 for each group. Statistical significance was calculated using the Mann-Whitney test. *P<0.05, **P<0.01.

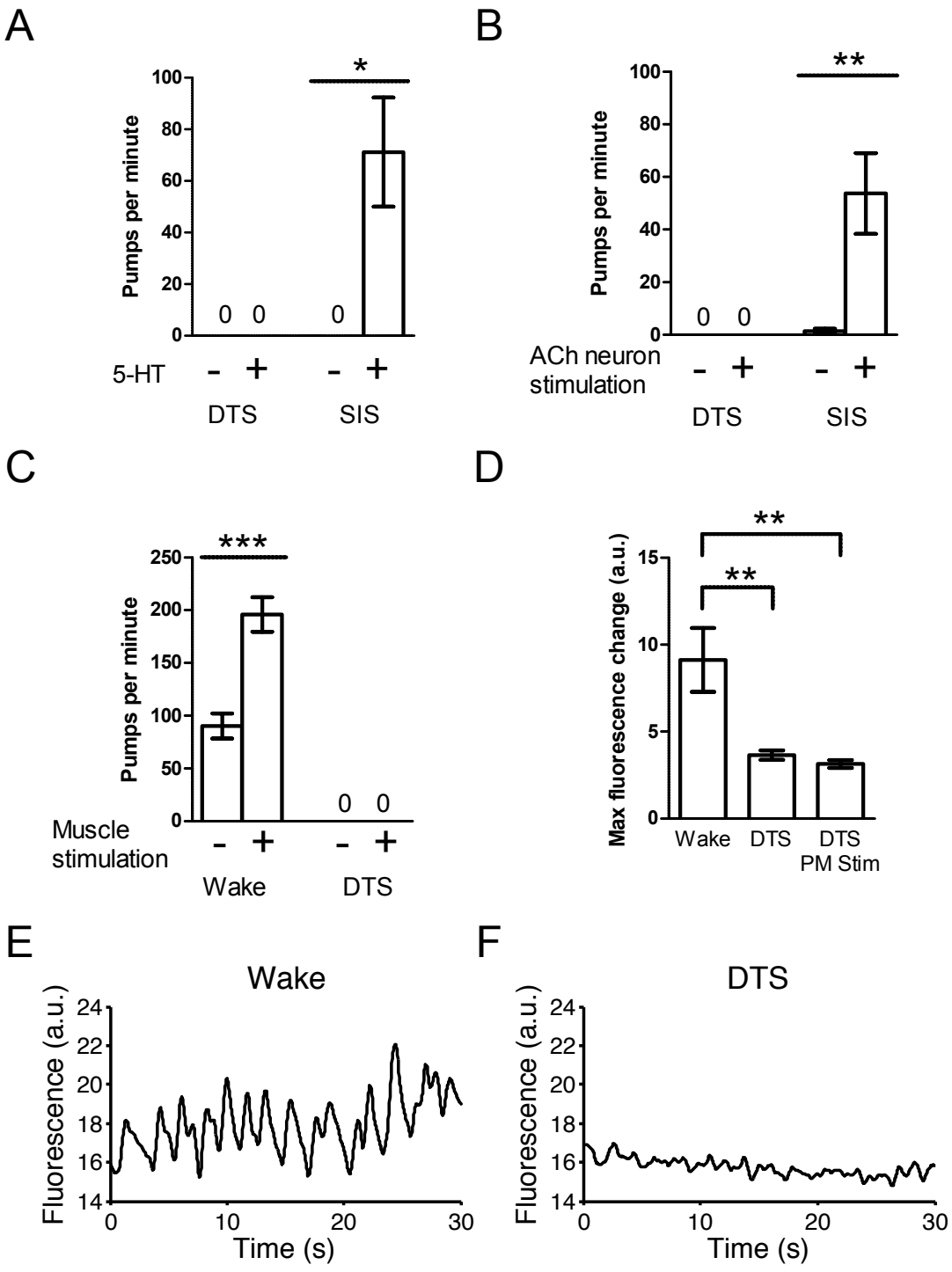

Figure 3.7: The pharyngeal nervous system can excite feeding during SIS but not during DTS. A: 10 mM 5-HT stimulates feeding during SIS but not during DTS. N=8-

10. **B:** Optogenetic excitation of all cholinergic pharyngeal neurons (AChN) by wide-field fluorescence stimulates feeding in worms on bacterially seeded agar plates during SIS but not DTS. N=13 for each group. **C:** Optogenetic excitation of pharyngeal muscle stimulates feeding in the presence of 10 mM 5-HT during wake but not during DTS. N=10. **D:** Ca^{2+} transients are absent from pharyngeal muscle during DTS, and cannot be stimulated by muscle excitation. The difference between maximum and minimum GCaMP6s intensity of a region of the metacorpus of the pharynx during an approximately 30 second interval was calculated for each condition to measure the magnitude of Ca^{2+} transients. N=10. **E:** GCaMP6s fluorescence from a region of the metacorpus from one representative worm during wake. **F:** GCaMP6s fluorescence from a region of the metacorpus from one representative worm during DTS. a.u. denotes arbitrary units in D, E, and F. Statistical significance was calculated using Student's *t*-test. *P<0.05, **P<0.01, ***P<0.001.

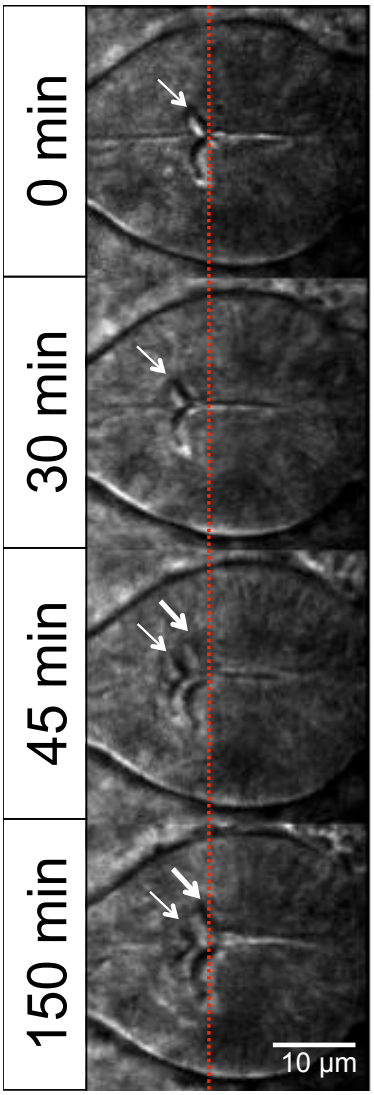

Figure 3.8: **The pharyngeal cuticle is replaced during DTS**. Pictures show a wild-type posterior pharynx at the start (0 minutes after pumping cessation), early (30 minutes after pumping cessation), early middle (45 minutes after pumping cessation), and end (150 minutes after pumping cessation) of the fourth larval stage (L4) DTS molt. Thin and thick arrows denote the L4 and adult grinders, respectively. Red dashed line represents the position of the L4 grinder at the beginning of the L4 DTS molt. Anterior is to the left.

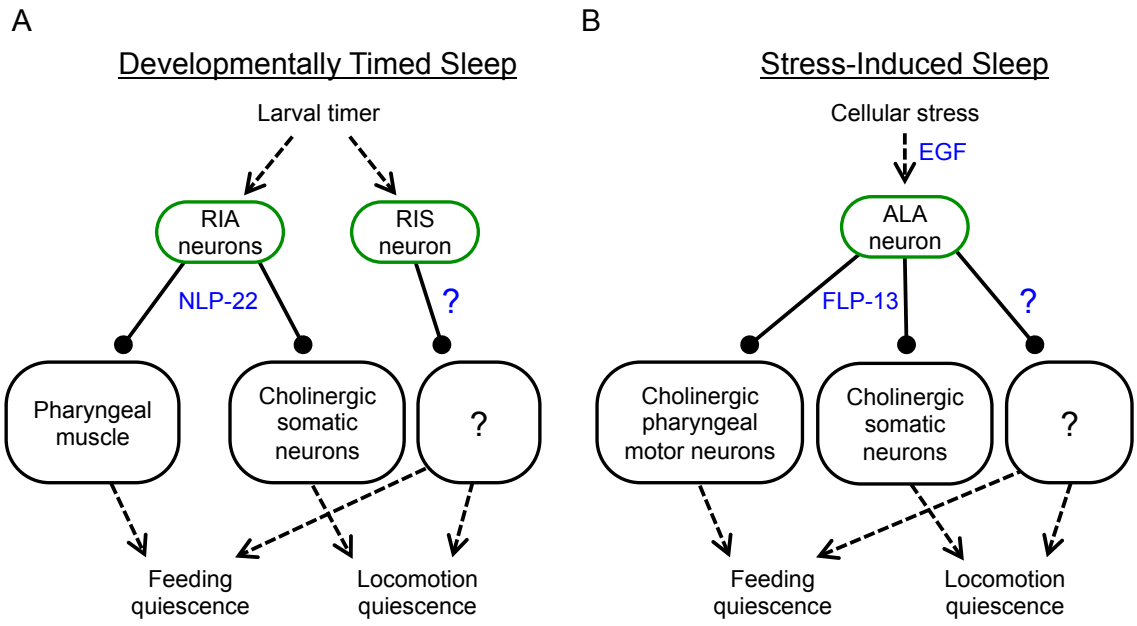

Figure 3.9: Model for quiescence regulation during SIS and DTS. Green ovals represent somatic interneurons and blue text represents molecular mechanisms. Solid lines with arrowheads represent positive regulation, and solid lines with balls on the end represent negative regulation. Dotted lines represent conceptual rather than molecular connections **A:** During DTS, an unidentified larval timer causes the RIA interneurons to release NLP-22. NLP-22 inhibits feeding by acting directly on pharyngeal muscles, and inhibits locomotion via cholinergic neurons. The RIS interneuron also regulates feeding and locomotion quiescence during DTS. **B:** Cellular stress triggers release of LIN-3/EGF from an unknown source, which then activates the ALA interneuron, causing release of FLP-13 and other neurotransmitter(s). FLP-13 inhibits feeding and locomotion by acting on pharyngeal and somatic (non-pharyngeal) cholinergic neurons, respectively.

Table 3.1: Mutants studied in Figures 3 and 4

Gene	Δ	Vertebrate homolog	Reason chosen	Reference
gsa-1	G	Gαs	reduced lethargus quiescence; resistant to isoflurane	(Saifee et al., 2011; Schwarz and Bringmann, 2013)
acy-1	G	Adenylate cyclase	reduced lethargus quiescence	(Iwanir et al., 2013)
pde-4	L	PDE4	reduced lethargus quiescence	(Singh et al., 2014)
kin-2	L	PKA regulatory subunit	reduced lethargus quiescence; resistant to isoflurane	(Saifee et al., 2011; Belfer et al., 2013)
goa-1	D	Gαi/o	reduced lethargus quiescence	(Singh et al., 2014)
goa-1	L	Gαi/o	resistant to halothane	(van Swinderen et al., 2001)
egl-30	G	Gαq	reduced lethargus quiescence; resistant to halothane	(Hawasli et al., 2004; Schwarz and Bringmann, 2013)
eat-16	L	Gαq RGS	resistant to halothane and isoflurane	(van Swinderen et al., 2001)
dgk-1	L	DGK-θ	resistant to halothane	(van Swinderen et al., 2002)
gpa-12	L	Gα12	activation inhibits feeding	(van der Linden et al., 2003)
tpa-1	L	PKCδ	suppresses effects of *gpa-12* activation	(van der Linden et al., 2003)
eat-6	L	Na^+/K^+ ATPase	depolarized pharyngeal muscle	(Davis et al., 1995)
egl-19	G	L-type Ca^{2+} channel	prolonged pharyngeal action potential	(Lee et al., 1997)
tom-1	L	Tomosyn	increased neurotransmission	(Dybbs et al., 2005)
slo-1	L	BK channel	increased neurotransmission; resistant to halothane	(Wang et al., 2001; Hawasli et al., 2004)
unc-77	G	NALCN channel	resistant to halothane	(Humphrey et al., 2007)
unc-64	N	Syntaxin	resistant to halothane and isoflurane	(van Swinderen et al., 1999)
unc-7	L	Innexin	resistant to halothane	(Morgan et al., 1990)
tbh-1	L	Tyramine β-hydroxylase	opposes 5-HT response	(Wragg et al., 2007)
egl-4	L	PKG	reduced lethargus quiescence	(Raizen et al., 2008)

Δ: change in function; D: dominant negative; N: neomorph; G: gain; L: loss

Table 3.2: Detailed data for Figures 3 and 4

Gene	Δ	mutant; *flp-13* overexpression							mutant; *nlp-22* overexpression						
		ppm	SD	Sig	bpm	SD	Sig	N	ppm	SD	Sig	bpm	SD	Sig	N
gsa-1	G	133.5	55.6	***	13.5	8.4	***	14	31.6	24.0	ns	13.8	8.5	***	15
acy-1	G	69.6	69.1	*	3.2	4.0	ns	15	39.6	25.6	ns	11.0	8.5	***	15
pde-4	L	130.5	74.8	***	3.8	4.1	ns	12	22.2	28.5	ns	7.4	6.3	**	15
kin-2	L	132.6	61.4	***	2.4	3.0	ns	15	22.0	14.9	ns	10.6	8.4	***	15
goa-1	D	91.6	64.1	***	6.8	5.5	***	15	24.0	15.3	ns	3.6	4.1	ns	15
goa-1	L	103.0	55.7	***	7.2	5.8	***	15	23.4	27.9	ns	6.8	4.6	**	15
egl-30	G	78.4	57.1	**	5.0	4.5	*	15	38.8	27.1	ns	4.2	4.9	ns	15
eat-16	L	71.2	44.6	*	7.2	8.1	***	15	3.6	3.6	ns	5.2	5.6	ns	15
dgk-1	L	136.4	43.7	***	5.2	7.2	*	15	41.4	46.7	ns	1.2	1.5	ns	15
gpa-12	L	87.8	85.5	***	0.4	1.1	ns	15	11.6	9.5	ns	1.6	2.2	ns	15
tpa-1	L	64.2	52.7	*	0.8	1.4	ns	15	21.6	18.6	ns	0.6	1.2	ns	15
eat-6	L	59.6	34.6	ns	2.4	2.4	ns	14	36.8	34.6	ns	1.0	1.9	ns	15
egl-19	G	90.4	64.4	***	0.4	1.5	ns	15	16.0	13.2	ns	1.4	2.7	ns	15
tom-1	L	24.2	41.8	ns	0.2	0.8	ns	15	24.6	31.4	ns	1.4	2.5	ns	15
slo-1	L	32.6	25.8	ns	2.2	5.4	ns	15	50.2	50.6	ns	1.0	1.9	ns	15
unc-77	G	33.8	41.9	ns	0.2	0.8	ns	15	32.8	27.5	ns	1.0	1.5	ns	15
unc-64	N	27.0	34.8	ns	0.4	1.1	ns	14	16.8	18.6	ns	1.0	2.4	ns	15
unc-7	L	87.2	57.6	***	0.0	0.0	ns	15	27.8	16.8	ns	1.2	1.9	ns	15
tbh-1	L	8.2	23.9	ns	0.0	0.0	ns	15	45.8	42.1	ns	1.8	4.1	ns	15
egl-4	L	9.4	24.2	ns	0.4	1.1	ns	15	37.4	34.1	ns	0.8	1.8	ns	15
None		5.8	12.2		0.2	0.8		15	28.0	30.9		1.0	1.9		15

Δ: change in function; D: dominant negative; N: neomorph; G: gain; L: loss

Underlined indicates twitching phenotype; ppm indicates pumps/minute; bpm indicates body bends/minute

* $p<0.05$, ** $p<0.01$, *** $p<0.001$, by Dunnett's multiple comparison test after one way ANOVA.

CHAPTER 4: General Discussion and Future Directions

The goal of this work was to understand how the neural circuit controlling *C. elegans* feeding operates during wake and sleep. Using pharmacological, genetic, and optogenetic approaches, I identified a small circuit of cholinergic neurons that degenerately controls pumping rate. I subsequently identified two distinct mechanisms that underlie feeding quiescence during different sleep states, revealing that behaviorally indistinguishable invertebrate sleep states can be physiologically distinct.

I found that although ablation of most cholinergic pharyngeal neurons does not affect behavior, optogenetic manipulation of these neurons revealed their functions. Though they have been investigated by laser ablation, the functions of many somatic neurons are also poorly understood (de Bono and Maricq, 2005). By acutely stimulating and inhibiting individual neurons, it will be possible to identify roles for redundant or degenerate neurons, for which ablation has no effect, in a state dependent manner. For example, a systematic screen similar to the one I performed could identify neurons that promote or inhibit egg laying or defecation in different behavioral states, such as sleep or starvation.

The pharyngeal nervous system is robust, evolvable, and degenerate

Degeneracy, the ability of structurally distinct elements of a system to perform the same function under certain conditions (Tononi et al., 1999), is ubiquitous throughout biology. The nature of these elements can vary widely, from nucleotides to entire organs (Edelman

and Gally, 2001). Theoretical work suggests that degeneracy represents a compromise between robustness, or the insensitivity of a system to a specific set of conditions, and evolvability, or the capacity of a system to generate new phenotypes (Whitacre and Bender, 2010).

Laser ablation experiments have previously demonstrated the robustness of the pharyngeal nervous system, as killing most classes of pharyngeal neurons has no obvious effect on feeding (Avery and Horvitz, 1989; Raizen et al., 1995). However, I have demonstrated that acute excitation or inhibition of many classes of pharyngeal cholinergic neurons does affect feeding rate, in apparent conflict with the laser ablation results. A possible explanation for this discrepancy is that the system may be homeostatically regulated, such that when some neurons are destroyed then others will compensate to replace their function. Recent theoretical experiments have demonstrated that homeostatic compensation after alterations in circuit function, such as might be caused by laser ablation, can lead to either restoration of function or pathological alteration of function, depending on the alteration (O'Leary et al., 2014). Thus, perhaps after ablation of M2 the homeostatic mechanisms allow for recovery of function, while these mechanisms produce aberrant behavior after MC ablation. Detailed analysis of neural activity patterns is required to further explore these ideas.

The evolvability of the pharyngeal nervous system has only become apparent more recently. The predatory nematode *Pristionchus pacificus,* which diverged from *C. elegans* approximately 300 million years ago (Pires-daSilva and Sommer, 2004), has morphological features consistent with its altered diet, such as the tooth-like denticle that

it uses to prey on beetles and other nematodes. Despite this difference in morphology and feeding strategy, *C. elegans* and *P. pacificus* have a very similar synaptic connectivity of their pharyngeal nervous systems, and the morphologies of pharyngeal neuronal process are nearly identical (Bumbarger et al., 2013). There is also evidence of functional conservation between the species: the M4 neuron is required for peristalsis and can promote pumping in *C. elegans*, and M4 ablation in *P. pacificus* causes a mild decrease in peristalsis and pumping rates (Chiang et al., 2006; Song and Avery, 2012; Steciuk et al., 2014). Just as I found in *C. elegans*, the M2 neurons are excitatory for pumping in a third species of nematode, *Panagrolaimus sp. PS1159* (Chiang et al., 2006). Anatomical reconstructions of pharyngeal nervous systems of even more diverse nematode species, including the fungal feeder *Aphelenchus avenae* (Ragsdale et al., 2010), reveal at least partial anatomical homology with *C. elegans* pharyngeal nervous system, though the functional homology of pharyngeal neurons is difficult to test due to the lack of transgenic tools available in these species. While it is unclear if these similarities in function and morphology are due to independent evolution from a common ancestor with a very different pharyngeal nervous system structure or represent only slight deviations from an ancestor with a pharyngeal nervous system similar to those described, the structure of the pharyngeal nervous system appears to have evolutionarily advantageous properties (Katz and Lillvis, 2014). Experimental evolution in *E. coli* has shown that evolvability is subject to natural selection (Woods et al., 2011), suggesting that in fact the structure and function of pharyngeal nervous system of *C. elegans* and other nematodes may have been selected for because of its evolvability.

As expected from a system that is robust and evolvable, I found that the pharyngeal nervous system has neural and genetic degeneracy: the cholinergic MC, M2, and M4 motor neurons each can directly stimulate pumping, and the MC neurons can act via nicotinic or muscarinic acetylcholine receptors. The implications of neural degeneracy are best understood in the crustacean stomatogastric nervous system, where computational and experimental studies have found that different neuromodulators can invoke similar activity patterns on the single neuron (Harris-Warrick and Flamm, 1987) or network level (Saideman et al., 2007; Rodriguez et al., 2013), and similar network outputs can be achieved through different combinations of cellular parameters (Prinz et al., 2004; Schulz et al., 2007; Goaillard et al., 2009; Gutierrez et al., 2013). In this system, as well as in the leech heartbeat system, a high degree of individual variability has been found in a population of animals that produce similar behaviors in their native conditions (Bucher et al., 2005; Norris et al., 2007a; 2007b), suggesting that natural selection has set constraints on the output of the system rather than on the mechanisms by which the system generates the output (Edelman and Gally, 2001). Thus, each animal can respond in a different manner to changes in environment or physiology, leading to subsequent selection for animals that respond favorably to any prolonged change in conditions. This difference in fitness after a change in conditions has been observed in the mollusc, where individual variability is not apparent under normal conditions but is revealed by different responses to an injury (Sakurai et al., 2014). If this change in environment persists, organisms that have responded in a favorable way will be selected for over organisms that respond less favorably even if their initial fitness was similar, as

has been demonstrated by experimental evolution in *E. coli* (Ostrowski et al., 2005; 2008).

In this context, it is intriguing to speculate how the neural and genetic degeneracy of the pharyngeal nervous system contributes to the fact that species that have diverged for 300 million years perform different pharyngeal behaviors despite having the same complement of neurons with similar morphology (Bumbarger et al., 2013). For a system to be degenerate it must have multi-functional components, and many pharyngeal neurons are both highly connected and have sensory endings and neuromuscular synapses (Albertson and Thomson, 1976, WormWiring.org), suggesting these neurons are indeed multi-functional. I did not directly examine individual variability in the ability of different classes of cholinergic neurons to stimulate pumping, but the degeneracy of the pharyngeal nervous system suggests worms can produce similar feeding behavior by different mechanisms. This means that some worms might respond differently to certain perturbations, and the subsequent differences in fitness will lead to the development of new species with similar underlying neural circuits and genetics (Edelman and Gally, 2001). For example, if different lines of *C. elegans* were to evolve in isolation under the same conditions for tens of thousands of generations, as was done experimentally with *E. coli* (Wiser et al., 2013), the gross morphology of the pharyngeal nervous system may be similar across each line, but the underlying mechanisms of feeding regulation may vary in ways that can be revealed by exposing the lines to different environments.

In addition to providing robustness, degeneracy can be a means for allowing a system to respond appropriately to a given perturbation under different behavioral states (Gutierrez

et al., 2013). Depending on other cellular or network parameters, or during different behavioral states, the same neuromodulator can have disparate effects on network function (Gutierrez and Marder, 2014). The relatively simple behavioral repertoire of *C. elegans* means that its behavior is readily quantified, so behavioral states and effects of neuromodulator manipulation can be clearly distinguished (de Bono and Maricq, 2005). While activation of MC, M2, or M4 has similar effects on pumping rate in my experiments, it is possible that under different conditions their effects on behavior will diverge. Testing this will require performing similar experiments on worms raised or maintained under different conditions, such as different types of food or atmospheric conditions, or in the presence of various neuromodulators.

Many aspects of pharyngeal nervous system function are still not well understood

Although we now have evidence that multiple pharyngeal cholinergic neurons control pumping, we do not yet know the activity patterns of these neurons under any conditions. Electrophysiological recordings from pharyngeal muscle show MC-dependent depolarizations that resemble post-synaptic potentials, suggesting the MC neurons may provide rhythmic input onto pharyngeal muscle (Raizen et al., 1995). However, I have shown that tonic depolarization of the MC neurons or pharyngeal muscle is sufficient to drive rapid pumping, suggesting the MC neurons may not have rhythmic activity. Electrophysiological recordings from the neurons is not yet possible, so an important next step will be to develop and implement fluorescent Ca^{2+} and voltage reporters with sufficient speed and signal-to-noise ratio to monitor the activity of these neurons. Whole

brain activity imaging has recently been performed in *C. elegans* (Schrödel et al., 2013; Prevedel et al., 2014), an approach that can be applied to the pharyngeal nervous system using a recently identified gene promoter fragment specific to pharyngeal neurons (Stefanakis et al., 2015). Once activity patterns are determined for each neuron in a particular context, we will be able to better understand how pumping is controlled on a single pump basis, and how various environmental and physiological factors are integrated to set pump rate.

Although MC, M2, and M4 are degenerate in terms of their ability to stimulate pumping, and EAT-2 and GAR-3 are degenerate for the ability to respond to MC stimulation, this may only be true when pump rate is used as the sole output measurement of the system. In reality, the pharynx consists of 20 muscle cells that do not contract in perfect synchrony (Fang-Yen et al., 2009), so it is possible that pumps stimulated by different neurons are not functionally identical. Indeed, recent work suggests that the M1 motor neurons are involved in an additional pharyngeal behavior, spitting, that requires altered patterns of muscle contraction (Bhatla et al., 2015). High speed imaging of pharyngeal pumping during stimulation of various neurons will likely reveal differences in muscle contraction patterns during feeding and help to define more precise roles for each class of cholinergic neurons.

In order to directly relate my results to data from the well-established invertebrate neural circuits of the leech, crustacean, and mollusc, activity patterns of *C. elegans* pharyngeal neurons must be identified. However, while quantifying neural activity in *C. elegans* is difficult, *C. elegans* is more genetically tractable than many other invertebrates. Since the

genetic basis of neuronal function and synaptic neurotransmission is highly conserved (Bargmann, 1998), the genetic basis of degeneracy in *C. elegans* is likely to be similar with that in mammals. Thus, identification of genetic mechanisms that control degeneracy, robustness, and evolvability in *C. elegans* will shed light on how these processes function in higher animals, complementing the circuit approaches used in other invertebrates.

FLP-13 and NLP-22 generate similar behaviors via different mechanisms

Overexpression of FLP-13 or NLP-22 causes essentially identical cessation of feeding and locomotion, but I found that these neuropeptides act via different pathways. Two FLP-13 receptors have recently been identified in the Raizen lab, DMSR-1 (Michael Iannacone, Jessie Zhou, Jinzhou Yuan, and David Raizen, personal communication) and FRPR-4 (Matthew Nelson and David Raizen, submitted). Preliminary experiments reveal that neither receptor is expressed in pharyngeal or somatic motor neurons, so FLP-13 may act on interneurons or inhibitory motor neurons, or via additional receptors.

The pathways acting downstream of NLP-22 overexpression are less clear, as multiple attempts by me (unpublished observations) and by others (Jinzhou Yuan and Kun He Lee, personal communication) to use a forward genetic screen to identify mutants that suppressed the effects of NLP-22 overexpression have not yielded any strong suppressors, implying that either NLP-22 acts on multiple receptors or the NLP-22 receptor is essential for survival. Neither cholinergic neuron stimulation after NLP-22 overexpression or during DTS nor direct muscle stimulation during DTS stimulated

pumping, suggesting pharyngeal muscle is inexcitable under these conditions. The difficulty suppressing this pumping quiescence suggests that it is important for survival, perhaps because it prevents the deleterious effects of the disruption of pharyngeal cuticle formation during the molt (Frand et al., 2005; Straud et al., 2013; George-Raizen et al., 2014), but the mechanisms generating this quiescence are unclear. There are multiple possible explanations for decreased muscle excitability during DTS: Ca^{2+} may be highly buffered, voltage gated Ca^{2+} channels may be blocked, or the membrane conductance may be dramatically increased. Intracellular recordings from pharyngeal muscle during DTS will be informative in distinguishing these possibilities.

Peptidergic regulation of sleep may also be degenerate

Although *C. elegans* has just 302 neurons, it has at least 91 neuropeptide genes encoding more than 250 unique neuropeptides (Janssen et al., 2010; Hobert, 2013). The somnogenic neuropeptide genes *nlp-22* and *flp-13* were identified from a neuropeptide gene overexpression screen in the Raizen lab that is less than 25% complete, so more somnogenic neuropeptides likely remain to be identified. Additionally, null mutations in *flp-13* or *nlp-22* reduce but do not abolish SIS and DTS quiescence, suggesting other neuropeptides act in parallel to promote quiescence. In support of this notion, zebrafish neuropeptides associated with sleep/wake states do not each promote unique aspects of sleep/wake behavior, but appear to act degenerately to regulate partially overlapping clusters of behaviors (Richter et al., 2014). For example, galanin and nociceptin have similar effects on waking activity but opposite effects on movement duration (Woods et

al., 2014). Given the number of neuropeptides in *C. elegans*, it seems likely that the peptidergic regulation of behavioral quiescence in *C. elegans* is equally complex, with neuropeptides acting in parallel to NLP-22 and FLP-13 with similar but not identical effects on different aspects of behavior. In other words, the regulation of feeding inhibition during *C. elegans* sleep may be degenerate.

Degeneracy may explain the ubiquity of sleep as well as the difficulty in ascertaining the primary function of sleep across species. If different subprograms of sleep can be triggered in multiple ways, then individual variability in the use of these mechanisms would be expected. As conditions change over time, different species evolve that use a unique subset of these mechanisms. As species continue to evolve, the subsets of mechanisms used to regulate sleep will begin to differ, as will the physiological processes that are best suited to occur during sleep. Therefore, while sleep may be important across different species, the processes happening during sleep could vary widely. This may explain the dramatic differences in sleep duration seen across mammals (Siegel, 2008) and part of the challenge in defining the precise function of sleep.

Behaviorally identical states are not necessarily physiologically homogenous

Until the mid-1930s, sleep in all animals was identified by three behavioral characteristics: decreased responsiveness to environmental stimuli, reversibility, and an increased threshold to arousal (Kleitman, 1929). Until the development of the electroencephalogram (EEG) allowed the first observation of ongoing neural activity in the human brain during sleep (Gibbs et al., 1935; Loomis et al., 1935a), it was thought

that during sleep the brain was essentially at rest (Kleitman, 1929). Subsequent research revealed that EEG activity patterns during sleep are variable (Loomis et al., 1935b; 1936) and thus mammalian sleep can be divided into physiologically distinct states based on EEG activity patterns (Blake and Gerard, 1937; Loomis et al., 1937). More recently, the discovery that sleep can be triggered by both circadian (Borbély, 1982) and non-circadian factors (Krueger et al., 1982), such as bacterial infection (Toth and Krueger, 1988), through at least partly distinct neural pathways (Saper et al., 2005; 2012) suggests a second type of heterogeneity in sleep. While the functional and physiological differences between REM and non-REM sleep are widely appreciated, the differences between stress- or infection-induced sleep and circadian sleep, or between sleep in infants and adults (Blumberg et al., 2014), are less well understood.

As was the case in humans before the development of the EEG (Kleitman, 1929), sleep in non-mammals is defined by behavioral criteria: locomotion and feeding quiescence, rapid reversibility, reduced sensory responsiveness, and homeostasis (Campbell and Tobler, 1984; Allada and Siegel, 2008; Cirelli and Tononi, 2008; Siegel, 2008; Zimmerman et al., 2008). When combined with my data presented here, it becomes clear that recently identified sleep states in other model organisms, including the zebrafish *Danio rerio* (Zhdanova et al., 2001) and *Drosophila* (Hendricks et al., 2000), may not be as physiologically homogenous as they superficially appear. In fact, there is already evidence for the complexity of behavioral sleep states in *Drosophila.* A recent study found that daytime sleep and nighttime sleep are regulated by at least partly distinct mechanisms (van Alphen et al., 2013), while another group found that different circuits regulate sleep in young and older flies (Kayser et al., 2014), and a third group showed

that mutations that decrease stress-induced sleep do not have a strong effect on baseline sleep (Lenz et al., 2015). Together, these results demonstrate that even though there is no evidence of REM/non-REM sleep in flies and sleep appears behaviorally homogenous, *Drosophila* has physiologically distinct sleep states. It would be surprising if sleep in all species were not similarly complex.

APPENDIX: Simultaneous optogenetic stimulation of individual pharyngeal neurons and monitoring of feeding behavior in intact *Caenorhabditis elegans*

Nicholas F Trojanowski[1, 2] and Christopher Fang-Yen[1, 2]

(1) Department of Bioengineering, School of Engineering and Applied Science

(2) Department of Neuroscience, Perelman School of Medicine

University of Pennsylvania, Philadelphia, PA 19104

This chapter is a slightly modified version of a paper in press in *C. elegans*, Methods and Applications, G. Haspel and D. Biron, Eds.

Christopher Fang-Yen assisted with revising the manuscript.

Abstract

Optogenetic approaches have proven powerful for examining the role of neural circuits in generating behaviors, especially in systems where electrophysiological manipulation is not possible. Here I describe a method for optogenetically manipulating single pharyngeal neurons in intact *C. elegans* while monitoring pharyngeal behavior. This approach provides bidirectional and dynamic control of pharyngeal neural activity simultaneously with a behavioral readout, and has allowed me to test hypotheses about the roles of individual pharyngeal neurons in regulating feeding behavior.

Introduction

The nematode *C. elegans* is a powerful tool for studying the function of neural circuits, in large part due to its genetic tractability and known synaptic connectivity (Xu and Kim, 2011; Bargmann and Marder, 2013). Since it is not currently possible to electrophysiologically manipulate the activity of the *C. elegans* nervous system in intact animals (Goodman et al., 2012), the primary method for studying the roles of specific neurons in behavior has been ablation of these neurons in young larvae using a laser beam, and observation of behavior in adults (Bargmann and Avery, 1995; Fang-Yen et al., 2012). However, laser ablation is a permanent, unidirectional manipulation of a neural circuit that does not easily allow the assessment of functional redundancy or developmental compensation (Steger et al., 2005). It is therefore suboptimal for understanding dynamic phenomena like neural activity.

Optogenetic techniques, which involve using light-sensitive ion channels to manipulate neural activity and behavior, are ideal for precise temporal control of neural activity in behaving animals, as they afford bidirectional and dynamic manipulation (Deisseroth, 2010). To date, most optogenetic experiments in *C. elegans* have been performed by illuminating the entire worm after expressing light-sensitive proteins in a desired subset of neurons (Husson et al., 2013). However, the cellular specificity of this approach – and therefore its utility for functionally dissecting neural circuits – has been limited by the difficulty of finding a promoter that drives gene expression only in the desired neurons. Genetic intersection approaches have been used (Davis et al., 2008; Voutev and Hubbard, 2008; Schmitt et al., 2012; Wei et al., 2012), but even these are not guaranteed to provide the desired overlap. Furthermore, when using promoters with high cellular specificity a

different strain is required to study each subset of neurons, making it impossible to study the functions of multiple neurons in a single worm. To solve this problem, multiple groups have developed different methods for using patterned light to illuminate arbitrary parts of the worm corresponding to neurons of interest. The first of these studies was done using immobilized worms and optically monitoring Ca^{2+} levels in neurons of interest (Guo et al., 2009). More recent work has used locomotion as a behavioral readout of circuit function (Leifer et al., 2011; Stirman et al., 2011; Kocabas et al., 2012).

Here, I describe a method for using spatially restricted optogenetic illumination to investigate the behavioral effects of manipulating individual neurons in the pharynx (feeding organ). The pharyngeal neural circuit is one of the simplest in the worm, containing 20 neurons of 14 classes. However, experiments in which each of the 14 classes of pharyngeal neurons were ablated found only 3 classes for which ablation caused a clearly identifiable deficit in feeding behavior (Avery and You, 2012), perhaps due to circuit redundancy. Using an optogenetic approach, I uncovered genetic and neural degeneracy in the circuit for excitation of pharyngeal pumping (Trojanowski et al., 2014).

I use a digital micromirror device (DMD) to focus light in defined patterns on worms that express light sensitive excitatory (e.g. blue-light-sensitive ion channel Channelrhodopsin-2 (ChR2)) (Zhang et al., 2007b) or inhibitory microbial opsins (e.g. blue-light-powered proton pump (Mac) from *Leptosphaeria maculans*) (Waschuk et al., 2005; Chow et al., 2010; Okazaki et al., 2014). To stimulate single neurons, I take advantage of the fact that the pharynx is internal and use polystyrene beads to immobilize worms (Kim et al., 2013). This affords submicron spatial resolution without pharmacological manipulation. I

use particle image velocimetry to automatically track movement of pharyngeal muscles during optogenetic manipulations. This approach improves on both the lack of specificity present in typical optogenetic experiments and the lack of sensitivity and intra-observer variability inherent in manual observation (Raizen et al., 2012).

Materials

Optical table (at least 1.5 m X 1.2 m surface)

473 nm laser (e.g. Shanghai Laser and Optics Century model BL473T3-150)

Leica DMI3000B inverted microscope and associated filter cubes

Leica Plan Apo 63X oil immersion objective lens with N.A.= 1.4

Photometrics DV2 multichannel imaging system

Cooled CCD camera with software capable of 30 frames per second (e.g. Andor iXon 885 and Andor SOLIS software)

1024 by 768 pixel digital micromirror device (DMD) with Discovery 4100 Explorer software (Discovery 4100 DLP, Texas Instruments/Digital Light Innovations)

Power meter (e.g. Coherent FieldMate)

MATLAB software

Aluminum mounting box for DMD control board (approx. 15 cm X 20 cm)

6.24 mm focal length aspheric lens (e.g. Thorlabs C110TME-A)

75 mm focal length planoconvex lens (e.g. Thorlabs LA1608-A)

100 mm focal length, 2-inch diameter achromatic lens (e.g. Thorlabs AC508-100-A)

2 200 mm focal length, 2-inch diameter achromatic lenses (e.g. Thorlabs AC508-200-A)

~7 mirrors (e.g. Thorlabs PF20-03-P01 and PF10-03-P01)

2 irises (e.g. Thorlabs ID15)

Longpass dichroic filter (e.g. Thorlabs DMLP490R)

Hardware for mounting each optic

Post holders (e.g. Thorlabs UPH3)

Posts (e.g. Thorlabs TR3)

Lens and mirror mounts (e.g. Thorlabs LMR1, LMR2, KM100, KM200)

Post clamps (e.g. Thorlabs RA45)

1/4"-20 cap screws (e.g. Thorlabs HW-KIT2)

8-32 cap screws (e.g. Thorlabs HW-KIT3)

Sodium fluorescein

NGM buffer (NGM from (Stiernagle, 2006) but without agar, cholesterol, or peptone)

Agarose

Serotonin HCl

Slides and coverslips

0.5 mm thick plastic shim stock (Ardus Yellow 0.020 Inches)

250 mL beaker

50 mL centrifuge tube

Disposable spatulas (e.g. VWR International 80081-188)

2.5% (v/v) suspension of 50 nm diameter polystyrene beads (Polysciences 08691-10)

Nematode strains expressing opsins in neurons of interest

Methods

The methods will be described in 5 sections: **A**: Building the rig; **B**: Constructing the worm strains; **C**: Immobilizing the worms; **D**: Performing the experiments; and **E**: Analyzing the data.

Building the rig

In the optical setup, a laser beam is first expanded in diameter by about 10 times by a telescope consisting of two lenses (Fig. 1). This laser beam is routed via mirrors to the DMD, which restricts the beam to a set of a pixels selected by computer. Next, the image on the DMD is relayed to an intermediate image plane of the microscope with 2X magnification using lenses with focal lengths 100 mm and 200 mm. Finally the image is relayed again to the worm via a relay lens system composed of a 200 mm focal length lens and the objective lens. The steps for constructing this setup are described below, and a schematic is depicted in Figure 1.

Before starting work, obtain the appropriate laser protection eyewear, light curtains, and other safety equipment. Consult your laser safety protection officer to determine what is needed.

1. Place the microscope and laser on an optical table and secure them so that they will not inadvertently move in relationship to the rest of the table. (see Note 1)

2. Mount each mirror or lens in an appropriate mount, and attach each mount to a post and post holder. Fasten post holders to the table in an out of the way location so that they are secure while you are performing the other steps.

3. Mount the DMD by attaching the DMD to a KM200 mirror mount and attaching the control board to the mounting case using screws and board standoffs. Ensure that the DMD power cable can be plugged in to the control board after mounting.

4. Place two irises in the path of the laser, and adjust them and the laser so that the laser beam is perfectly horizontal and passes directly through the center of the irises.

5. Place the 6.24 mm focal length lens and the 75 mm focal length lens so they are 81.24 mm apart (the sum of the focal lengths), beyond the irises. The lenses should be oriented according to their design specifications, with the sides designed for short conjugate distance facing each other.

6. Align these lenses so the beam passes through the center of the lenses and is collimated (i.e. neither converging nor diverging) after exiting the 75 mm focal length lens. (see Note 2)

7. Install a filter cube and dichroic filter that reflects light from the desired port through the back of the objective. For GFP optics, use a longpass dichroic filter that reflects

wavelengths shorter than 500 nm and transmits wavelengths longer than 500 nm. (see Note 3)

8. Place one of the 200 mm lenses 200 mm away from the back of the objective, along the light path, with the rounded side facing the microscope. (see Note 4)

9. Place the other 200 mm lens 400 mm beyond the first 200 mm lens, along the light path. The curved side should face away from the microscope. (see Note 5).

10. Place the 100 mm lens 300 mm beyond the furthest 200 mm lens. The curved side should face the 200 mm lens.

11. Place the DMD 100 mm beyond the 100 mm lens. Screw down loosely, as the position will likely need to be adjusted later. (see Note 6)

12. Plug in the DMD and use the Discovery 4100 Explorer software to set it so that all the mirrors are in the ON position.

13. Use mirrors as necessary to project the laser beam onto the DMD. (see Note 7)

14. Adjust the angle of the DMD so that with the mirrors in the ON position, the laser beam is reflected along the optical path of the microscope, through the center of the 100 and 200 mm lenses. (see Note 8)

15. Place a glass slide at an angle in the light path shortly after the beam leaves the laser by taping the slide to an optical post. (see Note 9)

16. Set up the power meter so the light reflected off the glass slide hits the center of the sensor.

17. Place a red filter in the transillumination light path to enable behavioral observation during the optogenetics experiments without off-target stimulation effects.

18. To allow independent analysis of the green (GFP/targeting) and red (brightfield/behavior) signals, attach the DV2 and camera to the imaging port of the microscope.

19. Align the DV2 according to the instructions that come with the device. (see Note 10)

20. Register the DMD coordinates to the field of view of the camera. Create a series of images that contain a square moving in a matrix across the DMD. (see Note 11)

21. Prepare a slide with a thin layer of 1 M sodium fluorescein in water or glycerol between two shims under a coverslip and place it on the microscope stage.

22. Pass the series of images to the DMD (step 20) and record where (if at all) a fluorescent spot appears on the camera.

23. Compute the correspondence matrix of the coordinates passed to the DMD and coordinates where fluorescence was detected.

24. Use this matrix to define an image transformation between the DMD and the camera.

Creating worm strains

1. In general, the same strains that are used for whole worm optogenetics can be used for this method. (see Note 12)

2. These worms should be grown in the dark following standard procedures. Where needed, add 2 μL of 100 mM all-*trans* retinal (ATR) in ethanol to the bacterial suspension immediately before seeding. (see Note 13)

3. Laser ablations, if desired, can be performed as previously described (Bargmann and Avery, 1995; Fang-Yen et al., 2012).

Preparing agarose pads

1. Prepare 6 slides by placing 0.5 mm thick shims, approximately 1 cm by 2 cm, on each end of each slide.

2. Prepare agarose pads by mixing 0.20 g agarose and 4 mg 5-HT into 2 mL of NGM (10% agarose, 10 mM 5-HT) in a 50 mL centrifuge tube. (see Note 14)

3. Swirl the mixture gently so that the agarose is evenly dispersed in the liquid rather than a large clump, but avoid getting too much of the mixture on the sides of the tube.

4. Rest the lid on top of the centrifuge tube, but do not screw it on.

5. Place the centrifuge tube in a 250 mL beaker.

6. Fill the beaker to ~50 mL with tap water, just above the level of liquid in the centrifuge tube.

7. Microwave the beaker and centrifuge tube for 50 seconds at high power, at which point the agarose mixture should be clear, and may have some bubbles.

8. Using a disposable plastic spatula, place a drop of agarose mixture about 1 cm in diameter onto the middle of a slide prepared with shims and immediately cover this slide with a second slide (see Note 15).

9. Make slides until all the agarose has been used. (see Note 16)

10. Allow slides to set for at least 1 minute before adding worms.

Steps 11-16 should be performed quickly for optimal immobilization

11. Load 1.5 µL of a 2.5% (v/v) suspension of 50 nm diameter polystyrene beads into a 20 µl pipettor (Kim et al., 2013). (see Note 17)

12. Remove top slide from one of the pads and place the slide with the pad onto a plate lid on the microscope stage.

13. Use bacteria to stick up to 10 worms onto the bottom of a worm pick, but do not put them on the pad yet.

14. Expel the 1.5 uL of beads onto the pad.

15. Gently, and as quickly as possible, place the pick into the beads and allow the worms to transfer into the beads on the pad. (see Note 18)

16. Quickly place a coverslip on top of the pad to immobilize the worms.

17. Wait 5-10 minutes before performing experiments to allow the worms to habituate.

Performing the experiments

1. Set the frame rate of the camera and the laser power. (see Note 19).

2. Place a slide on the microscope stage and find a worm at 10x on the microscope under brightfield illumination. (see Note 20)

3. Switch to 63x and move the pharynx of the worm into the center of the field of view under brightfield illumination. (see Note 21)

4. Manually take a z-stack of the pharyngeal neurons by illuminating the entire field using the DMD, and focusing through the relevant regions. This illumination period should be less than 1 second.

5. If desired, use MATLAB convert the images into JPEG files. MATLAB scripts for this and all other steps are available upon request. (see Note 22).

6. Identify the images in the z-stack that most clearly show the neurons of interest.

7. Use the roipoly function in MATLAB to select the regions of these images you would like to use to stimulate each neuron. (see Note 23 and Fig. 2B and C)

8. Use MATLAB to create an image mask that that contains the value 1 for the region you outlined in the previous step and the value 0 elsewhere, and transform this file into DMD coordinates using the transformation computed in step A23. (see Note 24)

9. Create a Discovery 4100 script that tells the DMD which images to display and at which times they should be displayed. (see Note 25)

10. Acquire a baseline recording of behavior without any illumination. (see Note 26)

11. Run each script while recording from both the red and green channels. (see Note 27)

Analyzing the data

The following steps should be repeated for each experiment.

1. If desired, convert the images into JPEG files. (see Note 22)

2. Use the roipoly function in MATLAB to draw a ROI around the brightest part of the neuron that was stimulated during the experiment. (see Note 28)

3. Use MATLAB to track the pixel intensity of this region over the course of experiment.

4. Use MATLAB to identify the times at which the intensity of this region sharply increased or decreased. These are the times at which the stimulus was turned on and off, respectively.

5. Use MATLAB to select the rectangular region of the terminal bulb just anterior to the grinder. (see Note 29 and Fig. 2A)

6. Using the freely available package PIVlab, a Time-Resolved Digital Particle Image Velocimetry Tool for MATLAB, track the velocity this region over time. (see Note 30)

7. Use this trace of velocity over time to identify the times at which a pump occurred by drawing a threshold and recording the times at which a positive-going threshold crossing occurs. (see Note 31)

8. Determine the number of pumps that occur during each interval in which the stimulus is on or off. (see Note 32)

9. Divide the number of pumps in a stimulus interval by the length of that stimulus interval to find the average pump rate. (see Note 33)

Notes

Note 1: My setup uses a Leica DMI3000B inverted microscope with a Leica Plan Apo 63X oil immersion objective lens with N.A.= 1.4. Any microscope with a port that allows direct access to the back of the objective should suffice. An inverted microscope may be easier to set up due to the lower height of the fluorescence illumination path, but an upright microscope could be used as well.

Note 2: The distance between the 6.24 mm lens and the 75 mm lens must be ~81.24 mm, but the distances from 75 mm lens to the irises, between the irises, and between the irises and the laser, can be arbitrary. My rig is partially designed to work with a 532 nm laser as well as a 473 nm laser, so I use a system of mirrors and a dichroic beam splitter to allow me to use these two lasers through the same optical path. If you only wish to use one laser, you can aim it directly through the irises, though I find it useful to have the beam reflect off at least one mirror before entering the irises, because it is easier to precisely adjust the tilt angle of the mirror than that of the laser.

Note 3: For the Leica DMI3000B, the fluorescent light port in the rear of the microscope contained optics of unknown parameters, so I used a side auxiliary port and custom filter cube (Nuhsbaum Inc.) that allowed direct access to the back of the objective.

Note 4: You should adjust this position so that a sharp back-scattered image through the objective forms 200 mm away beyond the lens. It is difficult to measure the 200 mm distance from the back of the objective to this lens precisely, so you may need to adjust this lens empirically later. If this lens needs to be adjusted after all the other lenses are set

up, it may be easier to adjust the position of the microscope rather than move all the optics.

Note 5: Due to spatial constraints, I put a mirror between the 200 mm lenses. This is fine so long as the total distance along the light path between the lenses is 400 mm.

Note 6: The 100 mm distance here should be adjusted empirically so that a crisp back-scattered image from the microscope appears on the DMD and is centered on the grid of mirrors, covering it completely.

Note 7: The laser beam should just barely cover the DMD. If this is not the case, then you likely need to adjust the two smaller lenses so that the beam is not changing in size after it exits the 75 mm lens.

Note 8: To do this, the light must be incident onto the DMD from the lower right, if you are facing the DMD. I find that is easiest to use multiple mirrors to reflect the laser beam at the correct angle, as this provides multiple degrees of freedom for adjustment

Note 9: This will allow a large amount of the light to pass through but will reflect a small fraction without disrupting the direction of the laser beam. You can measure the light power reflected and the light power at the objective to determine the percentage of light that is reflected, and use this relationship to determine the light power at the objective at any time.

Note 10: Alternatively, a beam splitter could be built in house with similar optics to those in the DV2.

Note 11: In order to target a specific region of the microscope stage, you must first identify the DMD coordinates that correspond to this region. This process will need to be repeated if any of the optics are inadvertently bumped, so make sure that all of the optics are tightly fastened to the table before beginning this step.

Note 12: It is essential that the opsin of interest is tagged with an appropriate fluorescent protein (I used blue light to excite ChR2 and Mac, so I used opsins tagged with YFP or GFP). However, I found that for some transgenes the ChR2::YFP was not bright enough to resolve neuron processes (for example, *zxIs6[unc-17p::ChR2(H134R)::YFP + lin-15(+)]*), likely because the ChR2 is membrane bound. After confirming expression in the relevant cell bodies, I crossed strains containing dim transgenes into a strain that expressed cytoplasmic GFP under the same promoter (I used *vsIs48[unc-17::GFP]*). I found this particularly useful for looking at off-target effects during ablation experiments, were I wanted to determine the effect of stimulating processes near a cell body after killing the cell body.

Note 13: I stored ATR-seeded plates at 4°C for up to one week before use.

Note 14: I make the agarose mixture fresh for each experiment. 5-HT is necessary for inducing a basal pumping rate during immobilization. Other drugs can be added at this step as desired, though I found that adding too many ionic salts (more than 10mM) caused the polystyrene beads to clump and made immobilization difficult.

Note 15: I have found that the flexibility of the plastic spatulas makes it easier to get all the agarose out of the centrifuge tube, compared to stainless steel spatulas, and their low thermal mass may prevent premature cooling of the agarose.

Note 16: I am usually able to make 6 slides from 2 mL of agarose solution.

Note 17: I store 100 µL aliquots of polystyrene beads at 4°C between uses.

Note 18: When the pads contain 5-HT, the beads clump quickly after they are added to the pad, which reduces the quality of immobilization. Thus, I try to have the beads on the pad for as little time as possible before I add the cover slip.

Note 19: I use an exposure time of 30 ms, which produces a frame rate of 32.7 Hz. I set the laser power so that the irradiance of the laser at the objective is approximately 37 mW/mm^2, well above the saturation irradiance of ChR2 (Grossman et al., 2011). These settings can be adjusted to increase the visibility of the fluorescent signal, if necessary.

Note 20: Because of the way the DV2 splits the camera field of view, it is important that the head of the worm is close to aligned with the long direction of each channel's field of view (within ~30 degrees). If the head is not aligned in this manner, rotate the slide or select a different worm on the slide. Do not rotate the camera, or you will have to re-register the DMD and camera images.

Note 21: It is important that the grinder is visible in the camera's field of view, since its motion will later be used to quantify feeding rate. It is also important that the locations of

the neurons of interest are visible in the camera. For pharyngeal neurons, this should not be an issue as long as the worm is aligned as described in Note 20.

Note 22: The Andor iXon 885 and Andor SOLIS software produce images as multipage TIFF files. I find it easier to work with JPEG files than multipage TIFF files, but this is a lossy compression and may increase noise.

Note 23: This should be a region slightly larger than the cell body – about 2-3 μm in diameter – to allow constant stimulation as the neural cell bodies move during the pump. It is important that the neuron of interest remains in this region during the entire experiment, because the fluorescent signal from this neuron will be used to determine the times of stimulation *post hoc*. Counterintuitively, I found it difficult to immobilize some paralyzed mutants, in which case I found it necessary to use a substantially larger stimulus region to ensure the neuron of interest was stimulated during the entire experiment.

Note 24: The DMD mirrors can be set in either the ON or OFF position, so I pass an image that contains 1s (representing ON) in locations corresponding to the area of the stage I wish to illuminate and 0s (representing OFF) elsewhere.

Note 25: The DMD works by reading in images that represent the pattern it should display and displaying this pattern, then pausing for a defined period, then reading in the next file, and so on. For my experiments, I begin with an all-off image for 5 seconds, followed by 5 seconds of illumination of the neuron of interest, followed by an all-off image for 5 seconds, repeating up to 10 times and ending with an all-off image.

Note 26: I record the baseline for 30 seconds.

Note 27: I wait 2-3 minutes between running each script, i.e. between each neuron I stimulate. I found that the behavior was most robust when experiments were performed within 90 minutes of immobilization.

Note 28: Here I find it better to use a ROI smaller than that used for the experiment, because it is easier to detect changes in brightness when just looking at the brightest parts of the neuron.

Note 29: I found that using a rectangle that extends from the anterior edge of the terminal bulb to the grinder, and is just slightly wider than the grinder, provides the best signal.

Note 30: Tracking the velocity of this region over time will show a series of spikes, each representing a pump: a positive change in velocity represents the movement of the grinder towards the posterior, and a negative change in velocity represents anterior movement.

Note 31: I found that using a threshold of half of the maximum velocity provided high sensitivity and specificity, though a wide range of threshold values will give the same result on a good recording.

Note 32: I did this for each stimulus interval by finding the number of pumps for which the value (pump time – stimulus time) was greater than 0 but less than the time between when the stimulus turned on and when it turned off.

Note 33: The pumping rate during the stimulus-off windows is sometimes lower the

initial baseline, likely due to post-excitatory inhibition, so I typically do not use these values for looking at the effect of neuron stimulation. Rather, I use the pumping rate that I get from step D10 as the baseline.

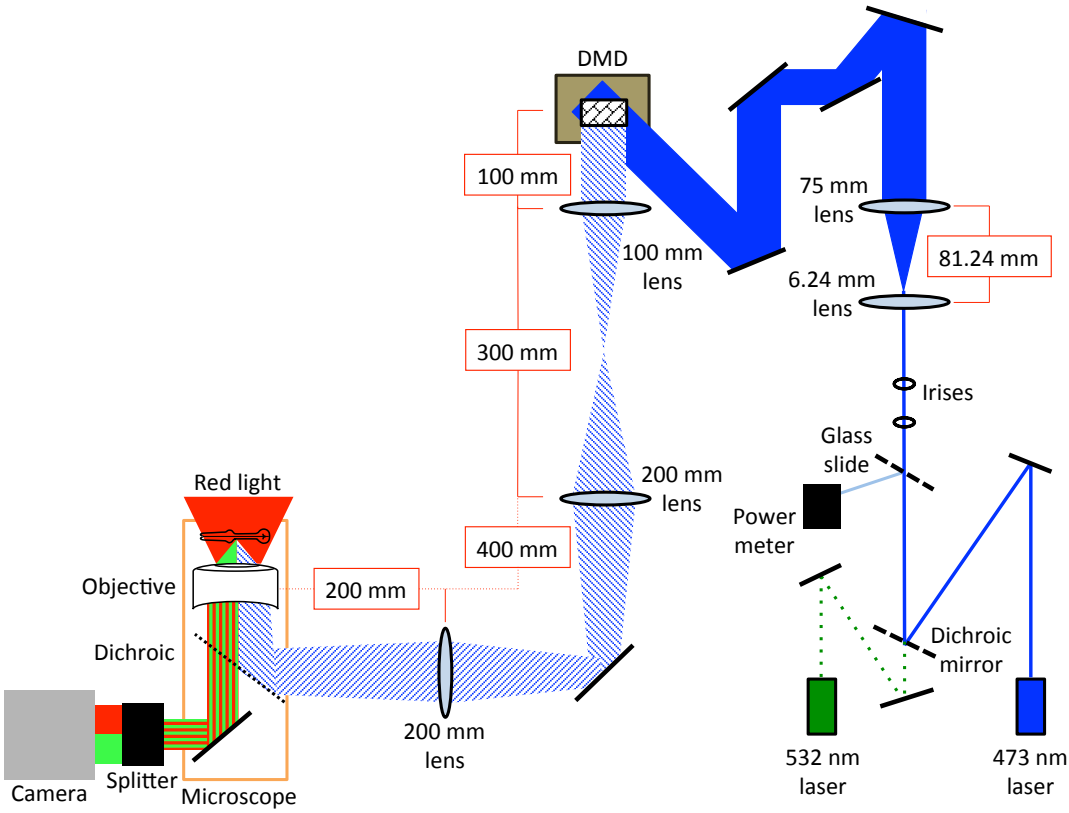

Figure A.1: Setup for single neuron stimulation of pharyngeal neurons. Light leaves the blue laser and is reflected off a mirror (black line) and dichroic beam splitter. A small percentage of the light is then reflected to a power meter to monitor laser output. The light then passes through two irises before being expanded through a telescope composed of two lenses. The beam is then, through a series of mirrors, reflected onto the DMD (brown box) such that it covers the entire grid of mirrors. This beam then passes through a series of lenses along the light path. It then enters the microscope through an auxiliary port, where it is reflected by a dichroic on a custom filter cube into the back of the objective. The stage of the microscope is illuminated with red light. This red light and the green light emitted by fluorescent proteins then pass through a DV2 beam splitter, which separates the red and green channels, which are then recorded by a camera.

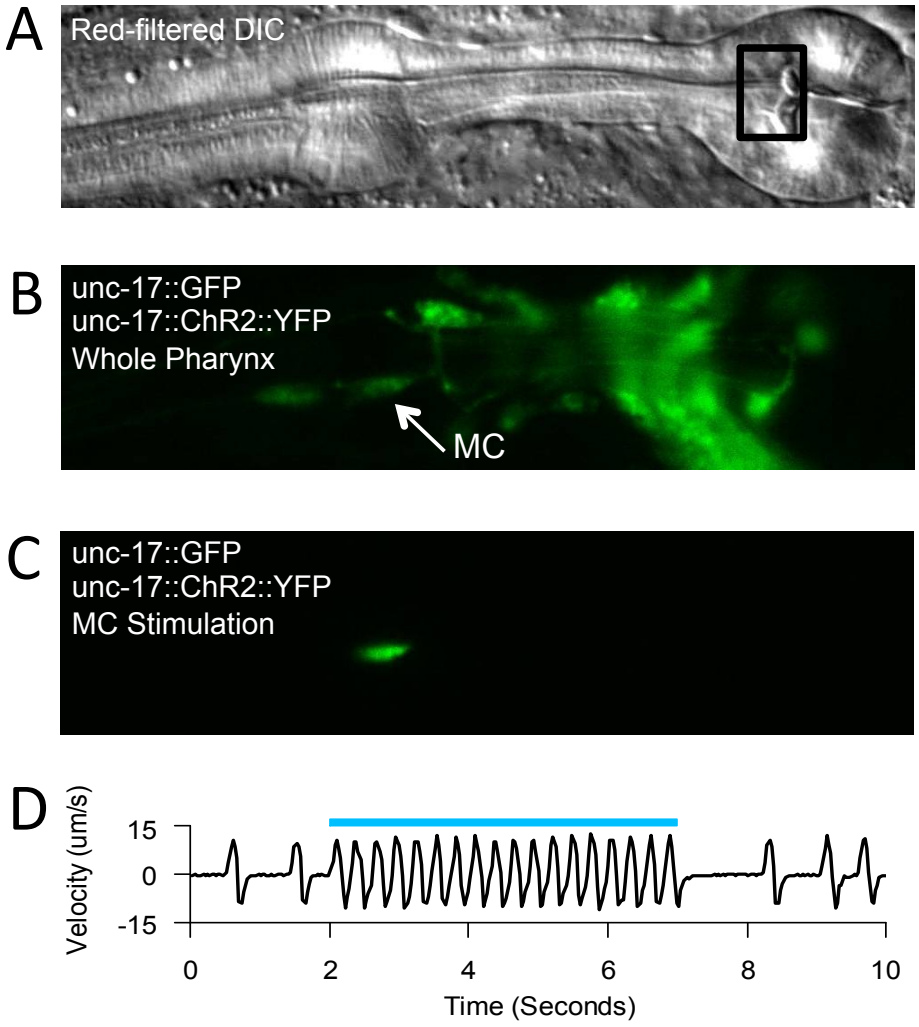

Figure A.2: Stimulation of single pharyngeal neurons. A: DIC image of the pharynx. Black box denotes region used for velocity calculations. **B**: wide field GFP fluorescence image of the same field of view as in A. The arrow points to an MC soma. **C**: GFP fluorescence image of the same field of view as in A and B, during selective illumination of an MC soma. **D**: Velocity from PIV algorithm during ChR2-mediated stimulation of the MC neurons. Each peak in the velocity represents a pump. The blue bar represents timing of laser illumination.

BIBLIOGRAPHY

Akerboom J et al. (2013) Genetically encoded calcium indicators for multi-color neural activity imaging and combination with optogenetics. Frontiers in Molecular Neuroscience 6:2.

Albertson DG, Thomson JN (1976) The pharynx of *Caenorhabditis elegans*. Philosophical Transactions of the Royal Society, Series B, Biological Sciences 275:299–325.

Alfonso A, Grundahl KM, Duerr JS, Han H-PP, Rand JB (1993) The *Caenorhabditis elegans unc-17* gene: a putative vesicular acetylcholine transporter. Science 261:617–619.

Alkema MJ, Hunter-Ensor M, Ringstad N, Horvitz HR (2005) Tyramine functions independently of octopamine in the *Caenorhabditis elegans* nervous system. Neuron 46:247–260.

Allada R, Siegel JM (2008) Unearthing the phylogenetic roots of sleep. Current Biology 18:R670–R679.

Avery L (1993a) Motor neuron M3 controls pharyngeal muscle relaxation timing in *Caenorhabditis elegans*. Journal of Experimental Biology 175:283–297.

Avery L (1993b) The genetics of feeding in *Caenorhabditis elegans*. Genetics 133:897–917.

Avery L, Horvitz HR (1987) A cell that dies during wild-type *C. elegans* development

can function as a neuron in a *ced-3* mutant. Cell 51:1071–1078.

Avery L, Horvitz HR (1989) Pharyngeal pumping continues after laser killing of the pharyngeal nervous system of *C. elegans*. Neuron 3:473–485.

Avery L, Horvitz HR (1990) Effects of starvation and neuroactive drugs on feeding in *Caenorhabditis elegans*. Journal of Experimental Zoology 253:263–270.

Avery L, Raizen DM, Lockery SR (1995) Electrophysiological methods. Methods in Cell Biology 48:251–269.

Avery L, Shtonda BB (2003) Food transport in the *C. elegans* pharynx. Journal of Experimental Biology 206:2441–2457.

Avery L, Thomas JH (1997) Feeding and defecation: Section II Feeding. Cold Spring Harbor Laboratory Press 33:679–716.

Avery L, You Y-J (2012) *C. elegans* feeding. Wormbook:1–23.

Bargmann CI (1998) Neurobiology of the *Caenorhabditis elegans* genome. Science 282:2028–2033.

Bargmann CI, Avery L (1995) Laser killing of cells in *Caenorhabditis elegans*. Methods in Cell Biology 48:225–250.

Bargmann CI, Horvitz HR (1991a) Chemosensory neurons with overlapping functions direct chemotaxis to multiple chemicals in *C. elegans*. Neuron 7:729–742.

Bargmann CI, Horvitz HR (1991b) Control of larval development by chemosensory

neurons in *Caenorhabditis elegans*. Science 251:1243–1246.

Bargmann CI, Marder E (2013) From the connectome to brain function. Nature Methods 10:483–490.

Bastiani CA, Gharib S, Simon MI, Sternberg PW (2003) *Caenorhabditis elegans* G(q)alpha regulates egg-laying behavior via a PLCbeta-independent and serotonin-dependent signaling pathway and likely functions both in the nervous system and in muscle. Genetics 165:1805–1822.

Beets I, Janssen T, Meelkop E, Temmerman L, Suetens N, Rademakers S, Jansen G, Schoofs L (2012) Vasopressin/oxytocin-related signaling regulates gustatory associative learning in *C. elegans*. Science 338:543–545.

Belfer SJ, Chuang H-S, Freedman BL, Yuan J, Norton M, Bau HH, Raizen DM (2013) Caenorhabditis-in-drop array for monitoring *C. elegans* quiescent behavior. Sleep 36:689–698G.

Benzer S (1971) From the gene to behavior. Journal of the American Medical Association 218:1015–1022.

Bhatla N, Droste R, Sando SR, Huang A, Horvitz HR (2015) Distinct neural circuits control rhythm inhibition and spitting by the myogenic pharynx of *C. elegans.* Current Biology 25:2075–2089.

Bhatla N, Horvitz HR (2015) Light and hydrogen peroxide inhibit *C. elegans* feeding through gustatory receptor orthologs and pharyngeal neurons. Neuron 85:804–818.

Blake H, Gerard RW (1937) Brain potentials during sleep. American Journal of Physiology 119:692–703.

Blumberg MS, Gall AJ, Todd WD (2014) The development of sleep–wake rhythms and the search for elemental circuits in the infant brain. Behavioral Neuroscience 128:250–263.

Borbély AA (1982) A two process model of sleep regulation. Human Neurobiology 1:195–204.

Brenner S (1973) The genetics of behaviour. British Medical Bulletin 29:269–271.

Brenner S (1974) The genetics of *Caenorhabditis elegans*. Genetics 77:71–94.

Brundage L, Avery L, Katz A, Kim UJ, Mendel JE, Sternberg PW, Simon MI (1996) Mutations in a *C. elegans* G(q)alpha gene disrupt movement, egg laying, and viability. Neuron 16:999–1009.

Bucher D, Prinz AA, Marder E (2005) Animal-to-animal variability in motor pattern production in adults and during growth. Journal of Neuroscience 25:1611–1619.

Bumbarger DJ, Riebesell M, Rödelsperger C, Sommer RJ (2013) System-wide rewiring underlies behavioral differences in predatory and bacterial-feeding nematodes. Cell 152:109–119.

Byerly L, Masuda MO (1979) Voltage-clamp analysis of the potassium current that produces a negative-going action potential in *Ascaris* muscle. Journal of Physiology 288:263–284.

Campbell DT, Hille B (1976) Kinetic and pharmacological properties of the sodium channel of frog skeletal muscle. Journal of General Physiology 67:309–323.

Campbell SS, Tobler I (1984) Animal sleep: a review of sleep duration across phylogeny. Neuroscience and Biobehavioral Reviews 8:269–300.

Cassada RC, Russell RL (1975) The dauerlarva, a post-embryonic developmental variant of the nematode *Caenorhabditis elegans*. Developmental Biology 46:326–342.

Chalfie M, Sulston JE, White JG, Southgate E, Thomson JN, Brenner S (1985) The neural circuit for touch sensitivity in *Caenorhabditis elegans*. Journal of Neuroscience 5:956–964.

Charlie NK, Thomure AM, Schade MA, Miller KG (2006) The Dunce cAMP phosphodiesterase PDE-4 negatively regulates G alpha(s)-dependent and G alpha(s)-independent cAMP pools in the *Caenorhabditis elegans* synaptic signaling network. Genetics 173:111–130.

Chase DL, Koelle MR (2007) Biogenic amine neurotransmitters in *C. elegans.* Wormbook:1–15.

Chen T-W, Wardill TJ, Sun Y, Pulver SR, Renninger SL, Baohan A, Schreiter ER, Kerr RA, Orger MB, Jayaraman V, Looger LL, Svoboda K, Kim DS (2013) Ultrasensitive fluorescent proteins for imaging neuronal activity. Nature 499:295–300.

Cheong MC, Artyukhin AB, You Y-J, Avery L (2015) An opioid-like system regulating feeding behavior in *C. elegans*. eLife 4.

Chiang J-TA, Steciuk M, Shtonda BB, Avery L (2006) Evolution of pharyngeal behaviors and neuronal functions in free-living soil nematodes. Journal of Experimental Biology 209:1859–1873.

Cho JY, Sternberg PW (2014) Multilevel modulation of a sensory motor circuit during *C. elegans* sleep and arousal. Cell 156:249–260.

Choi S, Chatzigeorgiou M, Taylor KP, Schafer WR, Kaplan JM (2013) Analysis of NPR-1 reveals a circuit mechanism for behavioral quiescence in *C. elegans*. Neuron 78:869–880.

Choi S, Taylor KP, Chatzigeorgiou M, Hu Z, Schafer WR, Kaplan JM (2015) Sensory neurons arouse *C. elegans* locomotion via both glutamate and neuropeptide release. PLoS Genetics 11:e1005359.

Chow BY, Han X, Dobry AS, Qian X, Chuong AS, Li M, Henninger MA, Belfort GM, Lin Y, Monahan PE, Boyden ES (2010) High-performance genetically targetable optical neural silencing by light-driven proton pumps. Nature 463:98–102.

Cirelli C (2009) The genetic and molecular regulation of sleep: from fruit flies to humans. Nature Reviews Neuroscience 10:549–560.

Cirelli C, Tononi G (2008) Is sleep essential? PLoS Biology 6:e216.

Cong X, Wang H, Liu Z, He C, An C, Zhao Z (2015) Regulation of sleep by insulin-like peptide system in *Drosophila melanogaster*. Sleep 38:1075–1083.

Corsi AK, Wightman B, Chalfie M (2015) A transparent window into biology: A primer

on *Caenorhabditis elegans*. Genetics 200:387–407.

Crocker A, Sehgal A (2010) Genetic analysis of sleep. Genes & Development 24:1220–1235.

Crocker A, Shahidullah M, Levitan IB, Sehgal A (2010) Identification of a neural circuit that underlies the effects of octopamine on sleep:wake Behavior. Neuron 65:670–681.

Croll NA, Smith JM (1978) Integrated behaviour in the feeding phase of *Caenorhabditis elegans* (Nematoda). Journal of Zoology 184:507–517.

Croll NA, Smith JM, Zuckerman BM (1977) The aging process of the nematode *Caenorhabditis elegans* in bacterial and axenic culture. Experimental Aging Research 3:175–189.

Cunningham KA, Hua Z, Srinivasan S, Liu J, Lee BH, Edwards RH, Ashrafi K (2012) AMP-activated kinase links serotonergic signaling to glutamate release for regulation of feeding behavior in *C. elegans*. Cell Metabolism 16:113–121.

Dabbish NS, Raizen DM (2011) GABAergic synaptic plasticity during a developmentally regulated sleep-like state in *C. elegans*. Journal of Neuroscience 31:15932–15943.

Davis MW, Fleischhauer R, Dent JA, Joho RH, Avery L (1999) A mutation in the *C. elegans* EXP-2 potassium channel that alters feeding behavior. Science 286:2501–2504.

Davis MW, Morton JJ, Carroll D, Jorgensen EM (2008) Gene activation using FLP

recombinase in *C. elegans*. PLoS Genetics 4:e1000028.

Davis MW, Somerville D, Lee RYN, Lockery SR, Avery L, Fambrough DM (1995) Mutations in the *Caenorhabditis elegans* Na,K-ATPase alpha-subunit gene, *eat-6*, disrupt excitable cell function. Journal of Neuroscience 15:8408–8418.

de Bono M, Bargmann CI (1998) Natural variation in a neuropeptide Y receptor homolog modifies social behavior and food response in *C. elegans*. Cell 94:679–689.

de Bono M, Maricq AV (2005) Neuronal substrates of complex behaviors in *C. elegans*. Annual Review of Neuroscience 28:451–501.

Dean T, Xu R, Joiner WJ, Sehgal A, Hoshi T (2011) *Drosophila* QVR/SSS modulates the activation and C-type inactivation kinetics of shaker K^+ channels. Journal of Neuroscience 31:11387–11395.

Deisseroth K (2010) Optogenetics. Nature Methods 8:26–29.

Dent JA, Davis MW, Avery L (1997) *avr-15* encodes a chloride channel subunit that mediates inhibitory glutamatergic neurotransmission and ivermectin sensitivity in *Caenorhabditis elegans*. The EMBO Journal 16:5867–5879.

Dieterich C, Clifton SW, Schuster LN, Chinwalla A, Delehaunty K, Dinkelacker I, Fulton L, Fulton R, Godfrey J, Minx P, Mitreva M, Roeseler W, Tian H, Witte H, Yang S-P, Wilson RK, Sommer RJ (2008) The *Pristionchus pacificus* genome provides a unique perspective on nematode lifestyle and parasitism. Nature Genetics 40:1193–1198.

Doi M, Iwasaki K (2002) Regulation of retrograde signaling at neuromuscular junctions by the novel C2 domain protein AEX-1. Neuron 33:249–259.

Doncaster CC (1962) Nematode feeding mechanisms. 1. Observations on *Rhabditis* and *Pelodera*. Nematologica 8:313–320.

Donlea JM, Leahy A, Thimgan MS, Suzuki Y, Hughson BN, Sokolowski MB, Shaw PJ (2012) Foraging alters resilience/vulnerability to sleep disruption and starvation in *Drosophila.* Proceedings of the National Academy of Sciences of the United States of America 109:2613–2618.

Driver RJ, Lamb AL, Wyner AJ, Raizen DM (2013) DAF-16/FOXO regulates homeostasis of essential sleep-like behavior during larval transitions in *C. elegans*. Current Biology 23:501–506.

Dybbs M, Ngai J, Kaplan JM (2005) Using microarrays to facilitate positional cloning: identification of tomosyn as an inhibitor of neurosecretion. PLoS Genetics 1:6–16.

Edelman GM, Gally JA (2001) Degeneracy and complexity in biological systems. Proceedings of the National Academy of Sciences of the United States of America 98:13763–13768.

Edgley ML, Baillie DL, Riddle DL, Rose AM (2006) Genetic balancers. Wormbook:1–32.

Espinosa F, Fleischhauer R, McMahon A, Joho RH (2001) Dynamic interaction of S5 and S6 during voltage-controlled gating in a potassium channel. Journal of General

Physiology 118:157–170.

Fang-Yen C, Alkema MJ, Samuel ADT (2015) Illuminating neural circuits and behaviour in *Caenorhabditis elegans* with optogenetics. Philosophical Transactions of the Royal Society, Series B, Biological Sciences 370:20140212.

Fang-Yen C, Avery L, Samuel ADT (2009) Two size-selective mechanisms specifically trap bacteria-sized food particles in *Caenorhabditis elegans*. Proceedings of the National Academy of Sciences of the United States of America 106:20093–20096.

Fang-Yen C, Gabel CV, Samuel ADT, Bargmann CI, Avery L (2012) Laser microsurgery in *Caenorhabditis elegans*. Methods in Cell Biology 107:177–206.

Flavell SW, Pokala N, Macosko EZ, Albrecht DR, Larsch J, Bargmann CI (2013) Serotonin and the neuropeptide PDF initiate and extend opposing behavioral states in *C. elegans*. Cell 154:1023–1035.

Fleischhauer R, Davis MW, Dzhura I, Neely A, Avery L, Joho RH (2000) Ultrafast inactivation causes inward rectification in a voltage-gated K(+) channel from *Caenorhabditis elegans*. Journal of Neuroscience 20:511–520.

Foltenyi K, Greenspan RJ, Newport JW (2007) Activation of EGFR and ERK by rhomboid signaling regulates the consolidation and maintenance of sleep in *Drosophila*. Nature Neuroscience 10:1160–1167.

Francis MM, Evans SP, Jensen M, Madsen DM, Mancuso J, Norman KR, Maricq AV (2005) The Ror receptor tyrosine kinase CAM-1 is required for ACR-16-mediated

synaptic transmission at the *C. elegans* neuromuscular junction. Neuron 46:581–594.

Frand AR, Russel S, Ruvkun GB (2005) Functional genomic analysis of *C. elegans* molting. PLoS Biology 3:e312.

Franks CJ, Pemberton DJ, Vinogradova I, Cook A, Walker RJ, Holden-Dye LM (2002) Ionic basis of the resting membrane potential and action potential in the pharyngeal muscle of *Caenorhabditis elegans*. Journal of Neurophysiology 87:954–961.

Frézal L, Félix M-A (2015) *C. elegans* outside the Petri dish. eLife 4.

Garrison JL, Macosko EZ, Bernstein S, Pokala N, Albrecht DR, Bargmann CI (2012) Oxytocin/vasopressin-related peptides have an ancient role in reproductive behavior. Science 338:540–543.

Gazzaniga MS (1995) Principles of human brain organization derived from split-brain studies. Neuron 14:217–228.

George-Raizen JB, Shockley KR, Trojanowski NF, Lamb AL, Raizen DM (2014) Dynamically-expressed prion-like proteins form a cuticle in the pharynx of *Caenorhabditis elegans.* Biology Open 3:1139–1149.

Gibbs FA, Davis H, Lennox WG (1935) The electro-encephalogram in epilepsy and in conditions of impaired consciousness. Archives of Neurology & Psychiatry 34:1133–1148.

Goaillard J-M, Taylor AL, Schulz DJ, Marder E (2009) Functional consequences of animal-to-animal variation in circuit parameters. Nature Neuroscience 12:1424–1430

Golowasch J (2014) Ionic current variability and functional stability in the nervous system. BioScience 64:570–580.

Goodman MB, Lindsay TH, Lockery SR, Richmond JE (2012) Electrophysiological methods for *Caenorhabditis elegans* neurobiology. Methods in Cell Biology 107:409–436.

Gordus A, Pokala N, Levy S, Flavell SW, Bargmann CI (2015) Feedback from network states generates variability in a probabilistic olfactory circuit. Cell 161:215–227.

Grashow R, Brookings T, Marder E (2010) Compensation for variable intrinsic neuronal excitability by circuit-synaptic interactions. Journal of Neuroscience 30:9145–9156.

Greer ER, Pérez CL, Van Gilst MR, Lee BH, Ashrafi K (2008) Neural and molecular dissection of a *C. elegans* sensory circuit that regulates fat and feeding. Cell Metabolism 8:118–131.

Grossman N, Nikolic K, Toumazou C, Degenaar P (2011) Modeling study of the light stimulation of a neuron cell with channelrhodopsin-2 mutants. IEEE Transactions on Biomedical Engineering 58:1742–1751.

Gruninger TR, Gualberto DG, LeBoeuf B, Garcia LR (2006) Integration of male mating and feeding behaviors in *Caenorhabditis elegans*. Journal of Neuroscience 26:169–179.

Guo F, Yi W, Zhou M, Guo A (2011) Go signaling in mushroom bodies regulates sleep in *Drosophila*. Sleep 34:273–281.

Guo ZV, Hart AC, Ramanathan S (2009) Optical interrogation of neural circuits in *Caenorhabditis elegans*. Nature Methods 6:891–896.

Gutierrez GJ, Marder E (2014) Modulation of a single neuron has state-dependent actions on circuit dynamics. eNeuro 1.

Gutierrez GJ, O'Leary T, Marder E (2013) Multiple mechanisms switch an electrically coupled, synaptically inhibited neuron between competing rhythmic oscillators. Neuron 77:845–858.

Gürel G, Gustafson MA, Pepper JS, Horvitz HR, Koelle MR (2012) Receptors and other signaling proteins required for serotonin control of locomotion in *Caenorhabditis elegans*. Genetics 192:1359–1371.

Hajdu-Cronin YM, Chen WJ, Patikoglou GA, Koelle MR, Sternberg PW (1999) Antagonism between G(o)alpha and G(q)alpha in *Caenorhabditis elegans*: the RGS protein EAT-16 is necessary for G(o)alpha signaling and regulates G(q)alpha activity. Genes & Development 13:1780–1793.

Hall DH, Russell RL (1991) The posterior nervous system of the nematode *Caenorhabditis elegans*: serial reconstruction of identified neurons and complete pattern of synaptic interactions. Journal of Neuroscience 11:1–22.

Harris GP, Korchnak A, Summers PJ, Hapiak VM, Law WJ, Stein AM, Komuniecki PR, Komuniecki RW (2011) Dissecting the serotonergic food signal stimulating sensory-mediated aversive behavior in *C. elegans*. PLoS ONE 6:e21897.

Harris GP, Mills H, Wragg RT, Hapiak VM, Castelletto M, Korchnak A, Komuniecki RW (2010) The monoaminergic modulation of sensory-mediated aversive responses in *Caenorhabditis elegans* requires glutamatergic/peptidergic cotransmission. Journal of Neuroscience 30:7889–7899.

Harris-Warrick RM, Flamm RE (1987) Multiple mechanisms of bursting in a conditional bursting neuron. Journal of Neuroscience 7:2113–2128.

Hawasli AH, Saifee O, Liu C, Nonet ML, Crowder CM (2004) Resistance to volatile anesthetics by mutations enhancing excitatory neurotransmitter release in *Caenorhabditis elegans*. Genetics 168:831–843.

He C, Yang Y, Zhang M, Price JL, Zhao Z (2013) Regulation of sleep by Neuropeptide Y-like system in *Drosophila melanogaster*. PLoS ONE 8:e74237.

Hendricks JC, Finn SM, Panckeri KA, Chavkin J, Williams JA, Sehgal A, Pack AI (2000) Rest in *Drosophila* is a sleep-like state. Neuron 25:129–138.

Hendricks JC, Williams JA, Panckeri KA, Kirk D, Tello M, Yin JCP, Sehgal A (2001) A non-circadian role for cAMP signaling and CREB activity in *Drosophila* rest homeostasis. Nature Neuroscience 4:1108–1115.

Hill AJ, Mansfield R, Lopez JMNG, Raizen DM, Van Buskirk C (2014) Cellular stress induces a protective sleep-like state in *C. elegans*. Current Biology 24:2399–2405.

Hobert O (2013) The neuronal genome of *Caenorhabditis elegans*. Wormbook:1–106.

Hobson RJ, Hapiak VM, Xiao H, Buehrer KL, Komuniecki PR, Komuniecki RW (2006)

SER-7, a *Caenorhabditis elegans* 5-HT7-like receptor, is essential for the 5-HT stimulation of pharyngeal pumping and egg laying. Genetics 172:159–169.

Holden-Dye LM, Walker RJ (2007) Anthelmintic drugs. Wormbook:1–13.

Horvitz HR, Chalfie M, Trent C, Sulston JE, Evans PD (1982) Serotonin and octopamine in the nematode *Caenorhabditis elegans*. Science 216:1012–1014.

Huang C, Xiong C, Kornfeld K (2004) Measurements of age-related changes of physiological processes that predict lifespan of *Caenorhabditis elegans*. Proceedings of the National Academy of Sciences of the United States of America 101:8084–8089.

Humphrey JA, Hamming KS, Thacker CM, Scott RL, Sedensky MM, Snutch TP, Morgan PG, Nash HA (2007) A putative cation channel and its novel regulator: cross-species conservation of effects on general anesthesia. Current Biology 17:624–629.

Husson SJ, Gottschalk A, Leifer AM (2013) Optogenetic manipulation of neural activity in *C. elegans*: from synapse to circuits and behaviour. Biology of the Cell 105:235–250.

Husson SJ, Liewald JF, Schultheis C, Stirman JN, Lu H, Gottschalk A (2012) Microbial light-activatable proton pumps as neuronal inhibitors to functionally dissect neuronal networks in *C. elegans*. PLoS ONE 7:e40937.

Hwang JM, Chang D-J, Kim US, Lee Y-S, Park Y-S, Kaang B-K, Cho NJ (1999)

Cloning and functional characterization of a *Caenorhabditis elegans* muscarinic acetylcholine receptor. Receptors & Channels 6:415–424.

Iwanir S, Tramm N, Nagy S, Wright C, Ish D, Biron D (2013) The microarchitecture of *C. elegans* behavior during lethargus: Homeostatic bout dynamics, a typical body posture, and regulation by a central neuron. Sleep 36:385–395.

Jansen G, Thijssen KL, Werner P, van der Horst M, Hazendonk E, Plasterk RHA (1999) The complete family of genes encoding G proteins of *Caenorhabditis elegans*. Nature Genetics 21:414–419.

Janssen T, Lindemans M, Meelkop E, Temmerman L, Schoofs L (2010) Coevolution of neuropeptidergic signaling systems: from worm to man. Annals of the New York Academy of Sciences 1200:1–14.

Jarrell TA, Wang Y, Bloniarz AE, Brittin CA, Xu M, Thomson JN, Albertson DG, Hall DH, Emmons SW (2012) The connectome of a decision-making neural network. Science 337:437–444.

Jeon M, Gardner HF, Miller EA, Deshler J, Rougvie AE (1999) Similarity of the *C. elegans* developmental timing protein LIN-42 to circadian rhythm proteins. Science 286:1141–1146.

Joiner WJ, Crocker A, White BH, Sehgal A (2006) Sleep in *Drosophila* is regulated by adult mushroom bodies. Nature 441:757–760.

Jones D, Candido EP (1999) Feeding is inhibited by sublethal concentrations of toxicants

and by heat stress in the nematode *Caenorhabditis elegans*: relationship to the cellular stress response. Journal of Experimental Zoology 284:147–157.

Katz PS, Lillvis JL (2014) Reconciling the deep homology of neuromodulation with the evolution of behavior. Current Opinion in Neurobiology 29:39–47.

Kayser MS, Yue Z, Sehgal A (2014) A critical period of sleep for development of courtship circuitry and behavior in *Drosophila*. Science 344:269–274.

Kerr RA, Lev-Ram V, Baird G, Vincent P, Tsien RY, Schafer WR (2000) Optical imaging of calcium transients in neurons and pharyngeal muscle of *C. elegans*. Neuron 26:583–594.

Kiehn O, Dougherty KJ, Hägglund M, Borgius L, Talpalar A, Restrepo CE (2010) Probing spinal circuits controlling walking in mammals. Biochemical and Biophysical Research Communications 396:11–18.

Kim E, Sun L, Gabel CV, Fang-Yen C (2013) Long-term imaging of *Caenorhabditis elegans* using nanoparticle-mediated immobilization. PLoS ONE 8:e53419.

Kim K, Li C (2004) Expression and regulation of an FMRFamide-related neuropeptide gene family in *Caenorhabditis elegans*. Journal of Comparative Neurology 475:540–550.

Klapoetke NC et al. (2014) Independent optical excitation of distinct neural populations. Nature Methods 11:338–346.

Kleitman N (1929) Sleep. Physiol Rev 9:624–665.

Kocabas A, Shen C-H, Guo ZV, Ramanathan S (2012) Controlling interneuron activity in *Caenorhabditis elegans* to evoke chemotactic behaviour. Nature 490:273–277.

Koh K, Joiner WJ, Wu MN, Yue Z, Smith CJ, Sehgal A (2008) Identification of SLEEPLESS, a sleep-promoting factor. Science 321:372–376.

Konopka RJ, Benzer S (1971) Clock mutants of *Drosophila melanogaster*. Proceedings of the National Academy of Sciences of the United States of America 68:2112–2116.

Korswagen HC, Park JH, Ohshima Y, Plasterk RHA (1997) An activating mutation in a *Caenorhabditis elegans* Gs protein induces neural degeneration. Genes & Development 11:1493–1503.

Krueger JM, Pappenheimer JR, Karnovsky ML (1982) Sleep-promoting effects of muramyl peptides. Proceedings of the National Academy of Sciences of the United States of America 79:6102–6106.

Lee RYN, Lobel L, Hengartner MO, Horvitz HR, Avery L (1997) Mutations in the alpha$_1$ subunit of an L-type voltage-activated Ca^{2+} channel cause myotonia in *Caenorhabditis elegans*. The EMBO Journal 16:6066–6076.

Lee RYN, Sawin ER, Chalfie M, Horvitz HR, Avery L (1999a) EAT-4, a homolog of a mammalian sodium-dependent inorganic phosphate cotransporter, is necessary for glutamatergic neurotransmission in *Caenorhabditis elegans*. Journal of Neuroscience 19:159–167.

Lee Y-S, Park Y-S, Chang D-J, Hwang JM, Min CK, Kaang B-K, Cho NJ (1999b)

Cloning and expression of a G protein-linked acetylcholine receptor from *Caenorhabditis elegans*. Journal of Neurochemistry 72:58–65.

Lee Y-S, Park Y-S, Nam S, Suh S, Lee J, Kaang B-K, Cho NJ (2000) Characterization of GAR-2, a novel G protein-linked acetylcholine receptor from *Caenorhabditis elegans*. Journal of Neurochemistry 75:1800–1809.

Leifer AM, Fang-Yen C, Gershow M, Alkema MJ, Samuel ADT (2011) Optogenetic manipulation of neural activity in freely moving *Caenorhabditis elegans*. Nature Methods 8:147–152.

Lenz O, Xiong J, Nelson MD, Raizen DM, Williams JA (2015) Brain, Behavior, and Immunity. Brain, Behaviour, and Immunity 47:141–148.

Li C, Nelson LS, Kim K, Nathoo AN, Hart AC (1999) Neuropeptide gene families in the nematode *Caenorhabditis elegans*. Annals of the New York Academy of Sciences 897:239–252.

Li H, Avery L, Denk W, Hess GP (1997) Identification of chemical synapses in the pharynx of *Caenorhabditis elegans*. Proceedings of the National Academy of Sciences of the United States of America 94:5912–5916.

Li S, Dent JA, Roy R (2003) Regulation of intermuscular electrical coupling by the *Caenorhabditis elegans* innexin *inx-6*. Molecular Biology of the Cell 14:2630–2644.

Li Z, Li Y, Yi Y, Huang W, Yang S, Niu W, Zhang L, Xu Z, Qu A, Wu Z-X, Xu T (2012) Dissecting a central flip-flop circuit that integrates contradictory sensory cues

in *C. elegans* feeding regulation. Nature Communications 3:776–778.

Lieven von AF (2003) Functional morphology and evolutionary origin of the three-part pharynx in nematodes. Zoology 106:183–201.

Liewald JF, Brauner M, Stephens GJ, Bouhours M, Schultheis C, Zhen M, Gottschalk A (2008) Optogenetic analysis of synaptic function. Nature Methods 5:895–902.

Liu Y, LeBoeuf B, Garcia LR (2007) Gq-coupled muscarinic acetylcholine receptors enhance nicotinic acetylcholine receptor signaling in *Caenorhabditis elegans* mating behavior. Journal of Neuroscience 27:1411–1421.

Livingstone MS, Hubel DH (1981) Effects of sleep and arousal on the processing of visual information in the cat. Nature 291:554–561.

Loomis AL, Harvey EN, Hobart G (1935a) Potential rhythms of the cerebral cortex during sleep. Science 81:597–598.

Loomis AL, Harvey EN, Hobart G (1935b) Further observations on the potential rhythms of the cerebral cortex during sleep. Science 82:198–200.

Loomis AL, Harvey EN, Hobart G (1936) Electrical potentials of the human brain. Journal of Experimental Psychology 19:249–279.

Loomis AL, Harvey EN, Hobart G (1937) Cerebral states during sleep, as studied by human brain potentials. Journal of Experimental Psychology 21:127–144.

Los FCO, Ha C, Aroian RV (2013) Neuronal Goα and CAPS regulate behavioral and

immune responses to bacterial pore-forming toxins. PLoS ONE 8:e54528.

Mackiewicz M, Shockley KR, Romer MA, Galante RJ, Zimmerman JE, Naidoo N, Baldwin DA, Jensen ST, Churchill GA, Pack AI (2007) Macromolecule biosynthesis: a key function of sleep. Physiological Genomics 31:441–457.

Marder E (2011) Variability, compensation, and modulation in neurons and circuits. Proceedings of the National Academy of Sciences of the United States of America 108:15542–15548.

Marder E, Bucher D, Schulz DJ, Taylor AL (2005) Invertebrate central pattern generation moves along. Current Biology 15:R685–R699.

Marder E, Calabrese RL (1996) Principles of rhythmic motor pattern generation. Physiological Reviews 76:687–717.

Marder E, O'Leary T, Shruti S (2014) Neuromodulation of circuits with variable parameters: Single neurons and small circuits reveal principles of state-dependent and robust neuromodulation. Annual Review of Neuroscience 37:329–346.

Marder E, Taylor AL (2011) Multiple models to capture the variability in biological neurons and networks. Nature Neuroscience 14:133–138.

McKay JP, Raizen DM, Gottschalk A, Schafer WR, Avery L (2004) *eat-2* and *eat-18* are required for nicotinic neurotransmission in the *Caenorhabditis elegans* pharynx. Genetics 166:161–169.

Mello CC, Kramer JM, Stinchcomb D, Ambros VR (1991) Efficient gene transfer in *C.*

elegans: extrachromosomal maintenance and integration of transforming sequences. The EMBO Journal 10:3959–3970.

Mendel JE, Korswagen HC, Liu KS, Hajdu-Cronin YM, Simon MI, Plasterk RHA, Sternberg PW (1995) Participation of the protein G(o)alpha in multiple aspects of behavior in *C. elegans*. Science 267:1652–1655.

Miller KG, Alfonso A, Nguyen M, Crowell JA, Johnson CD, Rand JB (1996) A genetic selection for *Caenorhabditis elegans* synaptic transmission mutants. Proceedings of the National Academy of Sciences of the United States of America 93:12593–12598.

Miller KG, Emerson MD, Rand JB (1999) G(o)alpha and diacylglycerol kinase negatively regulate the G(q)alpha pathway in *C. elegans*. Neuron 24:323–333.

Monsalve GC, Van Buskirk C, Frand AR (2011) LIN-42/PERIOD controls cyclical and developmental progression of *C. elegans* molts. Current Biology 21:2033–2045.

Morgan PG, Kayser E-B, Sedensky MM (2007) *C. elegans* and volatile anesthetics. Wormbook:1–11.

Morgan PG, Sedensky MM, Meneely PM (1990) Multiple sites of action of volatile anesthetics in *Caenorhabditis elegans*. Proceedings of the National Academy of Sciences of the United States of America 87:2965–2969.

Mori I, Ohshima Y (1995) Neural regulation of thermotaxis in *Caenorhabditis elegans*. Nature 376:344–348.

Nagel G, Brauner M, Liewald JF, Adeishvili N, Bamberg E, Gottschalk A (2005) Light

Activation of Channelrhodopsin-2 in excitable cells of *Caenorhabditis elegans* triggers rapid behavioral responses. Current Biology 15:2279–2284.

Nagel G, Szellas T, Huhn W, Kateriya S, Adeishvili N, Berthold P, Ollig D, Hegemann P, Bamberg E (2003) Channelrhodopsin-2, a directly light-gated cation-selective membrane channel. Proceedings of the National Academy of Sciences of the United States of America 100:13940–13945.

Nagy S, Tramm N, Sanders J, Iwanir S, Shirley IA, Levine E, Biron D (2014) Homeostasis in *C. elegans* sleep is characterized by two behaviorally and genetically distinct mechanisms. eLife 3:e04380.

Nagy S, Wright C, Tramm N, Labello N, Burov S, Biron D (2013) A longitudinal study of *Caenorhabditis elegans* larvae reveals a novel locomotion switch, regulated by G s signaling. eLife 2:e00782–e00782.

Nathoo AN, Moeller RA, Westlund BA, Hart AC (2001) Identification of neuropeptide-like protein gene families in *Caenorhabditis elegans* and other species. Proceedings of the National Academy of Sciences of the United States of America 98:14000–14005.

Nelson MD, Fitch DHA (2011) Overlap extension PCR: an efficient method for transgene construction. Methods in Molecular Biology 772:459–470.

Nelson MD, Lee KH, Churgin MA, Hill AJ, Van Buskirk C, Fang-Yen C, Raizen DM (2014) FMRFamide-like FLP-13 neuropeptides promote quiescence following heat

stress in *Caenorhabditis elegans*. Current Biology 24:2406–2410.

Nelson MD, Raizen DM (2013) A sleep state during *C. elegans* development. Current Opinion in Neurobiology 23:824–830.

Nelson MD, Trojanowski NF, George-Raizen JB, Smith CJ, Yu C-C, Fang-Yen C, Raizen DM (2013) The neuropeptide NLP-22 regulates a sleep-like state in *Caenorhabditis elegans*. Nature Communications 4:2846.

Niacaris T, Avery L (2003) Serotonin regulates repolarization of the *C. elegans* pharyngeal muscle. Journal of Experimental Biology 206:223–231.

Norris BJ, Weaver AL, Wenning A, Garcia PS, Calabrese RL (2007a) A central pattern generator producing alternative outputs: pattern, strength, and dynamics of premotor synaptic input to leech heart motor neurons. Journal of Neurophysiology 98:2992–3005.

Norris BJ, Weaver AL, Wenning A, Garcia PS, Calabrese RL (2007b) A central pattern generator producing alternative outputs: phase relations of leech heart motor neurons with respect to premotor synaptic input. Journal of Neurophysiology 98:2983–2991.

Nurrish SJ, Ségalat L, Kaplan JM (1999) Serotonin inhibition of synaptic transmission: G(o)alpha decreases the abundance of UNC-13 at release sites. Neuron 24:231–242.

Okazaki A, Takahashi M, Toyoda N, Takagi S (2014) Optical silencing of *C. elegans* cells with light-driven proton pumps. Methods 68:425–430.

O'Leary T, Williams AH, Franci A, Marder E (2014) Cell types, network homeostasis,

and pathological compensation from a biologically plausible ion channel expression model. Neuron 82:809–821.

Ostrowski EA, Rozen DE, Lenski RE (2005) Pleiotropic effects of beneficial mutations in *Escherichia coli*. Evolution 59:2343.

Ostrowski EA, Woods RJ, Lenski RE (2008) The genetic basis of parallel and divergent phenotypic responses in evolving populations of *Escherichia coli*. Proceedings of the Royal Society, Series B, Biological Sciences 275:277–284.

Owald D, Lin S, Waddell S (2015) Light, heat, action: neural control of fruit fly behaviour. Philosophical Transactions of the Royal Society, Series B, Biological Sciences 370:20140211.

Papaioannou S, Holden-Dye LM, Walker RJ (2008) The actions of *Caenorhabditis elegans* neuropeptide-like peptides (NLPs) on body wall muscle of *Ascaris suum* and pharyngeal muscle of *C. elegans*. Acta Biologica Hungarica 59:189–197.

Papaioannou S, Marsden D, Franks CJ, Walker RJ, Holden-Dye LM (2005) Role of a FMRFamide-like family of neuropeptides in the pharyngeal nervous system of *Caenorhabditis elegans*. Journal of Neurobiology 65:304–319.

Parisky KM, Agosto J, Pulver SR, Shang Y, Kuklin E, Hodge JJL, Kang K, Liu X, Garrity PA, Rosbash M, Griffith LC (2008) PDF cells are a GABA-responsive wake-promoting component of the *Drosophila* sleep circuit. Neuron 60:672–682.

Perez-Mansilla B, Nurrish SJ (2009) A network of G-protein signaling pathways control

neuronal activity in *C. elegans*. Advances in Genetics 65:145–192.

Pierce SB, Costa M, Wisotzkey R, Devadhar S, Homburger SA, Buchman AR, Ferguson KC, Heller J, Platt DM, Pasquinelli AE, Liu LX, Doberstein SK, Ruvkun GB (2001) Regulation of DAF-2 receptor signaling by human insulin and *ins-1*, a member of the unusually large and diverse *C. elegans* insulin gene family. Genes & Development 15:672–686.

Pires-daSilva A, Sommer RJ (2004) Conservation of the global sex determination gene *tra-1* in distantly related nematodes. Genes & Development 18:1198–1208.

Prevedel R, Yoon Y-G, Hoffmann M, Pak N, Wetzstein G, Kato S, Schrödel T, Raskar R, Zimmer M, Boyden ES, Vaziri A (2014) Simultaneous whole-animal 3D imaging of neuronal activity using light-field microscopy. Nature Methods 11:727–730.

Prinz AA, Bucher D, Marder E (2004) Similar network activity from disparate circuit parameters. Nature Neuroscience 7:1345–1352.

Pujol N, Torregrossa P, Ewbank JJ, Brunet JF (2000) The homeodomain protein CePHOX2/CEH-17 controls antero-posterior axonal growth in *C. elegans*. Development 127:3361–3371.

Ragsdale EJ, Ngo PT, Crum J, Ellisman MH, Baldwin JG (2010) Reconstruction of the pharyngeal corpus of *Aphelenchus avenae* (Nematoda: Tylenchomorpha), with implications for phylogenetic congruence. Zoological Journal of the Linnean Society 161:1–30.

Raizen DM, Avery L (1994) Electrical activity and behavior in the pharynx of *Caenorhabditis elegans*. Neuron 12:483–495.

Raizen DM, Lee RYN, Avery L (1995) Interacting genes required for pharyngeal excitation by motor neuron MC in *Caenorhabditis elegans*. Genetics 141:1365–1382.

Raizen DM, Song B-M, Trojanowski NF, You Y-J (2012) Methods for measuring pharyngeal behaviors. Wormbook:1–13.

Raizen DM, Zimmerman JE, Maycock MH, Ta UD, You Y-J, Sundaram MV, Pack AI (2008) Lethargus is a *Caenorhabditis elegans* sleep-like state. Nature 451:569–572.

Rampin C, Cespuglio R, Chastrette N, Jouvet M (1991) Immobilisation stress induces a paradoxical sleep rebound in rat. Neuroscience Letters 126:113–118.

Rand JB (1989) Genetic analysis of the *cha-1-unc-17* gene complex in *Caenorhabditis.* Genetics 122:73–80.

Ranganathan R, Sawin ER, Trent C, Horvitz HR (2001) Mutations in the *Caenorhabditis elegans* serotonin reuptake transporter MOD-5 reveal serotonin-dependent and -independent activities of fluoxetine. Journal of Neuroscience 21:5871–5884.

Renn SC, Park JH, Rosbash M, Hall JC, Taghert PH (1999) A pdf neuropeptide gene mutation and ablation of PDF neurons each cause severe abnormalities of behavioral circadian rhythms in *Drosophila*. Cell 99:791–802.

Reynolds NK, Schade MA, Miller KG (2005) Convergent, RIC-8-dependent Galpha signaling pathways in the *Caenorhabditis elegans* synaptic signaling network.

Genetics 169:651–670.

Richmond JE, Jorgensen EM (1999) One GABA and two acetylcholine receptors function at the *C. elegans* neuromuscular junction. Nature Neuroscience 2:791–797.

Richter C, Woods IG, Schier AF (2014) Neuropeptidergic control of sleep and wakefulness. Annual Review of Neuroscience 37:503–531.

Robatzek M, Thomas JH (2000) Calcium/calmodulin-dependent protein kinase II regulates *Caenorhabditis elegans* locomotion in concert with a G(o)/G(q) signaling network. Genetics 156:1069–1082.

Rodriguez JC, Blitz DM, Nusbaum MP (2013) Convergent rhythm generation from divergent cellular mechanisms. Journal of Neuroscience 33:18047–18064.

Rogers CM, Franks CJ, Walker RJ, Burke JF, Holden-Dye LM (2001) Regulation of the pharynx of *Caenorhabditis elegans* by 5-HT, octopamine, and FMRFamide-like neuropeptides. Journal of Neurobiology 49:235–244.

Saideman SR, Blitz DM, Nusbaum MP (2007) Convergent motor patterns from divergent circuits. Journal of Neuroscience 27:6664–6674.

Saifee O, Metz LB, Nonet ML, Crowder CM (2011) A gain-of-function mutation in adenylate cyclase confers isoflurane resistance in *Caenorhabditis elegans.* Anesthesiology 115:1162–1171.

Saifee O, Wei L, Nonet ML (1998) The *Caenorhabditis elegans unc-64* locus encodes a syntaxin that interacts genetically with synaptobrevin. Molecular Biology of the Cell

9:1235–1252.

Sakurai A, Tamvacakis AN, Katz PS (2014) Hidden synaptic differences in a neural circuit underlie differential behavioral susceptibility to a neural injury. eLife 3.

Saper CB, Romanovsky AA, Scammell TE (2012) Neural circuitry engaged by prostaglandins during the sickness syndrome. Nature Neuroscience 15:1088–1095.

Saper CB, Scammell TE, Lu J (2005) Hypothalamic regulation of sleep and circadian rhythms. Nature 437:1257–1263.

Sawin ER, Ranganathan R, Horvitz HR (2000) *C. elegans* locomotory rate is modulated by the environment through a dopaminergic pathway and by experience through a serotonergic pathway. Neuron 26:619–631.

Schade MA, Reynolds NK, Dollins CM, Miller KG (2005) Mutations that rescue the paralysis of *Caenorhabditis elegans ric-8* (synembryn) mutants activate the G alpha(s) pathway and define a third major branch of the synaptic signaling network. Genetics 169:631–649.

Schinkmann K, Li C (1992) Localization of FMRFamide-like peptides in *Caenorhabditis elegans*. Journal of Comparative Neurology 316:251–260.

Schmitt C, Schultheis C, Husson SJ, Liewald JF, Gottschalk A (2012) Specific expression of Channelrhodopsin-2 in single neurons of *Caenorhabditis elegans*. PLoS ONE 7:e43164.

Schrödel T, Prevedel R, Aumayr K, Zimmer M, Vaziri A (2013) Brain-wide 3D imaging

of neuronal activity in *Caenorhabditis elegans* with sculpted light. Nature Methods 10:1013–1020.

Schulz DJ, Goaillard J-M, Marder E (2007) Quantitative expression profiling of identified neurons reveals cell-specific constraints on highly variable levels of gene expression. Proceedings of the National Academy of Sciences of the United States of America 104:13187–13191.

Schwarz J, Bringmann H (2013) Reduced sleep-like quiescence in both hyperactive and hypoactive mutants of the Galphaq gene *egl-30* during lethargus in *Caenorhabditis elegans*. PLoS ONE 8:e75853.

Selverston AI (2010) Invertebrate central pattern generator circuits. Philosophical Transactions of the Royal Society, Series B, Biological Sciences 365:2329–2345.

Serrano-Saiz E, Poole RJ, Felton T, Zhang F, La Cruz De ED, Hobert O (2013) Modular control of glutamatergic neuronal identity in *C. elegans* by distinct homeodomain Proteins. Cell 155:659–673.

Seugnet L, Suzuki Y, Merlin G, Gottschalk L, Duntley SP, Shaw PJ (2011) Notch signaling modulates sleep homeostasis and learning after sleep deprivation in *Drosophila*. Current Biology 21:835–840.

Seymour MK, Wright KA, Doncaster CC (1983) The action of the anterior feeding apparatus of *Caenorhabditis elegans* (Nematoda, Rhabdita). Journal of Zoology 201:527–539.

Ségalat L, Elkes DA, Kaplan JM (1995) Modulation of serotonin-controlled behaviors by G(o)alpha in *Caenorhabditis elegans*. Science 267:1648–1651.

Shang Y, Donelson NC, Vecsey CG, Guo F, Rosbash M, Griffith LC (2013) Short Neuropeptide F is a sleep-promoting inhibitory modulator. Neuron 80:171–183.

Sharabi K, Charar C, Friedman N, Mizrahi I, Zaslaver A, Sznajder JI, Gruenbaum Y (2014) The response to high CO_2 levels requires the neuropeptide secretion component HID-1 to promote pumping inhibition. PLoS Genetics 10:e1004529.

Shimozono S, Fukano T, Kimura KD, Mori I, Kirino Y, Miyawaki A (2004) Slow Ca^{2+} dynamics in pharyngeal muscles in *Caenorhabditis elegans* during fast pumping. EMBO Reports 5:521–526.

Shtonda BB, Avery L (2005) CCA-1, EGL-19 and EXP-2 currents shape action potentials in the *Caenorhabditis elegan*s pharynx. Journal of Experimental Biology 208:2177–2190.

Siegel JM (2005) Clues to the functions of mammalian sleep. Nature 437:1264–1271.

Siegel JM (2008) Do all animals sleep? Trends in Neurosciences 31:208–213.

Singh K, Chao MY, Somers GA, Komatsu H, Corkins ME, Larkins-Ford J, Tucey TM, Dionne HM, Walsh MB, Beaumont EK, Hart DP, Lockery SR, Hart AC (2011) *C. elegans* notch signaling regulates adult chemosensory response and larval molting quiescence. Current Biology 21:825–834.

Singh K, Ju JY, Walsh MB, DiIorio MA, Hart AC (2014) Deep conservation of genes

required for both *Drosphila melanogaster* and *Caenorhabditis elegans* sleep includes a role for dopaminergic signaling. Sleep 37:1439–1451.

Singh RN, Sulston JE (1978) Some observations on moulting in *Caenorhabditis elegans*. Nematologica 24:63–71.

Song B-M, Avery L (2012) Serotonin activates overall feeding by activating two separate neural pathways in *Caenorhabditis elegans*. Journal of Neuroscience 32:1920–1931.

Song B-M, Faumont S, Lockery SR, Avery L (2013) Recognition of familiar food activates feeding via an endocrine serotonin signal in *Caenorhabditis elegans*. eLife 2:e00329.

Soukas AA, Kane EA, Carr CE, Melo JA, Ruvkun GB (2009) Rictor/TORC2 regulates fat metabolism, feeding, growth, and life span in *Caenorhabditis elegans*. Genes & Development 23:496–511.

Starich TA, Lee RYN, Panzarella C, Avery L, Shaw JE (1996) *eat-5* and *unc-7* represent a multigene family in *Caenorhabditis elegans* involved in cell-cell coupling. Journal of Cell Biology 134:537–548.

Starich TA, Miller A, Nguyen RL, Hall DH, Shaw JE (2003) The *Caenorhabditis elegans* innexin INX-3 is localized to gap junctions and is essential for embryonic development. Developmental Biology 256:403–417.

Steciuk M, Cheong MC, Waite C, You Y-J, Avery L (2014) Regulation of synaptic transmission at the *Caenorhabditis elegans* M4 neuromuscular junction by an

antagonistic relationship between two calcium channels. G3 4:2535–2543.

Stefanakis N, Carrera I, Hobert O (2015) Regulatory logic of pan-neuronal gene expression in *C. elegans*. Neuron 87:733–750.

Steger KA, Avery L (2004) The GAR-3 muscarinic receptor cooperates with calcium signals to regulate muscle contraction in the *Caenorhabditis elegans* pharynx. Genetics 167:633–643.

Steger KA, Shtonda BB, Thacker CM, Snutch TP, Avery L (2005) The *C. elegans* T-type calcium channel CCA-1 boosts neuromuscular transmission. Journal of Experimental Biology 208:2191–2203.

Stent GS, Thompson WJ, Calabrese RL (1979) Neural control of heartbeat in the leech and in some other invertebrates. Physiological Reviews 59:101–136.

Stiernagle T (2006) Maintenance of *C. elegans*. Wormbook:1–11.

Stirman JN, Crane MM, Husson SJ, Wabnig S, Schultheis C, Gottschalk A, Lu H (2011) Real-time multimodal optical control of neurons and muscles in freely behaving *Caenorhabditis elegans*. Nature Methods 8:153–158.

Straud S, Lee I, Song B-M, Avery L, You Y-J (2013) The Jaw of the Worm: GTPase-activating protein EAT-17 regulates grinder formation in *Caenorhabditis elegans*. Genetics 195:115–125.

Sulston JE, White JG (1980) Regulation and cell autonomy during postembryonic development of *Caenorhabditis elegans*. Developmental Biology 78:577–597.

Tabuse Y, Miwa J (1983) A gene involved in action of tumor promoters is identified and mapped in *Caenorhabditis elegans*. Carcinogenesis 4:783–786.

Tomita J, Ueno T, Mitsuyoshi M, Kume S, Kume K (2015) The NMDA receptor promotes sleep in the fruit fly, *Drosophila melanogaster*. PLoS ONE 10:e0128101.

Tononi G, Cirelli C (2014) Sleep and the price of plasticity: from synaptic and cellular homeostasis to memory consolidation and integration. Neuron 81:12–34.

Tononi G, Sporns O, Edelman GM (1999) Measures of degeneracy and redundancy in biological networks. Proceedings of the National Academy of Sciences of the United States of America 96:3257–3262.

Toth LA, Krueger JM (1988) Alteration of sleep in rabbits by *Staphylococcus aureus* infection. Infection and Immunity 56:1785–1791.

Touroutine D, Fox RM, Stetina Von SE, Burdina AO, Miller DM III, Richmond JE (2005) *acr-16* encodes an essential subunit of the levamisole-resistant nicotinic receptor at the *Caenorhabditis elegans* neuromuscular junction. Journal of Biological Chemistry 280:27013–27021.

Trent C, Tsung N, Horvitz HR (1983) Egg-laying defective mutants of the nematode *Caenorhabditis elegans*. Genetics 104:619–647.

Trojanowski NF, Padovan-Merhar O, Raizen DM, Fang-Yen C (2014) Neural and genetic degeneracy underlies *Caenorhabditis elegans* feeding behavior. Journal of Neurophysiology 112:951–961.

Turek M, Lewandrowski I, Bringmann H (2013) An AP2 transcription factor Is required for a sleep-active neuron to induce sleep-like quiescence in *C. elegans*. Current Biology 23:2215–2223.

van Alphen B, Yap MHW, Kirszenblat L, Kottler B, van Swinderen B (2013) A dynamic deep sleep stage in *Drosophila*. Journal of Neuroscience 33:6917–6927.

Van Buskirk C, Sternberg PW (2007) Epidermal growth factor signaling induces behavioral quiescence in *Caenorhabditis elegans*. Nature Neuroscience 10:1300–1307.

van der Linden AM, Moorman C, Cuppen E, Korswagen HC, Plasterk RHA (2003) Hyperactivation of the G12-mediated signaling pathway in *Caenorhabditis elegans* induces a developmental growth arrest via Protein Kinase C. Current Biology 13:516–521.

van Swinderen B, Metz LB, Shebester LD, Crowder CM (2002) A *Caenorhabditis elegans* pheromone antagonizes volatile anesthetic action through a Go-coupled pathway. Genetics 161:109–119.

van Swinderen B, Metz LB, Shebester LD, Mendel JE, Sternberg PW, Crowder CM (2001) G(o)alpha regulates volatile anesthetic action in *Caenorhabditis elegans*. Genetics 158:643–655.

van Swinderen B, Saifee O, Shebester LD, Roberson R, Nonet ML, Crowder CM (1999) A neomorphic syntaxin mutation blocks volatile-anesthetic action in *Caenorhabditis*

elegans. Proceedings of the National Academy of Sciences of the United States of America 96:2479–2484.

Vinogradova I, Cook A, Holden-Dye LM (2006) The ionic dependence of voltage-activated inward currents in the pharyngeal muscle of *Caenorhabditis elegans*. Invertebrate Neuroscience 6:57–68.

Voutev R, Hubbard EJA (2008) A "FLP-Out" system for controlled gene expression in *Caenorhabditis elegans*. Genetics 180:103–119.

Wang Z-W, Saifee O, Nonet ML, Salkoff L (2001) SLO-1 potassium channels control quantal content of neurotransmitter release at the *C. elegans* neuromuscular junction. Neuron 32:867–881.

Ward S, Thomson JN, White JG, Brenner S (1975) Electron microscopical reconstruction of the anterior sensory anatomy of the nematode *Caenorhabditis elegans*. Journal of Comparative Neurology 160:313–337.

Waschuk SA, Bezerra AG, Shi L, Brown LS (2005) *Leptosphaeria* rhodopsin: bacteriorhodopsin-like proton pump from a eukaryote. Proceedings of the National Academy of Sciences of the United States of America 102:6879–6883.

Wei J-Z, Hale K, Carta L, Platzer EG, Wong C, Fang S-C, Aroian RV (2003) *Bacillus thuringiensis* crystal proteins that target nematodes. Proceedings of the National Academy of Sciences of the United States of America 100:2760–2765.

Wei X, Potter CJ, Luo L, Shen K (2012) Controlling gene expression with the Q

repressible binary expression system in *Caenorhabditis elegans*. Nature Methods 9:391–395.

Whitacre J, Bender A (2010) Degeneracy: A design principle for achieving robustness and evolvability. Journal of Theoretical Biology 263:143–153.

White JG, Southgate E, Thomson JN, Brenner S (1986) The structure of the nervous system of the nematode *Caenorhabditis elegans*. Proceedings of the Royal Society, Series B, Biological Sciences 314:1–340.

Wiser MJ, Ribeck N, Lenski RE (2013) Long-term dynamics of adaptation in asexual populations. Science 342:1364–1367.

Woods IG, Schoppik D, Shi VJ, Zimmerman S, Coleman HA, Greenwood J, Soucy ER, Schier AF (2014) Neuropeptidergic signaling partitions arousal behaviors in zebrafish. Journal of Neuroscience 34:3142–3160.

Woods RJ, Barrick JE, Cooper TF, Shrestha U, Kauth MR, Lenski RE (2011) Second-order selection for evolvability in a large *Escherichia coli* population. Science 331:1433–1436.

Wragg RT, Hapiak VM, Miller SB, Harris GP, Gray JM, Komuniecki PR, Komuniecki RW (2007) Tyramine and octopamine independently inhibit serotonin-stimulated aversive behaviors in *Caenorhabditis elegans* through two novel amine receptors. Journal of Neuroscience 27:13402–13412.

Wu M, Robinson JE, Joiner WJ (2014) SLEEPLESS is a bifunctional regulator of

excitability and cholinergic synaptic transmission. Current Biology 24:621–629.

Wu MN, Joiner WJ, Dean T, Yue Z, Smith CJ, Chen D, Hoshi T, Sehgal A, Koh K (2010) SLEEPLESS, a Ly-6/neurotoxin family member, regulates the levels, localization and activity of Shaker. Nature Neuroscience 13:69–75.

Xu XZS, Kim SK (2011) The early bird catches the worm: new technologies for the *Caenorhabditis elegans* toolkit. Nature Reviews Genetics 12:793–801.

Yaniv Y, Lakatta EG, Maltsev VA (2015) From two competing oscillators to one coupled-clock pacemaker cell system. Frontiers in Physiology 6:28.

Yeh E, Ng S, Zhang M, Bouhours M, Wang Y, Wang M, Hung WL, Aoyagi K, Melnik-Martinez K, Li M, Liu F, Schafer WR, Zhen M (2008) A putative cation channel, NCA-1, and a novel protein, UNC-80, transmit neuronal activity in *C. elegans*. PLoS Biology 6:e55.

You Y-J, Kim J, Cobb MH, Avery L (2006) Starvation activates MAP kinase through the muscarinic acetylcholine pathway in *Caenorhabditis elegans* pharynx. Cell Metabolism 3:237–245.

You Y-J, Kim J, Raizen DM, Avery L (2008) Insulin, cGMP, and TGF-β signals regulate food intake and quiescence in *C. elegans*: A model for satiety. Cell Metabolism 7:249–257.

Zhang F, Aravanis AM, Adamantidis AR, de Lecea L, Deisseroth K (2007a) Circuit-breakers: optical technologies for probing neural signals and systems. Nature

Reviews Neuroscience 8:577–581.

Zhang F, Wang L-P, Brauner M, Liewald JF, Kay K, Watzke N, Wood PG, Bamberg E, Nagel G, Gottschalk A, Deisseroth K (2007b) Multimodal fast optical interrogation of neural circuitry. Nature 446:633–639.

Zhang YC, Baldwin JG (2000) Ultrastructure of the post–corpus of *Zeldia punctata* (Cephalobina) for analysis of the evolutionary framework of nematodes related to *Caenorhabditis elegans* (Rhabditina). Proceedings of the Royal Society, Series B, Biological Sciences 267:1229–1238.

Zhdanova IV, Wang SY, Leclair OU, Danilova NP (2001) Melatonin promotes sleep-like state in zebrafish. Brain Research 903:263–268.

Zimmerman JE, Naidoo N, Raizen DM, Pack AI (2008) Conservation of sleep: insights from non-mammalian model systems. Trends in Neurosciences 31:371–376.